Collision phenomena in a quantum gas

Document Version:
Publisher's PDF, also known as Version of Record (includes final page, issue and volume numbers)

Please check the document version of this publication:

• A submitted manuscript is the version of the article upon submission and before peer-review. There can be important differences between the submitted version and the official published version of record. People interested in the research are advised to contact the author for the final version of the publication, or visit the DOI to the publisher's website.
• The final author version and the galley proof are versions of the publication after peer review.
• The final published version features the final layout of the paper including the volume, issue and page numbers.

[Link to publication](#)

COLLISION PHENOMENA IN A QUANTUM GAS

PHILIP DE GOEY

COLLISION PHENOMENA IN A QUANTUM GAS

Dit proefschrift is goedgekeurd door de promotoren
Prof. dr. B.J. Verhaar
Prof. dr. W. Glöckle
co-promotor: dr. J.T.M. Walraven

Aan Riny
Aan mijn ouders

CONTENTS

INTRODUCTION

I (DEGENERATE) QUANTUM GASES

Fritz London[1] was the first to ascribe the remarkable superfluid properties of liquid ^{4}He below the λ-point to the influence of quantum mechanics, more specifically to Bose–Einstein condensation of the helium atoms. The associated condensate wavefunction would extend over macroscopic distances and thus create a long-range order in the liquid. London therefore referred to superfluidity as a macroscopic quantum phenomenon. Bose–Einstein condensation of particles in the lowest-energy single-particle state has a parallel in fermionic systems: the condensation of fermions into the single-particle states within the Fermi sphere. Collectively, these two phenomena are often indicated as quantum degeneracy. Effects due to quantum degeneracy are noticeable in the regime

$$\lambda \, \rangle \, \ell \, \rangle \, \sigma, \tag{1}$$

where σ characterizes the linear dimensions of the atoms, $\ell = n^{-1/3}$ characterizes the mean spacing of the atoms and λ is the thermal de Broglie wavelength

$$\lambda = \left[\frac{2\pi\hbar^2}{mk_BT} \right]^{\frac{1}{2}}, \tag{2}$$

with k_B Boltzmann's constant and m the atomic mass.

Quantum degeneracy is known to play a role in such diverse systems as the electron gas in metals,[2] a gas of excitons in semiconductors,[3] the system of protons and neutrons in atomic nuclei,[4] the fermionic system ^{3}He,[5] neutron stars[6] and superconductors.[7] In the case of atomic nuclei, for instance, the condensation of nucleons within the Fermi sphere is an essential element in understanding the validity of the shell model. In the case of superconductivity Cooper-paired electrons take part in Bose–Einstein condensation.

All of these systems are commonly described by phenomenological theories. Landau,[8] for instance, was able to explain the superfluid behavior of ^{4}He by interpreting the liquid as an ideal gas of phonons and rotons. These theories, although very satisfactory for describing experimental phenomena, are difficult to justify rigorously from a microscopic point of view. For example, microscopic theories by Bogoliubov,[9] and Lee, Huang and Yang,[10] which were meant to serve as an explication of the degeneracy effects in Bose systems such as in superfluid ^{4}He, are only qualitatively applicable due to the marginal validity of the second inequality in Eq. (1): such theories are generally based on expansions in (powers of) $(n\sigma^3)^{\frac{1}{2}}$, of which only the lowest orders are calculated. The density of the helium fluid, for instance, is so high that the expansion parameter has a value not far from 1. The necessary calculation of the complete sum entails all complications of the many-body problem. Although in recent decades much progress has been achieved with respect to the many-body problem, it would be of great importance to dispose experimentally of a system showing quantum degeneracy in a regime for which the inequality $\ell\rangle\sigma$ is less marginally fulfilled.

In 1959 Hecht[11] pointed to some suitable candidates: atomic hydrogen H and its two heavier isotopes ^{2}H (=D=deuterium) and ^{3}H (=T=tritium) in their electron-spin polarized forms H↓, D↓ and T↓, to be created by a strong magnetic field $\vec{B}$ at low temperatures (↓ is the electron-spin projection along $\vec{B}$). The spin polarization is necessary to avoid the strong singlet attraction among a pair of atoms and the associated formation of molecules. Hecht's predictions were based on the quantum theorem of corresponding states, first formulated by de Boer.[12] This theorem applies to any collection of atomic or molecular species with interatomic potentials which can be written as

$$V(r) = \epsilon \, f(r/\sigma) \tag{3}$$

with a common function f of, for instance, Lennard-Jones form, but different choices for the pair of parameters ϵ and σ. The Hamiltonian of these systems can therefore be rewritten in self-evident notation as

2

$$H = \epsilon \left\{ -\frac{\hbar^2}{2m\epsilon\sigma^2} \sum_{i=1}^{N} \Delta_{\vec{r}_i/\sigma} + \sum_{\substack{i<j \\ 1}}^{N} f(r_{ij}/\sigma) \right\} \qquad (4)$$

so that the free energy acquires the form

$$F = N\epsilon \, F^*(T^*, n^*, \eta), \qquad (5)$$

with F^* a universal function only depending on Fermi-Dirac or Bose-Einstein statistics i.e. on the (anti-) symmetry requirement of the admissable states, while $n^*=n\sigma^3$ is the reduced density, $T^*=T/(\epsilon/k_B)$ the reduced temperature and

$$\eta = \frac{\hbar^2}{m\epsilon\sigma^2} \qquad (6)$$

the quantum parameter, a measure for the "quantumness" of a substance due to the finite value of $\hbar$. This makes it possible to express all thermodynamic properties of the collection of gases in a universal way. The exceptional value of η for ^{4}He, due to its weak van der Waals interaction and low atomic mass, explains that it remains liquid at not too high pressure at T=0 and is also thought to be responsible for its superfluidity. By extrapolation the even weaker van der Waals attraction and lighter mass of spin-polarized atomic hydrogen and its isotopes would give rise to even more exceptional properties: the critical temperature for the gas to liquid phase transition for T↓ would be as low as 0.95 K and for H↓ and D↓ even be shifted to negative values: they would remain gaseous at T=0 for not too high pressures. This feature indeed enables a less marginal second inequality (1) and, in principle, independently controllable temperature and density. Later more rigorous calculations by Nosanow and coworkers[13] using variational methods led to more definite predictions on the properties to be expected for the above-mentioned quantum gases.

Experimental work with the purpose of preparing the new quantum gases was stimulated strongly by the idea to cover the wall of the gas cell with a superfluid helium film. One of the advantages of this superfluid helium lining is the low binding energy of atoms to this

3

surface (for H atoms about 1 K in temperature units), so that the density of atoms on the surface remains limited down to very low temperatures and an enhanced surface decay is avoided. Silvera and Walraven[14] at the University of Amsterdam were the first to stabilize a H↓ gas with a density of roughly 10^{14} atoms per cm^3 for several minutes.

After this breakthrough in 1980 attempts to realize the regime of densities and temperatures where the first inequality of Eq. (1) is satisfied, became a subject of widespread interest, both theoretically and experimentally. In 1981 a group at MIT (Cline et al.) obtained almost completely "doubly-polarized" atomic hydrogen gas[15] (H↓⇑) in which also the proton spins are polarized. This increased the stability of the H gas dramatically. A gas of H↓⇑ is much more stable than H↓: the hyperfine interaction admixes a small fraction of the opposite electron-spin projection in the one-atom spin state, when the proton spin is up, which leads to a singlet component in the wavefunction of two scattering H atoms and therefore to a possiblity to recombine on the surface.

The creation of H↓⇑ opened the way to still higher densities by compression.[16,17,18] The maximum density ever reported[18] is roughly a factor of 5×10^4 higher than the densities first stabilized by Silvera and Walraven. However, the corresponding mean spacing $\ell = 115$ a_0 is still larger than the thermal de Broglie wavelength $\lambda = 45$ a_0 at the temperature of 570 mK used in Ref. 18. The value of the density needed to reach the regime where degeneracy effects are playing an important role are roughly a factor of 50 larger.

The work in Refs. 16 and 17 revealed the first evidence for a three-body recombination process in H↓⇑. Hess et al.[18] noted that the latter could also explain a large (factor 35) discrepancy, first pointed out by Ahn et al.,[19] between earlier lower-density measurements and theory: the then undiscovered three-body recombination process was misinterpreted as a two-body surface rate.

The three-body process, referred to in Refs. 16 and 17, is the recombination reaction H+H+H→H$_2$+H, where the electron spins of the doubly-polarized atoms are depolarized by a magnetic-dipole interaction. More in particular, the decay was ascribed to a mechanism for this process, introduced by Kagan et al.[20] for volume recombination. Explained in simple terms, this Kagan dipole mechanism
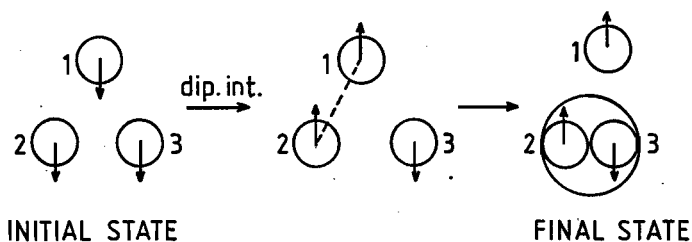
4

runs as follows. Two of the atoms, of which the electron spins precess differently in the magnetic-dipole field of the third one, obtain a singlet component in their wavefunction so that they may form a H_2 molecule.

A more detailed quantummechanical description makes clear that the final state of the third atom may be either an electron-spin up (double spin-flip: the total electron-spin magnetic quantum number changes by $2\hbar$) or down state (single spin-flip). The characteristics of the double-spin-flip are illustrated in a simple way in Fig. 1. The arrows represent the electron-spin projections during the various steps in the process. In the first step two of the colliding atoms interact via the dipole interaction. Each of them then acquires a small fraction of the opposite electron-spin projection in its wavefunction. As will be explained in Sec. II the total spin state of the two atoms remains purely triplet. However, the spin state of one of these atoms together with the third atom contains a singlet component. It therefore becomes possible for such a pair of atoms to recombine into a molecule in the same collision, the third atom also providing for combined energy-momentum conservation.

Comparing Kagan's results with experimental $H\downarrow\uparrow$ volume decay rates it turned out that the predicted rate constant had the correct order of magnitude, although the field dependence turned out to be incorrect. However, large discrepancies between experimental data and calculations by our group (see Chapters 2 and 3) for surface recombination, also based on the Kagan dipole mechanism, indicated

already that it is very unlikely that this mechanism alone can explain the observed decay. Several subsequent calculations of the rate constant for volume recombination, also by our Eindhoven group (see Chapters 4 and 5) made it likely that it is not the Kagan dipole mechanism that is responsible for the decay, but an alternative mechanism, the dipole-exchange mechanism, which is at least of equal importance to explain the measurements.

The theoretical aspects of these recent developments form the subject of this thesis. The theory of two- and three-body collisions underlies most of the work presented. Contrary to the general situation in the subject of atomic and molecular collisions which often allows for a (semi-)classical treatment, a full quantummechanical approach is needed in our case: although the quantum degeneracy regime $\lambda\rangle\ell\rangle\sigma$ has not yet been reached, the condition $\lambda\rangle\sigma$ characterizing a quantum gas has already been fulfilled since the first pioneering experiments in this field: λ increases beyond σ already at a few tens of kelvins.

To fulfil also the remaining part of the condition for Bose-Einstein condensation, most of the effort in the field of spin-polarized hydrogen has gone into the direction of decreasing the mean spacing by increasing the density, in particular by compression. The value of the three-body recombination rate observed for magnetic fields in the 5-10 T range, however, makes it probable that further progress to higher densities is limited by recombination heating. Experimentally, the recombination heating may possibly be removed from the gas by working with very thin samples, only on one side bounded by a helium surface and by a confining magnetic-field gradient in other directions.[21] Interestingly, theoretical analysis shows strong variations in the three-body recombination rate as a function of magnetic field. Possible this may lead to the selection of a B-field "window" where the three-body recombination is sufficiently slow to enable Bose-Einstein condensation. Both the theoretical work in this thesis, further work in our Eindhoven group[22] and recent experimental work at Harvard University[23] are first steps in this direction.

Other recent developments aim at wall-free confinement by static or dynamic field traps making use of evaporative cooling[24] or microwave cooling[25] to temperatures in the μK range or even lower. This might lead to a fulfilment of the degeneracy condition by

6

increasing λ beyond ℓ keeping the density very low thus causing three-body collisions to be of little significance. Although the prospects look promising, this field of cooling in a trap is still largely unexplored. In particular, it is still unknown at present how effective a cooling scheme will be in the final stage where atoms are to condense into the lowest quantum state in the field of the trap.

A very recent publication[26] calls attention for the special possibilities of realizing quantum degeneracy in doubly-polarized atomic deuterium D↑↓, using evaporative cooling in a magnetic trap. Due to Fermi statistics the lowest relative two-body partial wave in a three-body system then has a value of 1. This would imply a strong reduction of the two- and three-body rates and thus the possibility of combining cooling in a trap with compression. This reintroduces the subject of three-body recombination, but now in connection with a magnetic trap.

II INTERACTIONS

The quantum mechanical description of two- and three-body scattering forms the basis for the study of the decay of the density of spin-polarized atomic hydrogen gas. A collision of two (three) H atoms is in principle a process involving four (six) particles. However, previous experience gathered in particular in our group,[27] shows that this problem can be reexpressed with sufficient accuracy in the form of a two- (three-) atom Schrödinger equation, by introducing a number of effective interactions among the H atoms, i.e. the interactions to be dealt with below as points a, b and c. A few additional aspects of the interactions will subsequently be covered by points d,e and f.

a) Zeeman and hyperfine interactions

The effective spin Hamiltonian of a single H atom in the 1s ground state in an external magnetic field $\vec{B}$ is given by

$$H_{at} = 2\mu_e \vec{B}.\vec{S} - 2\mu_p \vec{B}.\vec{I} + a\,\vec{S}.\vec{I},\qquad(7)$$

where a=9.119×10^{-25} J, μ_e=928.48×10^{-26} J/T and μ_p=1.4106×10^{-26} J/T

are the hyperfine constant and the magnetic moments of electron and proton, respectively. Furthermore, $\vec{S}$, $\vec{I}$ are the electron- and proton-spin vectors (from which a factor of $\hbar$ has been extracted). For future convenience it is useful to express H_{at} and its eigenvalues also in temperature units. We then have a=68.169 mK, μ_e=0.67249 K/T and μ_p=1.0217 mK/T. The two Zeeman terms of Eq. (7) are invariant under separate rotations of the electon- and proton-spin vectors $\vec{S}$ and $\vec{I}$ about the direction of $\vec{B}$. The corresponding magnetic quantum numbers m_s and m_i are therefore good quantum numbers with respect to the Zeeman interaction. The Fermi contact hyperfine term of Eq. (7) is invariant under simultaneous rotations of electron and proton spins about an arbitrary axis. For this term alone, the total atomic-spin quantum numbers f and m_f, associated with the vector-operator $\vec{F}=\vec{S}+\vec{I}$, are good quantum numbers.

The (difference of) eigenvalues and eigenvectors of Eq. (7) are presented in Fig. 2 for magnetic fields of B=0 and B=10 T. Here, the electron- and proton-spin projections are denoted by ↑ or ↓, and ⇑ or ⇓, respectively. Furthermore, the mixing parameter $\epsilon \simeq a/[4B(\mu_e+\mu_p)]$ is small relative to 1 for the high magnetic field values to be considered in the following (B=4 T and higher). The large energy difference of about 13.5 K between the a,b states on the one hand and the c,d states on the other at B=10 T results from the electron-spin Zeeman interaction, while the remaining small energy splitting between the a and b levels and between the c and d states is caused by a combined influence of the hyperfine interaction and the Zeeman interaction of the proton.

At equilibrium for low temperatures T≲1.0 K the populations of the c and d states are completely negligible, while the a and b states are about equally populated. The small admixture of the "wrong" electron-spin projection in the a state is well-known[15] to lead to preferential depopulation of this state in a+a and a+b collisions at the wall, due to a singlet component which is already contained in the asymptotic spin states. The remaining gas sample consists of the doubly-polarized b atoms (↓⇓), with a much longer lifetime. For some time the decay of the gas has generally been ascribed to b→a relaxation through the magnetic-dipole interaction operating in *two-body* b+b collisions, taking place in the bulk and in the two-dimensional adsorbed gas. Our group was the first to point to a
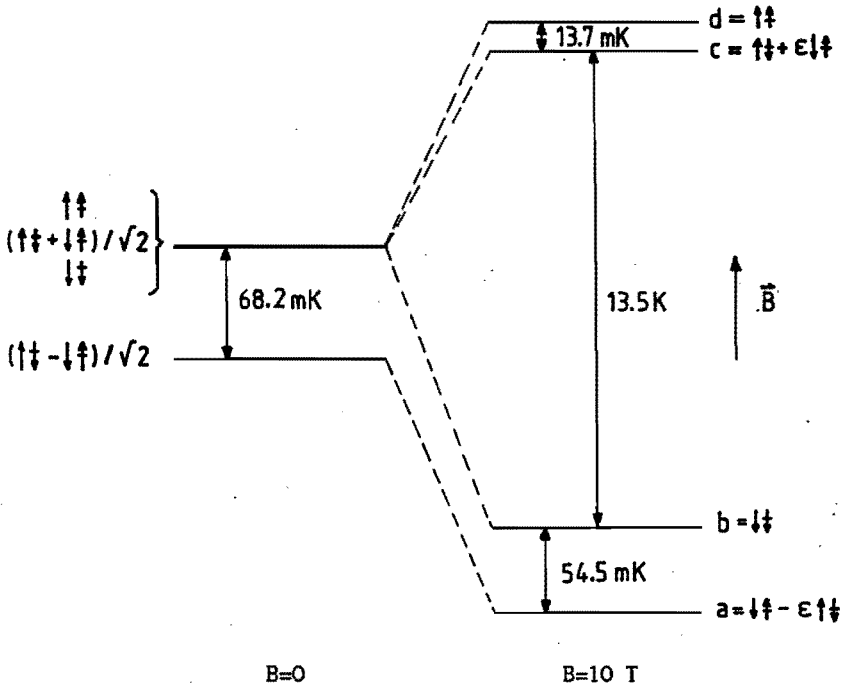
Fig. 2. *Eigenvalues and eigenstates of the effective one-atom*
Hamiltonian (7) for magnetic fields of B=0 and B=10 T.
The electron- and proton-spin projections are denoted by
↑ or ↓, and ⇑ or ⇓, respectively. The mixing parameter
$\epsilon \approx 2.5 \times 10^{-3}$ *for B=10 T.*

previously mentioned factor of 35 discrepancy[19] (see also Refs. 28-31)
between theoretical and experimental decay rates for the surface part
of the relaxation. The more recent experimental and theoretical
developments concentrate on a *three-body* recombination mechanism, in
which also the magnetic-dipole interaction is involved.

In this thesis we consider collisions of b-state atoms, which are
of importance for relaxation and recombination in the doubly-polarized
regime. The effective Hamiltonian of a two-atom system contains, apart
from a sum of expressions of the form (7) for each of the atoms, some
effective interatomic interactions, which will be discussed
subsequently.

9

b) Central interactions

The Coulomb interactions between electrons and protons of two H atoms give rise, through the Born-Oppenheimer approximation, to central interactions among the atoms of the form[27]

$$V^c(\vec{r}) = \mathscr{P}_{s=1} \ V^c_{s=1}(r) + \mathscr{P}_{s=0} \ V^c_{s=0}(r) \equiv$$

$$V_{direct}(r) + V_{exch}(r) \ \vec{S}_1 \cdot \vec{S}_2,$$

(8)

where $\vec{r}$ is the relative coordinate of the protons, while $\mathscr{P}_{s=0} = \frac{1}{4} - \vec{S}_1 \cdot \vec{S}_2$ and $\mathscr{P}_{s=1} = \frac{3}{4} + \vec{S}_1 \cdot \vec{S}_2$ are projection operators on the singlet and triplet subspaces of the total spin space, respectively. Furthermore, $V^c_{s=0}$ and $V^c_{s=1}$ are the singlet and triplet potentials, which are given as a function of r in Fig. 3. The two-atom problem comprises the relative atomic motion and the electron and proton spin degrees of freedom for each of the two atoms, the total center-of-mass
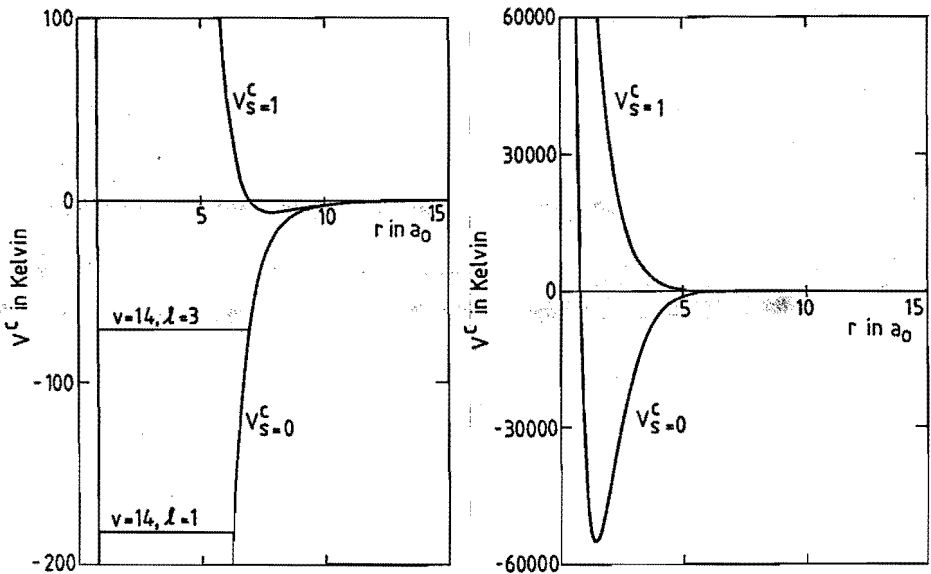
Fig. 3. The singlet and triplet H-H interactions $V^c_{s=0}(r)$ and $V^c_{s=1}(r)$ (in temperature units) as a function of the distance r between the protons. The energies of the bound states with quantum numbers $v=14$, $\ell=3$ and $v=14$, $\ell=1$ of $V^c_{s=0}$ are -72 K and -183 K, respectively.

motion being understood to be split off. Eq. (8) being invariant under separate rotations in relative orbital, 2-electron-spin and 2-proton-spin space, we have $\vec{L}$, $\vec{S}=\vec{S}_1+\vec{S}_2$ and $\vec{I}=\vec{I}_1+\vec{I}_2$ as conserved quantities and the associated quantum numbers ℓ, m_ℓ, s, m_s, i, m_i as good quantum numbers. Note that, contrary to common use, we use lower-case symbols for two-atom spin quantum numbers. Capital spin quantum numbers are reserved for future use in connection with the three-atom system. In actual calculations we use "state-of-the-art" $V^c_{s=1}$ and $V^c_{s=0}$ potentials,[32] including also relativistic, radiative, adiabatic and non-adiabatic corrections.

The singlet and triplet potentials display a completely different behavior at small distances. The singlet potential is strongly attractive and contains a large number of rotational-vibrational bound states. The more weakly bound ortho-states ($i=1$, ℓ=odd) appear to play an important role in three-body dipolar recombination, especially the two states with vibrational quantum number v=14 and rotational quantum numbers ℓ=3 and ℓ=1, which have a binding energy of 72 K and 183 K, respectively. The radial part of the wavefunction $\psi_{v\ell}(r)$ of the v=14,
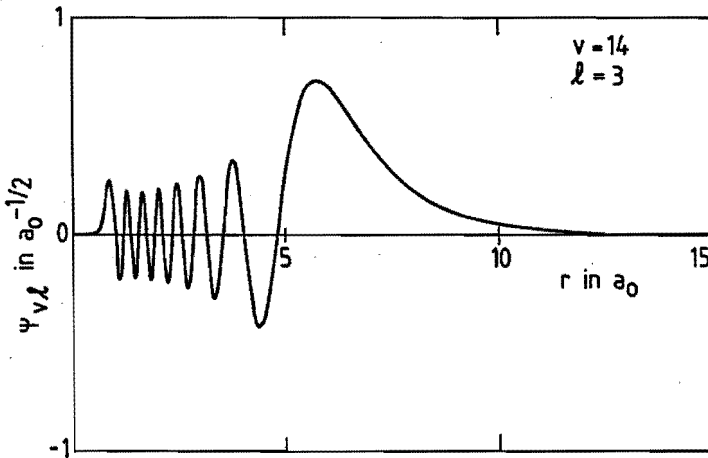
Fig. 4. *The radial part $\psi_{v\ell}(r)$ of the wavefunction of the bound state with quantum numbers v=14, ℓ=3 as a function of r, normalized as $\int |\psi_{v\ell}(r)|^2 dr = 1$. Note the lowe-r decrease due to the strong repulsion and centrifugal barrier, and the large-r tail due to weak binding.*
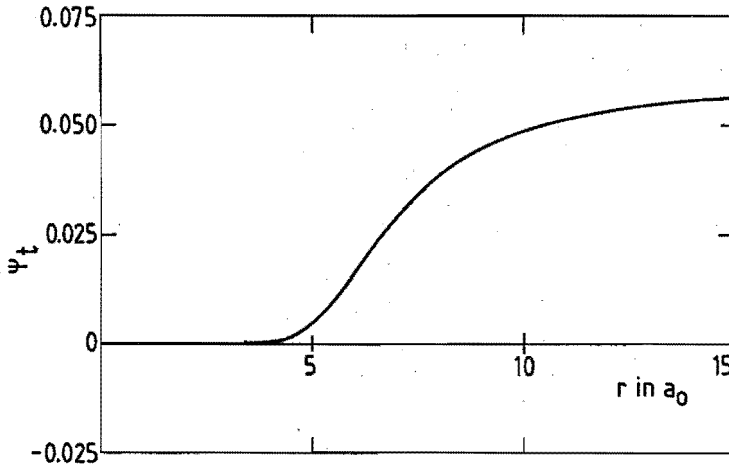
Fig. 5. *The spherically symmetric wavefunction* $\psi_t(r)$ *as a function of r, normalized so as to have the constant value* $(2\pi)^{-3/2}$ *for r→∞, describing triplet scattering at zero temperature.*

$\ell=3$ state is presented in Fig. 4. The triplet potential is strongly repulsive for small distances, due to the Pauli priciple for the electrons, but contains also a weakly attractive van der Waals tail for larger r values, which is too shallow to support bound states. In Fig. 5 the spherically symmetric triplet state $\psi_t(r)$ is given, which describes the scattering of two b atoms at T=0. This wavefunction is going to play a central role in subsequent chapters. There it is normalized so as to have the constant value $(2\pi\hbar)^{-3/2}$ beyond the range of the triplet potential. In the vertical scale of the figure the factor $\hbar^{-3/2}$ is left out.

The central interactions cannot cause transitions between s=1 and s=0, because s and m_s are good quantum numbers. Additional spin-dependent interactions are therefore responsible for the decay of the doubly-polarized gas. An obvious candidate is the electron-electron magnetic-dipole interaction. The much weaker electron-proton and proton-proton counterparts are negligible for our future purposes.

12

c) Electron-electron magnetic-dipole interaction

The spin flips causing the recombination during collisions of three b atoms are now believed to be induced by the magnetic-dipole interaction between the electrons of the atoms. From previous experience[27] it appears that in most circumstances it is sufficiently accurate to write it in the effective form:

$$V^d(\vec{r}) = -\frac{\mu_0}{4\pi}\, 4\mu_e^2 \left[\frac{3(\vec{S}_1\cdot\vec{r})(\vec{S}_2\cdot\vec{r}) - r^2(\vec{S}_1\cdot\vec{S}_2)}{r^5}\right]. \tag{9}$$

Herewith, the electronic magnetic moments are localized at the protons. It is clear thar $V^d(\vec{r})$ is only invariant under simultaneous rotations in orbital and total electron-spin space. The separate orbital and spin angular momenta are therefore not conserved. However, the total angular momentum $\vec{J}=\vec{L}+\vec{S}$ is a constant of the motion. Furthermore, it is useful to point out that $V^d(\vec{r})$ has the following structure in terms of irreducible spherical tensor operators[33] $Y^{(2)}$ and $\sum^{(2)}$ of rank 2:

$$V^d(\vec{r}) = \left\{Y^{(2)}(\hat{r},\hat{r})\cdot\sum\nolimits^{(2)}(\vec{S}_1,\vec{S}_2)\right\}_{00} \equiv \sum_{\mu=-2}^{2}(-1)^\mu\, Y^{(2)}_{-\mu}\,\sum\nolimits^{(2)}_{\mu}, \tag{10}$$

in which $\sum^{(2)}$ is built up from the two spin vector-operators and $Y^{(2)}$ similarly from $\hat{r}=\vec{r}/r$. Note that the components of $Y^{(2)}(\hat{r},\hat{r})$ are proportional to the spherical harmonics $Y_{2\mu}(\hat{r})$. Eq. (10) implies in particular a well-known selection rule for the initial and final s and s' values and for initial and final ℓ and ℓ' values: the "triangular condition", i.e. it must be possible to form a triangle with sides s,s' and 2 and similarly for ℓ,ℓ' and 2. Singlet-singlet and singlet-triplet transitions are thus forbidden. The fact that a parallel electron-spin state can only change into a parallel electron-spin state can also be understood from the symmetry of $V^d(\vec{r})$ under permutations of $\vec{S}_1$ and $\vec{S}_2$. A classical argument might also be instructive. The magnetic-dipole field of atom 1 at the position of atom 2 is equal to that of atom 2 at the position of 1. This results in a parallel precession of the electron spins in these fields. The atoms remain therefore in a triplet state. As first pointed out by

Kagan[20] a two-atom dipole interaction in a system of *three* b atoms does admix a singlet part in a two-atom subsystem (see Sec. I).

d) H-He interaction

At low temperatures (T ⪅ 0.3 K) the major part of the collisions takes place among H atoms adsorbed to the superfluid helium. The presence of the helium surface is responsible for many new and interesting aspects, both theoretical and experimental. Throughout this thesis we leave out the dynamics of the superfluid helium: it is assumed to act on the H atoms in the form of a static surface potential $V_w(z)$, depending on a coordinate perpendicular to the wall. With a few exceptions this is a general approach in this field: it is clear that the inclusion of a static surface forms, even for two H atoms, already a huge complication. The general "philosophy" is to find out to what extent experimental data on phenomena in the adsorbed H gas can be explained within this restricted framework. It cannot be excluded that eventually the inclusion of dynamical surface modes is inevitable.

Although the precise form of $V_w(z)$ is not known,[34] it has been found experimentally that its attractive van der Waals part is sufficiently strong to support a bound state $\phi_0(z)$. Very precise recent measurements based on the cryogenic H maser have provided an accurate value[35] for its binding energy: $\epsilon_0 = 1.01 \pm 0.01$ K. The single-particle motion of the adsorbed particles parallel to the surface is not influenced by V_w. The density of the adsorbed gas of H atoms increases strongly for decreasing temperatures. This, together with the three-atom dipolar recombination process, is the main reason for the rapid decay in compression experiments at low temperatures. In so far as we study surface collision processes in the following (Chapters 2 and 3), we will consider specific choices for $V_w(z)$ and for the associated eigenfunction $\phi_0(z)$.

e) H-H potential at helium surface

From previous calculations of two-body relaxation processes in the adsorbed gas[27] it may be concluded that the scattering of adsorbed b atoms is described fairly well by assuming that the atoms remain bound in the ϕ_0 state during the collision (2½D model[19]). The relative

14

motion parallel to the surface is decoupled from the z motion and can then be determined by solving a 2D Schrödinger equation, in which the 2D triplet interaction $\overline{V}^c_{s=1}(\rho)$ is given by the 3D potential $V^c_{s=1}(r)$ averaged over the motion of the atoms in the ϕ_0 state:

$$\overline{V}^c_{s=1}(\rho) = \int dz_1 \int dz_2 \ |\phi_0(z_1)|^2 \ |\phi_0(z_2)|^2 \ V^c_{s=1}(r).$$ (11)

Here, $r = [\rho^2 + (z_1-z_2)^2]^{\frac{1}{2}}$, $\vec{\rho}$ being the relative coordinate vector along the (plane) surface.

In Fig. 6 the 2D and 3D triplet potentials are given. As expected, the averaging process leads to a somewhat shallower well and a weaker repulsive part. We used the H-He potential calculated by Mantz and Edwards[34] to determine $\phi_0(z)$ and $\overline{V}^c_{s=1}(\rho)$. As an illustration Fig. 7 shows the lowest partial wave (m=0) of a low-energy (E=0.1K) 2D scattering state $\psi_{t\vec{k}}(\vec{\rho})$, of which $\exp(i\vec{k}.\vec{\rho})/(2\pi\hbar)$ is the undistorted part. The factor $1/\hbar$ is left out in the vertical scale in Fig. 7. On the basis of the effective-range theory, presented in Chapters 6-8, it may be deduced that $\psi_{t\vec{k}}(\vec{\rho})$ goes to zero logarithmically for a fixed
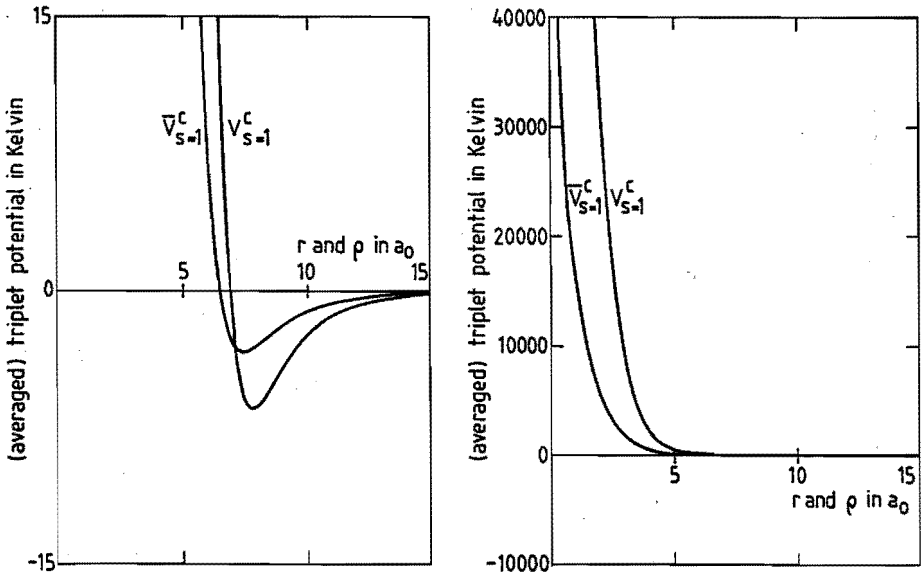
Fig. 6.   *The 3D and 2D triplet potentials $V^c_{s=1}(r)$ and $\overline{V}^c_{s=1}(\rho)$ (in temperature units) as a function of the 3D and 2D distances r and ρ, respectively.*
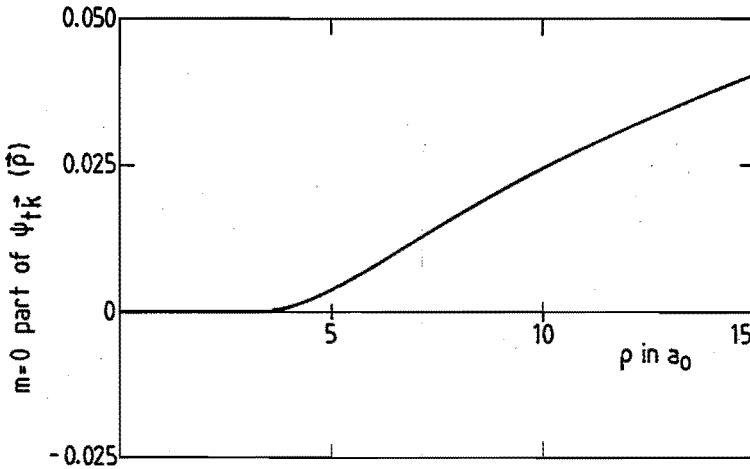
Fig. 7. The m=0 part of the wavefunction $\psi_{t\vec{k}}(\vec{\rho})$ as a function of ρ for 2D triplet scattering with energy E=0.1 K. The undistorted part is given by $\exp(i\vec{k}.\vec{\rho})/(2\pi)$. Comparing with Fig. 4, note the typical 2D behavior: a slower log ρ convergence for large ρ.

but arbitrary distance ρ when the collision energy E goes to zero.[36] This is a typical feature of 2D scattering. A 3D wavefunction goes to a finite limit for E→0 (see Fig. 5). This typical 2D behavior plays an essential role in the calculations of Chapters 2 and 3.

f) H-H-H central potential

Up to here it was assumed implicitly that the interaction of three scattering H atoms is given by a sum of pair interactions. However, this is not completely justified from the Born-Oppenheimer point of view. A genuine three-body term is bound to play a role in parts of three-atom configuration space where one atom is at close distance from both other atoms. In such a case, in particular, not only two-electron but also three-electron exchange plays a significant role.

We do not believe, however, that the above type of configurations come in to a significant extent. In the first place the three colliding atoms have parallel spin directions before the recombination

16

and repel each other at distances smaller than about 6 a_0. After the recombination process the molecule is in a weakly bound singlet state with widely separated atoms. Furthermore, the electron-spin configuration of the third H atom with each of the bound atoms is predominantly symmetric (75% s=1 and 25% s=0) (see also Fig. 7 of Chapter 5). The third atom is therefore repelled effectively by the molecule. We neglect corrections from a three-body potential term in the remainder of this thesis.

III SOME ASPECTS OF TWO- AND THREE-BODY SCATTERING

In this section we summarize some of the fundamentals of non-relativistic two- and three-particle scattering, used in Chapters 2-8. It is not our intention to present a complete and mathematically rigorous treatment of the theory. We try to follow a more intuitive approach and illustrate some of the equations in terms of Feynman-like diagrams. The background theory is discussed by Messiah,[37] Taylor,[38] Newton[39] and Glöckle.[40]

We first consider the scattering of two distinguishable particles, described by a stationary state $|\psi^{(\pm)}\rangle$ which is a solution of the Schrödinger equation

$$(H_0 + V - E)|\psi^{(\pm)}\rangle = 0, \qquad (12)$$

with outgoing-wave (+) or incoming-wave (-) asymptotic boundary conditions. The state $|\psi^{(+)}\rangle$ corresponds closely to the intuitive picture of a scattering process: at infinity it consists of an unperturbed plane wave plus a radially outgoing, in general anisotropic, wave. The state $|\psi^{(-)}\rangle$, on the contrary, has an unphysical plane wave plus ingoing radial wave behavior at infinity. Although unphysical, we shall see that such states play an important role in some of the expressions of this thesis in the form of final states in first-order collision amplitudes. In Eq. (12), H_0 is the sum of the (relative) kinetic energy operator and possible single-particle energy operators (e.g. of the type of Eq. (7) for H atoms), V the interaction between the particles and E the total energy. Eq. (12) is

a second-order differential equation in coordinate space, which can be
solved by numerical integration (potential scattering or coupled
channels[41]) and adjusting the solution to the proper asymptotic
boundary conditions for scattering.

For scattering by a rotationally symmetric potential $V(r)$ it is
useful to introduce the concept of the scattering phase shift. To show
the physical importance of this quantity we consider the special case
of 3D scattering and expand the wavefunction $\psi_{\vec{k}}^{(\pm)}(\vec{r})$ in spherical
harmonics with respect to the directions of the coordinate vector
$\vec{r}$ and the incident wavevector $\vec{k}$

$$\psi_{\vec{k}}^{(\pm)}(\vec{r}) = \sum_{\ell m_\ell} \frac{u_\ell^{(\pm)}(r)}{r} \; Y_{\ell m_\ell}^*(\hat{k}) \; Y_{\ell m_\ell}(\hat{r}). \tag{13}$$

The Schrödinger equation then reduces to a set of uncoupled radial
diffential equations for the functions $u_\ell^{(\pm)}(r)$.

If the potential is negligible beyond a certain range, these
functions can for large r be expressed as a combination of the regular
and irregular solutions $F_\ell(k,r)=\sqrt{\frac{\pi r}{2}} \; J_{\ell+\frac{1}{2}}(kr)$ and $G_\ell(k,r)=\sqrt{\frac{\pi r}{2}} \; N_{\ell+\frac{1}{2}}(kr)$
of the radial equations with $V\equiv0$

$$\begin{aligned}
u_\ell^{(\pm)}(r) &= a_\ell^{(\pm)} \Big[\cos\delta_\ell(k) \; F_\ell(k,r) - \sin\delta_\ell(k) \; G_\ell(k,r)\Big] \\
&\underset{r\to\infty}{\sim} k^{-\frac{1}{2}} a_\ell^{(\pm)} \sin[kr-\tfrac{1}{2}\ell\pi+\delta_\ell(k)]
\end{aligned} \tag{14}$$

Here, the coefficients $a_\ell^{(\pm)}$ are given by $\frac{4\pi}{\sqrt{k}}i^\ell(2\pi\hbar)^{-3/2}\exp(\pm i\delta_\ell(k))$,
when the undistorted plane-wave part of the full wavefunction
$\psi_{\vec{k}}^{(\pm)}(\vec{r})$ is normalized as $\exp(i\vec{k}.\vec{r})/(2\pi\hbar)^{3/2}$. We conclude from Eq. (14)
that the effect of the scattering potential is to shift the phase of
each partial wave ℓ by an amount $\delta_\ell(k)$. These phase shifts play an
important role in two-body scattering theory and will also be
considered in Chapters 6-8, where Eq. (14) is generalized to arbitrary
dimension $n\geq2$.

We will not go into this further, but rewrite Eq. (12) in order
to introduce the two-body t operator. By regarding the V term of Eq.
(12) artificially as an inhomogeneous term, it can be seen that $|\psi^{(\pm)}\rangle$
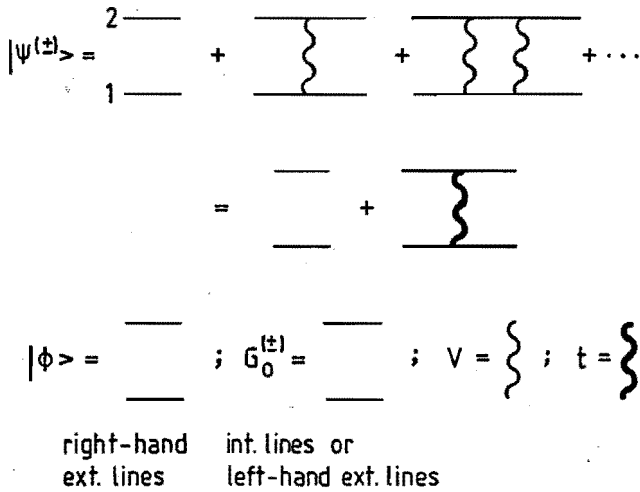
Fig. 8. *Graphical representation of full two-particle scattering*
state $|\psi^{(\pm)}\rangle$, *see Eq.* (16).

also obeys the Lippmann-Schwinger equation[37]

$$|\psi^{(\pm)}\rangle = |\phi\rangle + G_0^{(\pm)}(E) \, V \, |\psi^{(\pm)}\rangle, \tag{15}$$

where $|\phi\rangle$ is the undistorted wavefunction (i.e. a solution of Eq. (12) with $V \equiv 0$) and $G_0^{(\pm)}(E) = (E \pm i0 - H_0)^{-1}$ the free resolvent operator. Iterating Eq. (15) shows that the full scattering state can be obtained by summing a multiple-scattering series (Ref. 37 Chapter XIX):

$$|\psi^{(\pm)}\rangle = |\phi\rangle + G_0^{(\pm)}(E) \, V \, |\phi\rangle + G_0^{(\pm)}(E) \, V \, G_0^{(\pm)}(E) \, V \, |\phi\rangle + \ldots \ldots \tag{16}$$

$$\equiv |\phi\rangle + G_0^{(\pm)}(E) \, t(E) \, |\phi\rangle.$$

See Fig. 8 for a presentation in the form of Feynman-like diagrams.

The two-particle t operator is defined as a scattering operator which takes into account the complete "V-ladder" in the series of Eq. (16):
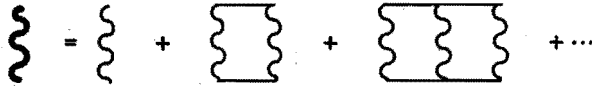
19

$$t(E) = V + V \; G_0^{(\pm)}(E) \; V + V \; G_0^{(\pm)}(E) \; V \; G_0^{(\pm)}(E) \; V + \ldots \ldots \qquad (17)$$

(see also Fig. 9). We note here that the series, presented in Eqs. (16) and (17) and in the following do not necessarily converge for an arbitrary potential V. We consider them as formal series in the same spirit as the well-known expansions in the coupling constant of "ladder" series of e.g. electron-electron scattering in quantum electrodynamics. In our case we do not calculate $|\psi^{(\pm)}\rangle$ or $t(E)$ by summing the series in Eqs. (16) and (17). Instead, we calculate for instance $t(E)$ by solving directly the Lippmann-Schwinger equation for the t operator:

$$t(E) = V + V \; G_0^{(\pm)}(E) \; t(E). \qquad (18)$$

A more rigorous introduction of the operator $t(E)$ can be based[40] directly on the defining equation (18) without resorting to series expansions. In momentum space Eq. (18) is an integral equation. It can be solved by matrix inversion after a numerical discretization and bringing the $V \; G_0^{(\pm)}(E) \; t(E)$ term to the left.

The t operator has in general non-vanishing matrix elements of the type $\langle \vec{k}' | t(E) | \vec{k} \rangle$ between states of arbitrary energy. It turns out, however, that the t matrix elements which determine the *asymptotic* form of the wavefunction for two-particle scattering, are those for which both initial and final states have energy E (the energy is conserved asymptotically). These on-shell t matrix elements are of special interest, because the most interesting physical observables for a two-body collision depend only on the asymptotic form of the

wavefunction. We also point out that the complete knowledge of the wavefunction in all space can be obtained from the half-shell t matrix elements only (i.e. in which the energy of the final state is variable). This follows directly from Eq. (16): the momentum representation of $|\psi^{(\pm)}\rangle$ is obtained by taking the inner product of the third member with an *arbitrary* plane-wave state, which is an eigenstate of $G_0^{(\pm)}(E)$. We finally note that for scattering of identical particles, we obtain the symmetrized scattering state by symmetrizing the driving term of Eq. (15).

We end the discussion of the two-body problem with some comments concerning the low-energy scattering of two b atoms in a doubly-polarized atomic hydrogen gas. The temperatures at which the experiments with atomic hydrogen are carried out are so low, that the typical size of wave packets representing the relative motion of colliding atoms is much larger than the interaction range $(\lambda\rangle\rangle\sigma)$, i.e. the gas is in the quantum regime (see Sec. I). Consequently, the relative wavenumbers k are so small that $k\sigma\langle\langle 1$. This implies that only the lowest partial wave of the undistorted plane wave enters the interaction region and is distorted. The corresponding phase shift and the related on-shell t matrix elements of this lowest partial wave for the scattering of two b atoms through the triplet potential can be expanded around their values for k=0. The behavior of the scattering is then determined by one (or a few) effective-range parameters.[42]

In Chapters 6-8 such an effective-range theory is introduced for low-energy scattering in arbitrary dimension $n\geq 2$. The primary purpose here is to find an effective-range theory for the case of a 2D gas, as an extension of the well-known[42] 3D formalism. We shall see that such an extension is not trivial. The 2D case is exceptional because it is the only integer dimension where the "centrifugal" potential for the lowest partial wave is attractive. This gives rise to a logarithmic k-dependence of the low-energy phase shift.

We now turn to three-body scattering. In this case there are two types of asymptotic scattering channels: two- and three-body fragmentation channels, in which one or no pairs are bound, respectively. For dipole recombination we need both channels. However, for convenience we consider in this introduction only the three-body fragmentation channel, the discussion of the other channel being

$$|\psi_0^{(\pm)}\rangle =$$
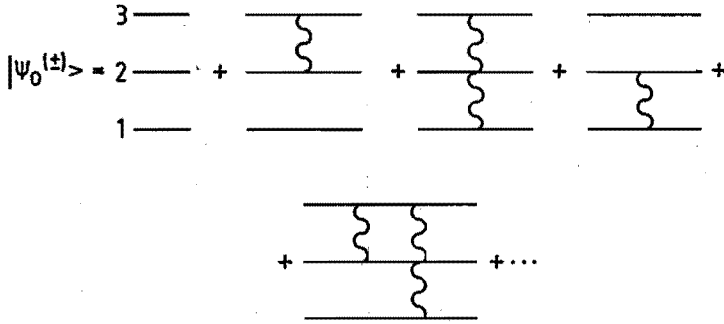
Fig. 10. Graphical representation of full three-particle scattering state $|\psi_0^{(\pm)}\rangle$ in terms of sequential operations of two-particle potentials V_i on the free three-particle state $|\phi_0\rangle$, see Eq. (19).

similar. We refer to Glöckle's monograph[40] for a treatment of this two-body fragmentation channel.

Analogous to the two-body problem, a full scattering eigenstate $|\psi_0^{(\pm)}\rangle$ of three distinguishable particles can be written as a multiple-scattering series (see Fig. 10)

$$|\psi_0^{(\pm)}\rangle = |\phi_0\rangle + G_0^{(\pm)}V_1|\phi_0\rangle + G_0^{(\pm)}V_2|\phi_0\rangle + G_0^{(\pm)}V_3|\phi_0\rangle + G_0^{(\pm)}V_1 G_0^{(\pm)}V_2|\phi_0\rangle + \ldots, \quad (19)$$

where we left out for simplicity the three-body energy argument E of the resolvent operators. The state $|\phi_0\rangle$ describes three free particles, i.e. a plane-wave state. The subscripts 0 of the states $|\phi_0\rangle$ and $|\psi_0^{(\pm)}\rangle$ here indicate the three-body fragmentation channel (compare with the index 1 used below for the other channel). The operators occurring in Eq. (19) and in the following, operate in the Hilbert space of three particles and are analogous to the two-body operators, introduced above. In Eq. (19) a pair interaction among pair i is denoted by V_i (we use the spectator-index notation,[40] i.e. i=1 for instance stands for particles 2 and 3).

We subsequently sum partial ladders of V_i operators to t_i operators with the help of Eq. (17) (Fig. 9) and obtain
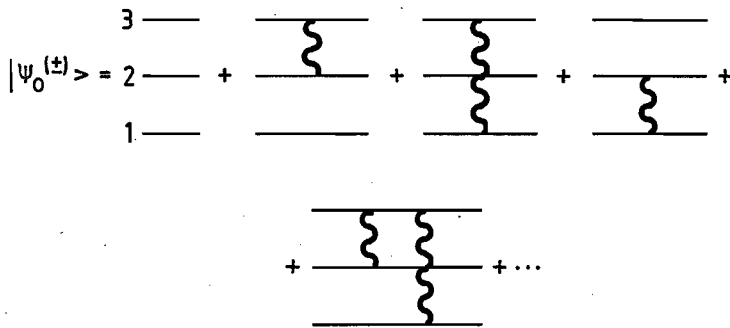
Fig. 11 *Graphical representation of full three-particle scattering*
state $|\psi_0^{(\pm)}\rangle$ in terms of sequential operations of
two-particle scattering operators t_i on the free
three-particle state $|\phi_0\rangle$, see Eq. (20).
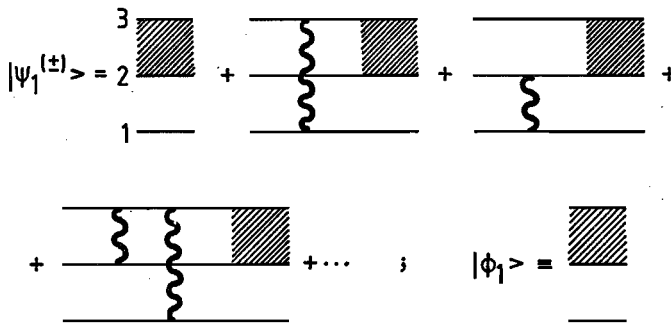
Fig. 12. *Graphical representation of the three-particle scattering*
state $|\psi_1^{(\pm)}\rangle$ in terms of sequential operations of
two-particle scattering operators t_i on the state $|\phi_1\rangle$ for
which pair 1 is bound (shaded pair) and particle 1 free,
see Eq. (21).

$$|\psi_0^{(\pm)}\rangle = |\phi_0\rangle + G_0^{(\pm)} t_1 |\phi_0\rangle + G_0^{(\pm)} t_2 |\phi_0\rangle + G_0^{(\pm)} t_3 |\phi_0\rangle + G_0^{(\pm)} t_1 G_0^{(\pm)} t_2 |\phi_0\rangle + \ldots . (20)$$

(see Fig. 11). In order to make a comparison with the situation for a
two-body fragmentation channel, we also present the corresponding
equation and figure (see Fig. 12) for such a channel:

$$|\psi_1^{(\pm)}\rangle = |\phi_1\rangle + c_0^{(\pm)}t_2|\phi_1\rangle + c_0^{(\pm)}t_3|\phi_1\rangle + c_0^{(\pm)}t_1c_0^{(\pm)}t_2|\phi_1\rangle + \ldots \qquad (21)$$

in which the index 1 indicates that pair 1 is bound. Note that $|\psi_0^{(\pm)}\rangle$ and $|\psi_1^{(\pm)}\rangle$ (and similarly $|\psi_2^{(\pm)}\rangle$ and $|\psi_3^{(\pm)}\rangle$) are exact eigenstates of the total three-body Hamiltonian and thus include all three-body correlations.

In Eqs. (20) and (21) two subsequent t operators never operate on the same pair i. In addition, in Eq. (21) t_1 never operates directly on $|\phi_1\rangle$. Eqs. (20) and (21) illustrate that a scattering event of three particles can be interpreted as a series of subsequent pair collisions. If we insert the completeness relation in terms of H_0 eigenstates between two subsequent t operators in Eqs. (20) and (21), we can associate a relative momentum state with each set of three internal lines in Figs. 10-12, add to such a set a $c_0^{(\pm)}$ "propagator" depending on the relative momenta and integrate over the latter, as in the case of regular Feynman diagrams. Note that energies of intermediate states, i.e. their H_0 eigenvalues, are in general different from E. This is sometimes interpreted as a violation of energy conservation in intermediate states, which is then ascribed to the finite lifetime of such states. Thus the t_i operators now induce transitions among plane-wave states with arbitrary two-body and three-body energy. In other words, the full off-shell t_i matrices are needed now.

Eqs. (20) and (21) do not usually provide a practical scheme for calculating a three-particle scattering state. We now turn to a set of equations upon which such a practical scheme can be based: the Faddeev equations. To obtain them for the three-body fragmentation channel, we separate the series of Eq. (20) (Fig. 11) into four parts:

$$|\psi_0^{(\pm)}\rangle = |\phi_0\rangle + \sum_{i=1}^{3} |\chi_i^F\rangle. \qquad (22)$$

The Faddeev components $|\chi_i^F\rangle$ are defined as the collection of terms in Eq. (20) (Fig. 11), in which a t_i operator is the "last" (i.e. left-hand) operator of a given diagram. E.g. the Faddeev component $|\chi_1^F\rangle$ is given by
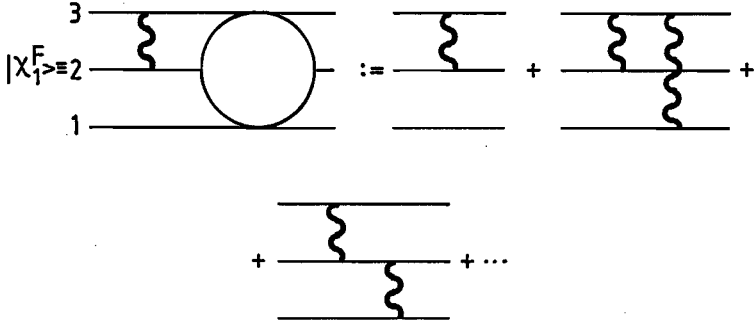
Fig. 13. Faddeev component $|x_1^F\rangle$ in terms of two-particle t_i operators, see Eq. (23).
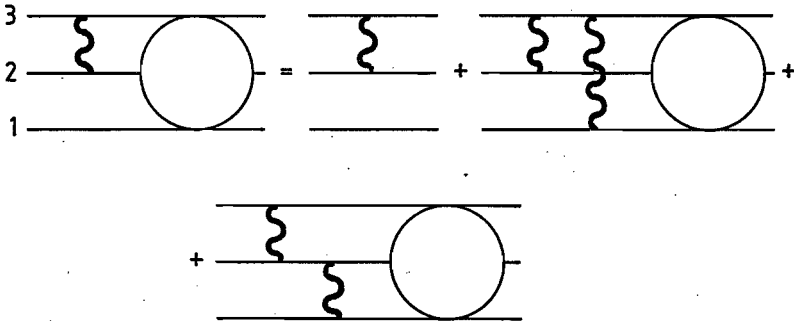
Fig. 14. One of the three coupled Faddeev equations, see Eq. (24).

$$|x_1^F\rangle = G_0^{(\pm)}t_1|\phi_0\rangle + G_0^{(\pm)}t_1G_0^{(\pm)}t_2|\phi_0\rangle + G_0^{(\pm)}t_1G_0^{(\pm)}t_3|\phi_0\rangle + \ldots . \qquad (23)$$

which is presented in Fig. 13. Eq. (23) can be rearranged as indicated in Eq. (24) (see Fig. 14). A similar procedure for the other components leads to Eqs. (25) and (26):

$$|x_1^F\rangle = G_0^{(\pm)}t_1|\phi_0\rangle + G_0^{(\pm)}t_1|x_2^F\rangle + G_0^{(\pm)}t_1|x_3^F\rangle \qquad (24)$$

$$|x_2^F\rangle = G_0^{(\pm)}t_2|\phi_0\rangle + G_0^{(\pm)}t_2|x_1^F\rangle + G_0^{(\pm)}t_2|x_3^F\rangle \qquad (25)$$

$$|x_3^F\rangle = G_0^{(\pm)}t_3|\phi_0\rangle + G_0^{(\pm)}t_3|x_1^F\rangle + G_0^{(\pm)}t_3|\psi_2^F\rangle . \qquad (26)$$

25

The coupled equations (24), (25) and (26) are the Faddeev equations.

For scattering of identical particles we have to symmetrize $|\psi_0^{(\pm)}\rangle$. To that end we replace the free state $|\phi_0\rangle$ in the above equations by a properly symmetrized state $S|\phi_0\rangle$, where S is the symmetrization operator (sum over six permutations without normalization constant). Furthermore, because of the fact that the particles are indistinguishable, the state vectors $|\chi_1^F\rangle$ can be expressed into each other by a simple permutation of particles, i.e. $|\chi_2^F\rangle$ and $|\chi_3^F\rangle$ can be written as $P_{12}P_{23}|\chi_1^F\rangle$ and $P_{13}P_{23}|\chi_1^F\rangle$, respectively. The operator P_{ij} exchanges particles i and j. The set of coupled Faddeev equations then effectively reduces to one equation, which reads, leaving out the spectator index:

$$|\chi^F\rangle = G_0^{(\pm)}(E)\ t(E)\ S\ |\phi_0\rangle + G_0^{(\pm)}(E)\ t(E)\ P\ |\chi^F\rangle, \qquad (27)$$

in which $P=P_{12}P_{23}+P_{13}P_{23}$. Eq. (27) is our final equation and is rewritten in Chapters 4 and 5 together with Eq. (22) for purposes of numerical solution.

It is clear that the evaluation of a three-body scattering wavefunction from Eq. (27) is much more complicated than the calculation of a two-atom state. It would therefore be very useful if an effective-range theory for three-particle scattering could be formulated in analogy to that for two-particle scattering. This has not been possible as yet. The difficulty encountered, if one would like to derive a three-body effective-range theory from a two-body one, is the occurrence of the full off-shell t matrix elements in the Faddeev equations, i.e. in intermediate states both the two-particle energy and the left-hand and right-hand momenta are not nessecarily small, even if the total energy E is low.

IV THIS THESIS

The contents of this thesis can be divided in three parts. The first part deals with three-body dipole recombination in the 2D H↓↑ gas (Chapters 2 and 3). The second part treats the analogous bulk phenomenon (Chapters 4 and 5). The formulation of a two-body

low-energy scattering theory in arbitrary dimension n$\geq$2 is considered in the third part (Chapters 6–8).

Each of the following chapters has been published (Chapter 2: Ref. 43, Chapter 4: Ref. 44, Chapter 6: Ref. 45, Chapter 7: Ref. 46 and Chapter 8: Ref. 47) or has been submitted for publication (Chapters 3 and 5). Within each of the three parts of this thesis the chapters are ordered according to their order of publication in the literature. As a possible drawback of this way of organization we point to the special role of the first half of Chapter 3. It contains the general theory of recombination in a quantum gas and as such has an introductory character: it may serve as a derivation of the expressions for rate constants in terms of three–body collision quantities on which all chapters dealing with three–body recombination are based. We now turn to a summary of the three parts.

Part A: Surface dipole recombination (Chapters 2 and 3)

In Chapters 2 and 3 we calculate the rate constant for H+H+H surface recombination on the basis of the Kagan dipole mechanism. In Chapter 2 we discuss the principal results of this calculation. The ideas behind the approach as well as the motivations for and implications of the approximations are more extensively studied in Chapter 3.

For volume recombination it had earlier been found,[20] that the Kagan mechanism is not able to explain the slowly decreasing magnetic–field dependence of the experimentally observed rate constant between B=5 T and B=10 T. In Chapters 2 and 3 we show that this conclusion also holds for surface dipole recombination. Furthermore, although the volume rate constants have the correct order of magnitude, it turns out that the surface rate constants are roughly an order of magnitude smaller than the observed values.

This suggests that an additional mechanism might play a role, which dominates over the Kagan dipole mechanism in the surface case, while it should lead to comparable contributions to the total rate constant for volume recombination, which change the rapid increase of the rate with B according to Kagan into a slowly decreasing one.

Part B: Volume dipole recombination (Chapters 4 and 5)

In Chapter 4 we introduce the dipole–exchange mechanism. In order
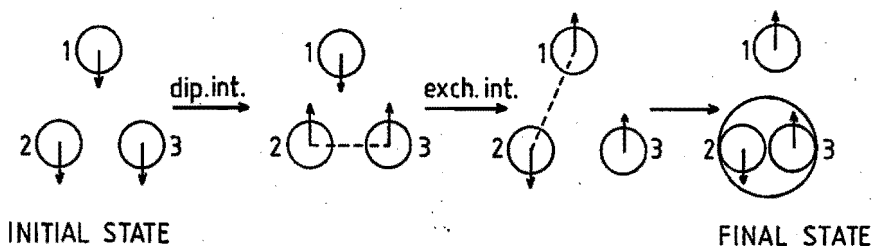
Fig. 15. Electron-spin projections of atoms during subsequent steps in
the dipole-exchange mechanism (double-spin-flip process).

to get an idea about the importance of this mechanism and about the
magnetic-field dependence of its contribution to the total rate
constant, we estimate this contribution for the easier case of volume
recombination.

The essential idea of the dipole-exchange mechanism can be
summarized as follows. In the Kagan picture the pair of atoms
interacting via the dipole interaction cannot form a molecular state.
If, however, one of the atoms of this pair exchanges its spin state
with the third atom, the dipole-interacting pair does acquire a
singlet component and therefore may recombine (see Fig. 15). The
exchange of electron spin states can take place through the exchange
part V_{exch} of the central interatomic interaction (8). This is
relatively strong so that a two-step process of this type does not
necessarily have a much lower probability than Kagan's single-step
process.

Simple calculations based on this new mechanism are presented in
Chapter 4 and lead to volume rate constants, which show the correct
tendency as a function of magnetic field. The absolute magnitude of
the rate, however, is difficult to estimate with a simple approach.

Therefore, we turn to a more exact determination of the volume
rate constant. This is started in the second half of Chapter 4 and
continued in Chapter 5. Ideally, one would like to carry out a
calculation which is rigorous, except for the treatment of the
electronic magnetic-dipole interaction as a first-order perturbation,
which is undoubtedly an excellent approximation. This would imply the
evaluation of a matrix element of the dipole interaction between an

28

initial state of the type $|\psi_0^{(+)}\rangle$ and a final state of the type $|\psi_1^{(-)}\rangle$, in both of which the central (singlet/triplet) interaction is included exactly. Within the framework of this thesis an important part of this task has been realized: the initial b+b+b collision wavefunction has been calculated rigorously by means of the identical-particle Faddeev equation (27). The final atom + molecule collision wavefunction, which is replaced by a free atom + molecule state by Kagan, is still treated approximately: the interaction of the final atom with the atoms of the molecule is taken into account in such a way that the molecule can undergo all changes of internal state except for break-up. This implies that only the V_{direct} term in Eq. (8) contributes. The contribution of the V_{exch} part vanishes automatically, so that an exchange of electron-spin states as in Fig. 15, i.e. the dipole-exchange mechanism, is not included.

The final results of this calculation are still in disagreement with experiment for fields B≤10 T. Since the calculation is complete except for the dipole-exchange mechanism, we are able to conclude finally that indeed the dipole-exchange mechanism is responsible for the remaining discrepancies.

This might be an appropriate place to mention for completeness that at the moment of completion of this thesis, our Eindhoven group is extending calculations to stronger fields B>10 T.

Part C: Low-energy scattering (Chapters 6, 7 and 8)

We then turn to the formulation of a low-energy parametrization of the two-particle phase shifts (and wavefunctions) in two and three dimensions, which is of major importance for the description of the decay kinetics of atomic hydrogen. In particular, this subject is relevant for part A where it is used to split off the temperature dependence of the 2D scattering wavefunction of three polarized atoms.

Verhaar at al.[36] already demonstrated the usefulness of an effective-range theory for scattering in a plane in analogy with the well-known concept for three dimensions. However, this approach was limited in the first instance to potentials which vanish exactly beyond a finite range. This restriction is relaxed in Chapter 6. In addition we show that the 2D formalism is not an ad-hoc variation on the 3D scheme: both the 2D and 3D versions are special cases of an

elegant general effective-range theory in dimension n≥2. Also, a Coulomb-type interaction γ/r may be included, γ being the strength parameter of the Coulomb interaction. The basis for the approach is formed by the interpretation of the parameters in the expansion for $\cot\delta(k)$ as "equivalent hard-sphere radii", with values such as to lead to the same energy dependence in the respective orders as for the actual potential. Thus, the value of an arbitrary effective-range parameter reduces to R for scattering by a hard spere of radius R. We prove that the parameters behave smoothly as a function of γ and n, in contrast to those of an alternative approach introduced by Bollé et al.[48]

Chapters 7 and 8 contain a further foundation of the formalism, for neutral-particle scattering ($\gamma=0$) and collisions of charged particles ($\gamma\neq0$), respectively. In these chapters we present conditions for the asymptotic behavior of the potential, which are sufficient for the formalism to be applicable. We find a smooth dependence of the scattering length a and effective range r_e on n and γ. This is compared with the (dimensional and continuity) problems of the scattering length defined by Bollé et al. for n→2 and γ→±0 (n=2). As an example we consider a square-well potential for $\gamma=0$ in Chapter 7. In Chapter 8 we further discuss the problem of how to take into account the effect of charges on the value of the neutral scattering length.

REFERENCES

[1] F. London, *Superfluids*, Vol. II (Wiley, New York, 1954).

[2] D. Pines, *The Many-Body Problem*, (Benjamin, New York, 1961).

[3] D. Snoke, J.P. Wolfe and A. Mysyrowics, Phys. Rev. Lett. $\underline{59}$, 827 (1987).

[4] L.C. Gomes, J.D. Walecka and V.F. Weisskopf, Ann. Phys. $\underline{3}$, 241 (1958).

[5] W.F. Brinkman and M.C. Cross, *Progr. in Low Temp. Phys.*, edited by D.F. Brewer (North-Holland, Amsterdam, 1978) Vol. VIIA p. 105.

[6] D. Pines and M.A. Alpar, Nature $\underline{316}$, 27 (1985).

[7] F. London, *Superfluids*, Vol. I (Dover, New York, 1961).

[8] L.D. Landau, J. Phys. (USSR) $\underline{5}$, 71 (1941); $\underline{11}$, 91 (1947).

[9] N.N. Bogoliubov, J. Phys. (USSR) $\underline{11}$, 23 (1947).

[10] T.D. Lee, K. Huang and C.N. Yang, Phys. Rev. $\underline{106}$, 1135 (1957).

[11] C.E. Hecht, Physica $\underline{25}$, 1159 (1959).

[12] J. de Boer, Physica $\underline{14}$, 139 (1948).

[13] L.H. Nosanov, L.J. Parish and F.J. Pinski, Phys. Rev. B $\underline{11}$, 191 (1975).

[14] I.F. Silvera and J.T.M. Walraven, Phys. Rev. Lett. $\underline{44}$, 164 (1980).

[15] B.W. Statt and A.J. Berlinsky, Phys. Rev. Lett. $\underline{45}$, 2105 (1980); R.W. Cline, T.J. Greytak and D. Kleppner, Phys. Rev. Lett. $\underline{47}$, 1195 (1981).

[16] R. Sprik, J.T.M. Walraven and I.F. Silvera, Phys. Rev. Lett. $\underline{51}$, 479 (1983); Erratum $\underline{51}$, 942 (1983); Phys. Rev. B $\underline{32}$, 5668 (1985).

[17] H.F. Hess, D.A. Bell, G.P. Kochanski, R.W. Cline, D. Kleppner and T.J. Greytak, Phys. Rev. Lett. $\underline{51}$, 483 (1983).

[18] H.F. Hess, D.A. Bell, G.P.Kochanski, D. Kleppner and T.J. Greytak, Phys. Rev. Lett. $\underline{52}$, 1520 (1984); D.A. Bell, H.F. Hess, G.P. Kochanski, S. Buchman, L. Pollack, Y.M. Xiao, D. Kleppner and T.J. Greytak, Phys. Rev. B $\underline{34}$, 7670 (1986).

[19] R.M.C. Ahn, J.P.H.W. van den Eijnde, C.J. Reuver, B.J. Verhaar and I.F. Silvera, Phys. Rev. B $\underline{26}$, 452 (1982).

[20] Yu. Kagan, I.A. Vartan'yants and G.V. Shlyapnikov, Zh. Eksp. Teor. Fiz. $\underline{81}$, 1113 (1981) [Sov. Phys. JETP $\underline{54}$, 590 (1981)].

[21] Yu. Kagan, G.V. Shlyapnikov and N.A. Glukhov, Pis'ma Zh. Eksp. Teor. Fiz. $\underline{41}$, 197 (1985) [JETP Lett. $\underline{41}$, 238 (1985)].

[22] H.T.C. Stoof, Ph. D. thesis, Eindhoven University of Technology, The Netherlands, (to appear).

[23] J.D. Gillaspy, I.F. Silvera and J.S. Brooks, Jpn. J. Appl. Phys. 26, 229 (1987) Suppl. 26-3 (Proc. 18th Int. Conf. on Low Temperature Physics, Kyoto, 1987).

[24] H.F. Hess, Bull. Am. phys. Soc. 30, 854 (1985); Phys. Rev. B 34, 3476 (1986); H.F Hess, G.P. Kochanski, J.M. Doyle, T.J. Greytak and D. Kleppner, Phys. Rev. B 34, 1602 (1986); R.V.E. Lovelace, C. Mehanian, T.J. Tommila and D.M. Lee, Nature 318, 30 (1985).

[25] I.F. Silvera, Jpn. J. Appl. Phys. 26, 245 (1987) Suppl. 26-3 (Proc. 18th Int. Conf. on Low Temperature Physics, Kyoto, 1987); and to be published.

[26] J.M.V.A. Koelman, H.T.C. Stoof, B.J. Verhaar and J.T.M. Walraven, Phys. Rev. Lett. 59, 676 (1987); Jpn. J. Appl. Phys. 26, 249 (1987) Suppl. 26-3 (Proc. 18th Int. Conf. on Low Temperature Physics, Kyoto, 1987).

[27] J.P.H.W. van den Eijnde, Ph. D. thesis, Eindhoven University of Technology, The Netherlands, 1984.

[28] J.P.H.W. van den Eijnde, C.J. Reuver and B.J. Verhaar, Phys. Rev. B 28, 6309 (1983).

[29] A. Lagendijk, Phys. Rev. B 25, 2054 (1982).

[30] A.E. Ruckenstein and E.D. Siggia, Phys. Rev. B. 25, 6031 (1982).

[31] B.W. Statt, Phys. Rev. B 25, 6035 (1982).

[32] B.J. Verhaar, J.M.V.A. Koelman, H.T.C. Stoof, O.J. Luiten and S.B. Crampton, Phys. Rev. A 35, 3825 (1987).

[33] D.M. Brink and G.M. Satchler, *Angular Momentum* (Oxford University Press, Oxford, 1962).

[34] I.B. Mantz and D.O. Edwards, Phys. Rev. B 20, 4518 (1979).

[35] W.N. Hardy, M.D. Hurlimann and R.W. Cline, to be published in Jpn. J. Appl. Phys. (Proc. 18th Int. Conf. on Low Temperature Physics, Kyoto, 1987).

[36] B.J. Verhaar, J.P.H.W. van den Eijnde, M.A.J. Voermans and M.M.J. Schaffrath, J. Phys. A 17, 595 (1984).

[37] A. Messiah, *Qauntum Mechanics*, Vol. II (North-Holland, Amsterdam, 1961).

[38] J.R. Taylor, *Scattering Theory* (Wiley, New York, 1972).

[39] R.G. Newton, *Scattering Theory of Waves and Particles* (McGraw-Hill, New York, 1966).

32

[40] W. Glöckle, *The Quantum Mechanical Few-Body Problem* (Springer-Verlag, Berlin, 1983).

[41] N. Austern, *Direct Nuclear Reaction Theories* (Wiley, New York, 1970).

[42] G.F. Chew and M.L. Goldberger, Phys. Rev. 75, 1637 (1949); H.A. Bethe, Phys. Rev. 76, 38 (1949).

[43] L.P.H. de Goey, J.P.J. Driessen, B.J. Verhaar and J.T.M. Walraven, Phys. Rev. Lett. 53, 1919 (1984).

[44] L.P.H. de Goey, T.H.M. v.d. Berg, N. Mulders, H.T.C. Stoof, B.J. Verhaar and W. Glöckle, Phys. Rev. B 34, 6183 (1986).

[45] B.J. Verhaar, L.P.H. de Goey, E.J.D. Vredenbregt and J.P.H.W. van den Eijnde, Phys. Lett. A 110, 371 (1985).

[46] B.J. Verhaar, L.P.H. de Goey, J.P.H.W. van den Eijnde and E.J.D. Vredenbregt, Phys. Rev. A 32, 1424 (1985).

[47] B.J. Verhaar, L.P.H. de Goey and E.J.D. Vredenbregt, Phys. Rev. A 32, 1430 (1985).

[48] D. Bollé and F. Gesztesy, Phys. Rev. Lett. 52, 1469 (1984); Phys. Rev. A 30, 1279 (1984).

Surface Three-Body Recombination in Spin-Polarized Atomic Hydrogen

L. P. H. de Goey, J. P. J. Driessen, and B. J. Verhaar
Department of Physics, Eindhoven University of Technology,
5600-MB Eindhoven, The Netherlands

J. T. M. Walraven
Natuurkundig Laboratorium der Universiteit van Amsterdam,
1018-XE Amsterdam, The Netherlands
(Received 12 July 1984)

We calculate the surface dipolar recombination rate L_s for spin-polarized hydrogen adsorbed on ^{4}He surfaces at temperatures in the 0.2- to 0.6-K regime and for magnetic fields up to 30 T. For a magnetic field of 7.6 T normal to the surface and 0.4 K we find $L_s = 1.3(3) \times 10^{-25}$ cm^4 s^{-1} increasing by 10%/T in the range of experimental interest. The anisotropy with the direction of the magnetic field is considerably smaller than in the case of the surface dipolar relaxation.

The recent observation[1] of three-body phenomena in high-density spin-polarized hydrogen (H↓) has focused considerable attention on a very interesting class of thresholdless recombination processes, first described by Kagan, Vartanyants, and Shlyapnikov.[2] Detailed understanding of these processes is of vital importance for H↓ research as they appear to limit the highest densities that may be achieved experimentally. In a recent publication Hess and co-workers[3] pointed out that effects previously attributed to an anomalously large surface two-body nuclear relaxation rate[4] could be accounted for by a surface analog of the Kagan process. In their analysis the surface rate was estimated by a scaling argument taken from Ref. 2.

We took up this interesting suggestion and present here the first detailed calculation of the three-body surface recombination rate L_s. We analyze the nature of the Kagan dipole mechanism and discuss the differences between recombination on a ^{4}He surface and in the bulk. We find that the scaling argument, which results from a model in which the relative motion of the H atoms on the surface is assumed to be identical to that in the volume, is not supported by detailed theory. It leads to an overestimate of the surface rate by an order of magnitude. We calculate $L_s = 1.3(3) \times 10^{-25}$ cm^4 s^{-1} for a magnetic field $B = 7.6$ T normal to the surface and temperature $T = 0.4$ K, to be compared[2] with an experimental value $L_s = 2.0(6) \times 10^{-24}$ cm^4 s^{-1} obtained[3] at the same field. In the range of experimental interest our results show an increase of the rate of recombination with growing field although this trend is weaker than theory predicts for the bulk process. Experiments show a decreasing behavior for growing fields.[3,5,6] The anisotropy of the Kagan mechanism is found to be

less than that of the two-body surface dipolar relaxation.[7] This feature is in common with a very recent experimental analysis of the surface rates by Bell et al.[8] but seems to contradict earlier low-temperature results obtained by Sprik et al.[6] using ^{3}He surfaces. We point out that in particular the large difference in absolute value indicates that the existing discrepancy[4] between theory and experimentally observed decay rates remains unresolved. We also calculated the bulk dipolar recombination process and find a rate which at 10 T is in agreement with results obtained by Kagan, Vartanyants, and Shlyapnikov,[2] although our field dependence is slightly weaker. Our value is $L_g = 8.5 \times 10^{-39}$ cm^6 s^{-1} ($B = 10$ T and $T \to 0$).

At low temperatures ($T \lesssim 1$ K) the available number of recombination channels for a system of H atoms is vastly reduced. Resonance recombination, dominant at room temperature, may be excluded entirely as the energies of the resonances are too elevated to permit thermal population.[9] The first description of a low-temperature recombination mechanism for H was given by Greben, Thomas, and Berlinsky.[9] This exchange-recombination process requires a collision between a pair of H atoms with singlet character in their initial state. A third body is required to conserve energy and momentum in the process. Besides H other atoms or surfaces may be effective as third body. One of the most fascinating features of the H↓ system is that the above mechanism implies (in combination with slow magnetic relaxation in high fields) preferential recombination and depletion of the "mixed" a state (a, b, c, and d are the hyperfine states in order of increasing energy). This process results in a gas of atoms in the "pure" b state, double-polarized hydrogen (H↓↑) in which both

    1919

electron and proton spins are polarized.

The Kagan process is the only recombination mechanism presented in the literature which may limit the stability of $H\downarrow\uparrow$. This process involves a combined relaxation-recombination mechanism which is thresholdless and in which the dipolar interaction between the electronic spins of the b-state atoms causes the spin flip required for recombination. We distinguish between single- and double-spin-flip processes and will show that the double-spin-flip process is dominant at low fields, whereas it may be suppressed entirely by application of a field $B \gtrsim 24$ T.

If we divide the triple of atoms in a bbb incoming state into a recombining pair (atoms 1 and 2) and a third body (atom 3), we note that one may neglect the electronic dipolar interaction between the atoms 1 and 2 as this interaction cannot cause triplet-singlet transitions. In principle the electronic-nuclear dipolar interaction may do so, but this process is believed to be much weaker. As a result only the difference in magnetic field experienced by the recombining atoms due to the third atom is effective in the recombination process. This causes the remarkable feature that even in the presence of an abundance of third bodies provided by the He surface a third H atom is required. In principle the interaction with a magnetic surface impurity may be present and may cause a similar process with a second-order character.

We write the transition amplitude f for recombination of atoms 1 and 2 as

$$f = \frac{\frac{2}{3}m_H}{2\pi\hbar^2} \langle \psi_f | V_{13}^d + V_{23}^d | \sum_P P\psi_i \rangle . \quad (1)$$

Here, m_H is the mass of the hydrogen atom, V_{ij}^d represents the dipolar interaction between atoms i and j, while the initial state $\sum_P P\psi_i$ is a symmetrized three-atom bbb state, P being a permutation operator. Following Kagan we approximate the initial state by only taking into account the spatial correlations between the atoms of the recombining pair and between the atoms interacting via the dipolar interaction. For instance, for the 13 term the initial state is written as

$$\psi_i = \phi_0(z_1)\phi_0(z_2)\phi_0(z_3)\psi_{\vec{k}_{12}}^t(\vec{p}_{12})\psi_{\vec{k}_{13}}^d(\vec{p}_{13})|bbb\rangle . \quad (2)$$

For each of the atoms we use a bound-state wave function[4] $\phi_0(z) \sim z\exp(-\alpha z)$. For $\alpha = 0.2a_0^{-1}$, ϕ_0 resembles the bound-state wave function in a Stwalley-type potential reproducing the experimen-

tal adsorption energy,[4] while for $\alpha \approx 0.15a_0^{-1}$ it resembles the Mantz and Edwards wave function.[10] The error bar for our L_s value corresponds with these values for α. In Eq. (2) $\psi_{\vec{k}}^t$ describes the relative motion of a pair of H atoms along the surface distorted by the triplet interaction averaged over the z motion ("$2\frac{1}{2}$-dimensional" model[4]) and normalized with plane-wave part $\exp(i\vec{k}\cdot\vec{p})$. Here $\vec{k}$ and $\vec{p}$ are two-dimensional momentum and position vectors. The final state ψ_f is assumed to be identical to that used by Kagan in the volume case, but expressed in cylindrical coordinates: the product of a final spin state $\sigma_f = +\frac{1}{2}$ or $-\frac{1}{2}$ of atom 3, a plane wave with three-dimensional momentum $\hbar\vec{q}_f(B,v,j,\sigma_f)$ for the motion of this atom relative to atoms 12, and a 12 molecular singlet state with vibrational and rotational quantum numbers vjm. In view of the rather high $H+H_2$ relative kinetic energy we neglect completely the influence of the helium surface on the final state, which at the same time reduces the expressions to a form manageable numerically. With this approximation we neglect a reduction of the available final-state phase space and a possible energy transfer to the center-of-mass motion or to the helium. These effects are estimated to be small.

We note that only ortho ($j =$ odd) final states are allowed, as the proton spins are unaffected by the process. Furthermore, we note that in the matrix element of Eq. (1) the spatial intergration is over relative coordinates. The essential difference from the volume case is the lack of translational invariance in the z direction, which causes the result to depend on the center-of-mass coordinate Z in this direction. The recombination rate is obtained by summing $|f|^2$ over final states, integrating over Z, and thermal averaging over initial momenta along the surface:

$$L_s = \sum_{vjm\sigma_f} \left\langle \frac{\pi q_f}{4m_H}\int dZ \int d\hat{q}_f \left| f_{vjm\sigma_f}(\vec{q}_f,Z)\right|^2 \right\rangle_{thermal}. \quad (3)$$

Notice that in two dimensions a $T \rightarrow 0$ approximation cannot be made. Instead we use a low-energy logarithmic k_{12},k_{13} dependence of f following from two-dimensional effective-range theory,[11] using the value $2.3a_0$ for the scattering length. It is appropriate to point out here that the same logarithmic character of f probably contributes to the failure of the above-mentioned scaling argument.

To evaluate L_s we reexpress the spin wave functions using the surface normal as the new quantization axis. If we represent the transfer of angular

1920

momentum from the spin system to the orbital system along this axis by $\mu\hbar$, we find an expression for L_s as an incoherent sum over μ:

$$L_s(\vec{B}) = \sum_{\sigma_f} \sum_{\mu=-2}^{2} L_s^{|\mu|\sigma_f}(B)[d^2_{\sigma_f+3/2,\mu}(\theta)]^2 = \sum_{\sigma_f} \sum_{n=0,2,4} A_{n\sigma_f}(B)P_n(\cos\theta) , \qquad (4)$$

where the d functions are reduced Wigner functions and θ is the angle between $\vec{B}$ and the surface normal. We note that the double–spin–flip contribution tends to dominate over the single–spin–flip one because of the relation

$$L_s^{|\mu|,+1/2}(B) = 4L_s^{|\mu|,-1/2}(2B).$$

For the dominant states $v = 14$, $j = 3$ and $j = 1$ (all other molecular states contribute at a negligible level), and various $|\mu|$ and $|m|$ combinations, we calculated the behavior of $|f|^2$ as a function of Z and of the projection $q_{f\parallel}$ of $\vec{q}_f$ along the surface. For $q_{f\parallel} \to q_f$ all $|f|^2$ surfaces show a strong decrease. Physically this is due to the absence of high relative momenta along the surface in the initial state. Essentially this is the same feature which gives rise to the strong B dependence of volume recombination. Because this argument applies in the surface case only for two coordinate directions instead of three, the B dependence of L_s is weaker
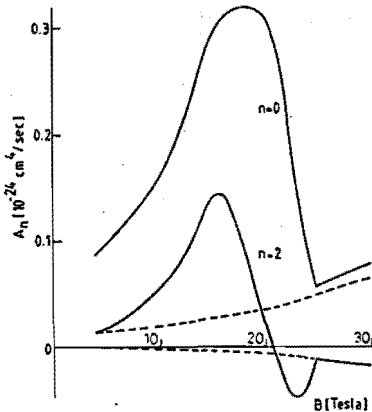
FIG. 1. Coefficients $A_n = \sum A_{n\sigma}$ of Legendre polynomials describing the surface recombination rate L_s for $a = 0.2a_0^{-1}$ at $T = 0.4$ K as a function of magnitude and direction of magnetic field (solid curves). The coefficient A_4 is omitted (magnitude $< 0.014 \times 10^{-24}$ cm^4 s^{-1}). The broken curves represent single–spin–flip contributions.

than that of L_g. In Fig. 1 we show the functions $A_{n\sigma}(B)$ for $T = 0.4$ K. The coefficients $A_{0\sigma}$ represent the recombination rate averaged over the direction of $\vec{B}$. The coefficients $A_{2\sigma}$ and $A_{4\sigma}$ express the anisotropy as a function of the field direction. The A_4 coefficients are negligibly small, whereas the A_2 are small for the single–spin–flip contribution ($\sigma_f = -\frac{1}{2}$) and at most half the A_0 value for the double–spin–flip process ($\sigma_f = +\frac{1}{2}$).

Although the absence of a strong anisotropy is in common with experimental indications,[8] both the B dependence and the absolute magnitude of L_s seem to be at variance with the experimental data, although it would be desirable to extend the measurements to the double–spin–flip cutoff at 24 T. The extreme sharpness of the bends at this cutoff is due to the above-mentioned low-energy approximation and is similar to the behavior in the volume $T \to 0$ limit. We find a rate which is growing by 70% from $B = 4$ to 9 T, whereas the experiments show a decrease by about the same amount. For $\theta = 0$ we calculate $L_s = 1.3(3) \times 10^{-25}$ cm^4 s^{-1} at $B = 7.6$ T. Experimentally a larger value will be observed because of the large probability for the c atom, originating from the double spin-flip process, to recombine in a subsequent collision.[8] This implies that the experimental value given by Hess and co-workers[3] has to be scaled down by approximately a factor 2×0.87, where 0.87 is the double spin-flip fraction. This leads to $L_s = 1.1(4) \times 10^{-24}$ cm^4 s^{-1}. An angular average reduces our theoretical L_s value by 25%. The calculated values show an increase by roughly a factor of 2 in the temperature range $0.2 - 0.6$ K.

We stress that to evaluate the surface dipolar recombination process rather substantial approximations had to be imposed. Hence, our present results do not provide the same level of accuracy as the results for surface dipolar relaxation. However, we are convinced that refinements of the theory are unlikely to resolve the large discrepancy with experiment.

1921

37

[1]R. Sprik, J. T. M. Walraven, and I. F. Silvera, Phys. Rev. Lett. 51, 479 (1983); H. F. Hess, D. A. Bell, G. P. Kochanski, R. W. Cline, D. Kleppner, and T. J. Greytak, Phys. Rev. Lett. 51, 483 (1983).

[2]Yu. Kagan, I. A. Vartan'yants, and G. V. Shlyapnikov, Zh. Eksp. Teor. Fiz. 81, 1113 (1981) [Sov. Phys. JETP 54, 590 (1981)]; Yu. Kagan, G. V. Shlyapnikov, I. A. Vartan'yants, and N. A. Glukhov, Pis'ma Zh. Eksp. Teor. Fiz. 35, 386 (1982) [Sov. Phys. JETP Lett. 35, 477 (1982)]. Note that Kagan *et al.* calculate the rate of direct three-body events, which is twice as small as the rate of loss of atoms in these events, for which we quote our results. Like Kagan *et al.* we do not consider the enhanced recombination probability of the third body discussed in Ref. 3. We thank T. J. Greytak for drawing our attention to these points and for sharing with us his private communication on this subject with Kagan.

[3]H. F. Hess, D. A. Bell, G. P. Kochanski, D. Kleppner, and T. J. Greytak, Phys. Rev. Lett. 52, 1520 (1984); D. A. Bell, G. P. Kochanski, L. Pollack, H. F. Hess, D. Kleppner, and T. J. Greytak, in *Proceedings of the Seventeenth International Conference on Low Temperature Physics,* edited by U. Eckern, A. Schmid, W. Weber, and H. Wühl (North-Holland, Amsterdam, 1984).

[4]J. P. H. W. van den Eijnde, C. J. Reuver, and B. J. Verhaar, Phys. Rev. B 28, 6309 (1983).

[5]R. W. Cline, T. J. Greytak, and D. Kleppner, Phys. Rev. Lett. 47, 1195 (1981); B. Yurke, J. S. Denker, B. R. Johnson, N. Bigelow, L. P. Lévy, D. M. Lee, and J. H. Freed, Phys. Rev. Lett. 50, 1137 (1983).

[6]R. Sprik, J. T. M. Walraven, G. H. van Yperen, and I. F. Silvera, Phys. Rev. Lett. 49, 153 (1982).

[7]A. Lagendijk, Phys. Rev. B 25, 2054 (1982); see also references in Ref. 4.

[8]D. A. Bell, G. P. Kochanski, D. Kleppner, and T. J. Greytak, in *Proceedings of the Seventeenth International Conference on Low Temperature Physics,* edited by U. Eckern, A. Schmid, W. Weber, and H. Wühl (North-Holland, Amsterdam, 1984).

[9]J. M. Greben, A. W. Thomas, and A. J. Berlinsky, Can. J. Phys. 59, 945 (1981).

[10]I. B. Mantz and D. O. Edwards, Phys. Rev. B 20, 4518 (1979).

[11]B. J. Verhaar, J. P. H. W. van den Eijnde, M. A. J. Voermans, and M. M. J. Schaffrath, J. Phys. A 17, 595 (1984).

38

CHAPTER 3

SURFACE THREE-BODY RECOMBINATION IN SPIN-POLARIZED ATOMIC HYDROGEN

L. Philip H. de Goey, Henk T.C. Stoof, J.M. Vianney A. Koelman and
Boudewijn J. Verhaar
Department of Physics, Eindhoven University of Technology,
5600 MB Eindhoven, The Netherlands

Jook T.M. Walraven
Natuurkundig Laboratorium der Universiteit van Amsterdam,
1018XE Amsterdam, The Netherlands

ABSTRACT

We study the theory of exchange and dipole recombination in $H\downarrow$,
starting from a) three-body scattering theory, b) a quantum Boltzmann
equation. On the basis of this we determine the rate of surface dipole
recombination for doubly-polarized hydrogen atoms adsorbed on a ^{4}He
film. The calculation is based on the Kagan mechanism adapted to a 2½D
initial state. We find a rate constant $L_s^{eff} = 2.7(7) \times 10^{-25}$ $cm^4 sec^{-1}$ at
B=7.6 T and T=0.4 K, which is roughly a factor of 6 smaller than the
experimental results. The magnetic-field dependence also disagrees
with experiment. A scaling approach, although leading to the correct
order of magnitude, is discussed and shown to be unsatisfactory. The
reliability of some of our approximations is estimated. We conclude
that the dipole-exchange mechanism is probably responsible for the
discrepancies with experiment.

I. INTRODUCTION

Since the pioneering work of London[1] in the early sixties, the
phenomena of superconductivity in metals and superfluidity in liquid
^{4}He are believed to be manifestations of quantum mechanics on a
macroscopic scale. Since then superfluidity has been observed in
liquid ^{3}He and in the lower part of the energy spectrum of atomic
nuclei. It is also believed to play a role in neutron stars. The
prospect of observing quantum phenomena on a macroscopic scale in
electron-spin polarized atomic hydrogen H↓ has strongly stimulated the
investigation of such a gas at low temperatures (T=80 mK-1 K) in
liquid-helium-covered sample cells.[2,3] Compared with the
above-mentioned systems, an attractive feature of H↓ is the
possibility to observe Bose-Einstein condensation in a wide range of
controllable circumstances of temperature and density. This feature is
related to the fact that H↓ is expected to remain in gaseous form even
for T→0, which should in addition facilitate a "first-principles"
interpretation of the observed phenomena. Up to now the decay of the
gas into H_2 molecules has been the major obstacle to reach the
density-temperature regime of interest.

Polarizing the electon spins in a strong magnetic field (B≃10 T)
strongly reduces the decay and densities in the range $n_H = 10^{16} - 10^{17} cm^{-3}$
were achieved. The next step towards Bose-Einstein condensation was
the creation of a doubly polarized H↓↑ gas, where both the electron
and proton spins are polarized. The double polarization is achieved by
the spontaneous selective recombination[4] of the hyperfine a-state
population as a result of the small admixture of the anti-parallel
electron-spin state (The 1s hyperfine levels of atomic H are as
usually labeled a,b,c,d in order of increasing energy).

The first experiments based on this mechanism still showed a slow
decay, which was interpreted for low temperatures in terms of b→a
surface relaxation, studied theoretically in Refs. 5-9, followed by
rapid recombination. In Ref. 8 it was first pointed out that this
interpretation led to a discrepancy of order 50 between experimental
and theoretical values for the b→a surface relaxation constant G_s.
Many attempts were made to resolve this discrepancy, in particular via
a three-dimensional calculation of the collision of adsorbed atoms[9]

and a possible role of surface dimers.[9,10]

Further experimental progress took place by compression[2,3] of H↓↕
to densities up to 4.5×10^{18} cm^{-3}. This is to be compared with the
critical density for the transition to the Bose-Einstein condensed
phase, predicted at $n_c = (m_H k_B T_c / 3.31\hbar^2)^{3/2} \simeq 1.6 \times 10^{19}$ cm^{-3} for an ideal
gas at $T_c = 100$ mK. The main obstacle to achieving higher densities
now turned out to be a process of magnetic-dipole induced
recombination in a three-body collision of b atoms, first described by
Kagan, Vartan'yants, and Shlyapnikov.[11] Hess et al.[12] first noticed
that this same process taking place at the surface could have been
responsible for the apparent discrepancy at lower densities. A
reanalysis of previous experiments and a new experiment by Reynolds et
al.[13] confirmed this and showed G_s to agree with theory taking into
account the roughness of the cell walls.

With respect to the three-body rate constant L the situation is
less satisfactory. For the bulk constant the magnitude is roughly in
agreement with Kagan's calculation for B=7.8 T. The field dependence,
however, shows a disagreement. At the temperatures relevant for
achieving Bose-Einstein condensation, the Kagan process takes place
primarily at the surface. The present paper deals with the theory of
this surface process. The main results were published earlier as a
short report[14] (further referred to as I).

The decay of H↓↕ through the three-body channel is described by
an additional n_H^3 term in the rate equation

$$\frac{dn_H}{dt} = -G^{eff} n_H^2 - L^{eff} n_H^3. \tag{1}$$

Like the two-body relaxation constant, L^{eff} is the sum of bulk and
surface contributions

$$L^{eff} = L_g^{eff} + L_s^{eff} \left\{ \frac{A}{V} \lambda^3(T) \exp(3\epsilon_0/kT) \right\}. \tag{2}$$

Here, A/V is the surface to volume ratio, λ the thermal de Broglie
wavelength and ϵ_0 the adsorption energy. It should be noted that the
effective rate constants include a subsequent recombination of the
final H atom in case its electron spin is flipped:

$$L_{g,s}^{eff} = L_{g,s}^{-\frac{1}{2}} + 2L_{g,s}^{+\frac{1}{2}}, \tag{3}$$

the superscripts $\pm\frac{1}{2}$ standing for the spin projection of this atom along $\vec{B}$. The constants $L_{g,s}^{-\frac{1}{2}}$ and $L_{g,s}^{+\frac{1}{2}}$ denote the pure single- and double-spin-flip contributions to the effective rate constants. In this paper we shall sometimes consider the rate constants

$$L_{g,s} = L_{g,s}^{-\frac{1}{2}} + L_{g,s}^{+\frac{1}{2}}, \tag{4}$$

representing the pure b+b+b → H_2+H recombination decay. For comparison with experiment, however, we present results of the separate contributions $L_s^{\pm\frac{1}{2}}$, as well as the total effective surface rate constant. A weight factor close to 2 for the double-spin-flip contribution has been considered in several experimental papers. Results to be presented here allow the derivation of L_s^{eff} for weight factors close to 2.

   In this paper we reexamine the results of I with respect to the surface rate constant L_s^{eff}. Throughout this paper we approximate the helium film as an inert surface, the effect of which on an H atom is represented by a potential well $V(z)$. In Sec. II we study the theory of recombination starting from three-body scattering theory. In view of the subtleties with respect to identical-particle aspects which have played a role in similar earlier two-body treatments,[5-9] it is useful to supplement this approach by a formalism in which the many-body and the identical-particle aspects are taken into account from the beginning. This is done in Sec. III on the basis of a quantum Boltzmann equation. In Sec. IV we specialize the previous general theory to dipole recombination. In Sec. V we review our method to calculate $L_s^{\pm\frac{1}{2}}$. In Sec. VI we describe our results. It turns out that they show some difference with I, primarily by the use of an H-H singlet potential, describing more accurately the H-H binding energy data. A major discrepancy still exists with experimental data, both with respect to absolute magnitude and field dependence. Furthermore, we add to I a set of intermediate results which lend themselves to physical interpretation. In Sec. VII we confront our method with the scaling procedure, described by Kagan et al.[15] We show that the scaling method is unsatisfactory, although the results do agree

roughly with experiment (as to magnitude, not to field dependence) and although it enables one to obtain an L_s^{eff} value without cumbersome calculations. One of our model assumptions in Secs. V and VI is the complete neglect of the influence of the helium surface on the final H_2+H state. In I we already pointed out briefly that some of the effects which arise when this assumption is relaxed, are estimated to be small. In Sec. VIII we describe how the estimate is carried out and present its results. Some conclusions of the present paper are given in Sec. IX.

II. THREE-BODY COLLISION THEORY

    In this and in the following sections we present a treatment of three-body recombination which applies to recombination in a 3D as well as in a 2D gas. Our starting point in the present section is the recombination probability per second for a system of three H atoms, after which we make the step to calculating the rate dN_H/dt due to formation of H_2 molecules in a gas of H atoms.

    The system of three H atoms, in the first instance to be treated as distinguishable particles, is in a normalized state $|\psi(t)\rangle$, evolving under the influence of the interatomic interactions from some "free" wave packet

$$|\psi^0(t)\rangle = \sum_\alpha \int d\vec{p}\, d\vec{q}\, f(\vec{p}\vec{q}\alpha)\, |\vec{p}\vec{q}\alpha\rangle\, e^{-iE_{\vec{p}\vec{q}\alpha}t/\hbar}. \qquad (5)$$

Here, $\vec{p}\vec{q}$ is a combination of 3D or 2D Jacobi relative momentum vectors,[16] depending on whether the initial state consists of bulk or adsorbed particles. The label α represents additional spin information, needed to specify the "free" eigenstates. In the 2D case it also specifies the bound state $\phi_0(z)$ of each H atom in the potential well at the wall. For the sake of definiteness we choose $\vec{p}$ to be the momentum of atom 1 relative to atom 2, while $\vec{q}$ is the momentum of atom 3 relative to the center of mass of atoms 1 and 2. The states $|\vec{p}\vec{q}\alpha\rangle$ are eigenstates with eigenvalue $E_{\vec{p}\vec{q}\alpha}$ of

$$H_0 = H - V \tag{6}$$

i.e. the Hamiltonian with interatomic interactions omitted (in the 2D case it still includes the interaction with the inert wall), and are normalized according to

$$\langle \vec{p}'\vec{q}'\alpha' | \vec{p}\vec{q}\alpha \rangle = \delta(\vec{p}'-\vec{p}) \; \delta(\vec{q}'-\vec{q}) \; \delta_{\alpha'\alpha}. \tag{7}$$

The wave packet $|\psi^0(t)\rangle$ is taken to have spatial dimensions small relative to $\mathcal{L}$, $\mathcal{L}^d$ being the macroscopic area (d = 2) or volume (d = 3) available to the atoms.

The wave packets $|\psi^0(-\tau)\rangle$ and $|\psi(-\tau)\rangle$ are assumed to be identical for times $-\tau$ with

$$\frac{\sigma}{v} < \tau < \frac{\mathcal{L}}{v}, \tag{8}$$

where σ characterizes the range of the interatomic interaction and v is a typical atomic velocity. Then

$$|\psi(0)\rangle = e^{-iH\tau/\hbar} \; e^{iH_0\tau/\hbar} \; |\psi^0(0)\rangle. \tag{9}$$

The condition $\tau < \mathcal{L}/v$ is imposed to avoid the necessity of taking into account the boundary of the area or volume $\mathcal{L}^d$ in the scattering process.

As in the usual treatment[16] we now rewrite the τ-"limit" in Eq. (9) as an ϵ-"limit":

$$e^{-iH\tau/\hbar} \; e^{iH_0\tau/\hbar} |\vec{p}\vec{q}\alpha\rangle = \frac{\epsilon}{\hbar} \int_{-\infty}^{0} dt' e^{\epsilon t'/\hbar} \; e^{iHt'/\hbar} \; e^{-iH_0t'/\hbar} \; |\vec{p}\vec{q}\alpha\rangle \tag{10}$$

$$= \frac{i\epsilon}{E_{\vec{p}\vec{q}\alpha} + i\epsilon - H} \; |\vec{p}\vec{q}\alpha\rangle,$$

in which ϵ is chosen such that

$$\frac{\sigma}{v} < \tau < \frac{\hbar}{\epsilon} < \frac{\mathcal{L}}{v}. \tag{11}$$

The validity of the first equality in Eq. (10) can be understood by separating the integration interval in parts ⟩ and ⟨ −τ. Mathematically the conditions (11) express the proper order of taking limits. That ε does not strictly go to zero is essential for one of the following steps in the derivation. From Eqs. (5), (9) and (10) we have

$$|\psi(0)\rangle = \sum_{\alpha} \int d\vec{p} \; d\vec{q} \; f(\vec{p}\vec{q}\alpha) \; |\psi^{(+)}(\vec{p}\vec{q}\alpha)\rangle . \tag{12}$$

in which

$$|\psi^{(+)}(\vec{p}\vec{q}\alpha)\rangle = \frac{i\varepsilon}{E_{\vec{p}\vec{q}\alpha} + i\varepsilon - H} |\vec{p}\vec{q}\alpha\rangle \equiv \Omega |\vec{p}\vec{q}\alpha\rangle \tag{13}$$

tends in the limit ε→0 to an eigenstate of H satisfying outgoing-wave scattering conditions with the same eigenvalue $E_{\vec{p}\vec{q}\alpha}$ and Ω is a three-body Møller wave operator.

We now consider the total transition probability to a subspace of stationary states $|\vec{q}_f n\rangle$ of a Hamiltonian H_3 obtained from H by subtracting the sum of the interactions of atom 3 with atoms 1 and 2:

$$H_3 = H - V^3 . \tag{14}$$

The label n denotes a particular molecular state of atoms 1 and 2, while $\vec{q}_f$ is a momentum of atom 3 relative to the molecular center of mass. In the case of surface recombination we neglect for phase-space reasons the possibility that a final atom is again adsorbed to the surface. The final state $|\vec{q}_f n\rangle$ then represents a state where a molecule and an atom without mutual interaction collide with the inert wall. The vector $\vec{q}_f$ therefore stands in this case for the three-dimensional relative momentum of atom and molecule as they impinge on the wall, as well as their total momentum component P_z relative to the surface. In principle the notation $|\vec{q}_f n\rangle$ should include an additional quantum number m_{s_3}. For simplicity this is omitted.

The transition probability $P_n(t)$ is given by

$$P_n(t) = \int d\vec{q}_f \left| \langle \psi^0_{\vec{q}_f n}(t) | \psi(t) \rangle \right|^2. \tag{15}$$

in which

$$|\psi^0_{\vec{q}_f n}(t)\rangle = |\vec{q}_f n\rangle \, e^{-iE_{\vec{q}_f n} t/\hbar}. \tag{16}$$

$E_{\vec{q}_f n}$ being the corresponding eigenvalue of H_3. The inner product in Eq. (15) can be written as

$$\langle \psi^0_{\vec{q}_f n}(t) | \psi(t) \rangle = \sum_\alpha \int d\vec{p} \, d\vec{q} \, f(\vec{p}\vec{q}\alpha) \, \langle \vec{q}_f n| \, e^{i(E_{\vec{q}_f n} - H)t/\hbar} \, |\psi^{(+)}(\vec{p}\vec{q}\alpha)\rangle. \tag{17}$$

As explained below, we also need the time derivative of this equation. Using Eq. (14) this can be expressed in a similar matrix element as in Eq. (17), but now containing an additional operator V^3.

We subsequently rewrite Eq. (17) with the help of Eq. (13), exchanging Ω with the exponential and using the Lippmann-Schwinger equation

$$\frac{i\epsilon}{E_{\vec{p}\vec{q}\alpha} + i\epsilon - H} = \frac{i\epsilon}{E_{\vec{p}\vec{q}\alpha} + i\epsilon - H_3} + \frac{1}{E_{\vec{p}\vec{q}\alpha} + i\epsilon - H_3} V^3 \frac{i\epsilon}{E_{\vec{p}\vec{q}\alpha} + i\epsilon - H}. \tag{18}$$

We omit the first term in the right-hand side anticipating the ϵ-limit. We then find an expression as Eq. (17) which contains not only an additional V^3 operator but also an energy denominator $(E_{\vec{p}\vec{q}\alpha} + i\epsilon - E_{\vec{q}_f n})^{-1}$.

Actually, in connection with the recombination rate we are not interested in $P_n(t)$ for a single wave packet, but in the transition probability per unit time

$$w_n = \frac{d}{dt} \langle P_n(t) \rangle, \tag{19}$$

where the brackets stand for an average over an ensemble of wave packets, thus simulating the situation of the three H atoms in a 2D or 3D gas. Through the averaging process $\langle P_n(t)\rangle$ becomes a linear function of t and therefore w_n a constant.

We thus obtain an expression for w_n containing the 3-body density matrix:

$$\rho_{\vec{p}'\vec{q}'\alpha',\vec{p}\vec{q}\alpha} = \langle f^*(\vec{p}'\vec{q}'\alpha')\ f(\vec{p}\vec{q}\alpha)\rangle = \frac{1}{\mathcal{L}^{2d}} \int_{\mathcal{L}^d} d\vec{R}\ e^{-i\vec{R}\cdot(\vec{q}'-\vec{q})/\hbar}$$

$$\times \int_{\mathcal{L}^d} d\vec{r}\ e^{-i\vec{r}\cdot(\vec{p}'-\vec{p})/\hbar}\ F_{\alpha'\alpha}(\vec{p}_1\vec{q}_1\vec{r}\vec{R}). \tag{20}$$

In the third member we have carried out a Wigner transformation.[17] Furthermore, we introduced the notation

$$\vec{p}_1 = \tfrac{1}{2}(\vec{p}' + \vec{p}), \quad \vec{q}_1 = \tfrac{1}{2}(\vec{q}' + \vec{q}). \tag{21}$$

We assume the system to be homogeneous, so that the Wigner distribution function F is independent of $\vec{r}$ and $\vec{R}$. For a non-degenerate gas F is taken to be a Maxwell-Boltzmann distribution in momenta, diagonal in α' and α, and normalized according to

$$\sum_\alpha \int d\vec{p}_1\ d\vec{q}_1\ F_{\alpha\alpha}(\vec{p}_1\vec{q}_1) = 1. \tag{22}$$

As Eq. (20) shows, the widths Δp and Δq of ρ as a function of $\vec{p}'-\vec{p}$ and $\vec{q}'-\vec{q}$, respectively, are of order $2\pi\hbar/\mathcal{L}$. We apply this in working out the expression for w_n:

$$w_n = \frac{i}{\hbar} \sum_\alpha \int d\vec{q}_f \int d\vec{p}_1 d\vec{q}_1 \int d(\vec{p}'-\vec{p})\ d(\vec{q}'-\vec{q})\ \rho_{\vec{p}'\vec{q}'\alpha,\vec{p}\vec{q}\alpha}$$

$$\times \left\{ \frac{1}{E_{\vec{p}'\vec{q}'\alpha} - i\epsilon - E_{\vec{q}_f n}} - \frac{1}{E_{\vec{p}\vec{q}\alpha} + i\epsilon - E_{\vec{q}_f n}} \right\} \tag{23}$$

$$\langle \vec{q}_f n|V^3\ e^{i(E_{\vec{q}_f n}-H)t/\hbar}|\psi^{(+)}(\vec{p}'\vec{q}'\alpha)\rangle^* \langle \vec{q}_f n|V^3\ e^{i(E_{\vec{q}_f n}-H)t/\hbar}|\psi^{(+)}(\vec{p}\vec{q}\alpha)\rangle.$$

Because of Eq. (11), the arguments $\vec{p}'\vec{q}'$ and $\vec{p}\vec{q}$ may be replaced by their average values $\vec{p}_1\vec{q}_1$ in all factors except for ρ. The $\vec{p}'-\vec{p}$, $\vec{q}'-\vec{q}$ integrals can then be evaluated by means of Eq. (20). We may subsequently take the limit $\epsilon \to 0$, with the associated replacement of

H by $E_{\vec{p}_i\vec{q}_i\alpha}$, leading to

$$w_n = \frac{2\pi}{\hbar} \frac{(2\pi\hbar)^{2d}}{\mathcal{L}^{2d}} \sum_\alpha \int d\vec{q}_f \int d\vec{p}_i d\vec{q}_i \; \delta(E_{\vec{p}_i\vec{q}_i\alpha} - E_{\vec{q}_f n})$$

$$\times \left| \langle \vec{q}_f n | V^3 | \psi^{(+)}(\vec{p}_i\vec{q}_i\alpha) \rangle \right|^2 F_{\alpha\alpha}(\vec{p}_i\vec{q}_i). \tag{24}$$

Eq. (24) is our final result for three distinguishable particles.

In the next step we include the identical-particle aspect. This may be done by replacing in Eq. (15) the wave packet $|\psi(t)\rangle$ by a symmetrized state:

$$\frac{1}{\sqrt{6}} \sum_P P \; |\psi(t)\rangle. \tag{25}$$

Note that for large negative t the six wave packets in this sum do not overlap, so that the resulting state is properly normalized. In addition we sum the right-hand side of Eq. (15) over the three identities of the final free atom. We thus end up with

$$w_n = \frac{\pi}{\hbar} \frac{(2\pi\hbar)^{2d}}{\mathcal{L}^{2d}} \sum_\alpha \int d\vec{q}_f \int d\vec{p}_i d\vec{q}_i \; \delta(E_{\vec{p}_i\vec{q}_i\alpha} - E_{\vec{q}_f n})$$

$$\times \left| \langle \vec{q}_f n | V^3 | \sum_P P\psi^{(+)}(\vec{p}_i\vec{q}_i\alpha) \rangle \right|^2 F_{\alpha\alpha}(\vec{p}_i\vec{q}_i). \tag{26}$$

Finally, we consider a gas of N_H atoms with

$$\binom{N_H}{3} \simeq \frac{N_H^3}{6}$$

triples. We thus have as a final result:

$$\frac{dN_H}{dt} = -2 \frac{N_H^3}{6} \sum_n w_n \tag{27}$$

i.e. the rate equation for recombination:

$$\frac{dn_H}{dt} = -L\, n_H^3$$

48

with n_H the 2D or 3D density and the rate constant

$$L = \frac{\pi}{3\hbar} (2\pi\hbar)^{2d} \langle \sum_n \sum_\alpha \int d\vec{q}_f \; \delta(E_{\vec{p}_i\vec{q}_i\alpha} - E_{\vec{q}_f n})$$
$$\left| \langle \vec{q}_f n | v^3 | \sum_P P \psi^{(+)}(\vec{p}_i\vec{q}_i\alpha) \rangle \right|^2 \rangle_{thermal} . \tag{28}$$

III. QUANTUM BOLTZMANN EQUATION

As motivated in Sec. I we now include the many-body and identical-particle aspects from the beginning in the form of the second-quantization formalism.

We enclose a system of N_H atoms in a square (cube) with volume $\mathcal{L}^d$ on the faces of which we impose periodic boundary conditions. At the end we take the limit $\mathcal{L} \to \infty$. The starting point is the BBGKY equation[18-20] for the two-particle distribution matrix

$$\frac{\partial F^2}{\partial t} + \frac{i}{\hbar} [H^2, F^2] = - \frac{i}{\hbar} \operatorname*{Tr}_3 \left[v^3, \; \Omega^3 \left\{ F^1(1)F^1(2)F^1(3) \right\} \Omega^{3\dagger} \right]. \tag{29}$$

in which we have introduced the molecular-chaos assumption in the right-hand side, neglecting the presence of initial correlations in the form of molecules, because any produced molecule disappears rapidly from the gas. The symbol Ω^3 stands for the three-particle Møller operator, introducing the atomic interactions in the "free" three-particle state. Furthermore, H^k is the full k-particle Hamiltonian and

$$v^3 = V(1,3) + V(2,3). \tag{30}$$

Note that H^3 and Ω^3 were denoted as H and Ω in the previous section. The curly-bracket factor stands for the sum over three-particle permutations:

$$\left\{ F^1(1)F^1(2)F^1(3) \right\} = \sum_P F^1(P1)F^1(P2)F^1(P3). \tag{31}$$

49

The trace Tr in Eq. (29) stands for a sum over momentum and spin states for particle 3. In Eq. (29) F^k is normalized according to

$$\operatorname*{Tr}_{1..k} F^k = \frac{N!}{(N-k)!}. \tag{32}$$

We use Eq. (29) to calculate the rate of formation of H_2 molecules for the pure recombination process:

$$
\begin{aligned}
\frac{dN_{H_2}}{dt} &= \frac{d}{dt} \operatorname*{Tr}_{1..N} \left[\mathscr{P}_S \, \rho^N \, \mathscr{P}_S \sum_{i\langle j} \sum_n \mathscr{P}_n(i,j) \right] \\
&= \tfrac{1}{2} \frac{d}{dt} \operatorname*{Tr}_{1,2} \left[F^2(1,2) \sum_n \mathscr{P}_n(1,2) \right] \\
&= \tfrac{1}{2} \operatorname*{Tr}_{1,2} \left[\frac{\partial F^2(1,2)}{\partial t} \sum_n \mathscr{P}_n(1,2) \right].
\end{aligned}
\tag{33}
$$

in which ρ^N is the N-particle density matrix, $\mathscr{P}_n(i,j)$ is the projection operator on a specific bound state of H-atoms i and j, and $\mathscr{P}_S$ is the projection operator on the symmetric part of N-particle Hilbert space. Note that the Tr-operations include all, not necessarily symmetric, N- and 2-particle states, although the formalism takes correctly into account the identical-particle aspects.

We now substitute the time derivative using Eq. (29). The commutator $[H^2, F^2]$ does not contribute, since $[H^2, \mathscr{P}_n] = 0$. In the contribution from the other commutator we introduce the three-particle transition operator[16] from the free state (subscript 0) to the molecular state with particle 3 free (subscript 3):

$$U_{30} = \sum_n \mathscr{P}_n(1,2) \, V^3 \Omega^3. \tag{34}$$

We thus find

$$\frac{dn_H}{dt} = -\frac{2}{\mathscr{L}d} \frac{dN_{H_2}}{dt} = -L \, n_H^3 \tag{35}$$

with

50

$$L = \frac{-1}{\hbar n_H^3 \mathcal{L}^d} \, \underset{123}{\mathrm{Tr}} \, \left[U_{30}\left\{F^1(1)F^1(2)F^1(3)\right\}\Omega^{3\dagger}\sum_n \mathscr{F}_n(1,2) \right.$$
$$\left. - \sum_n \mathscr{F}_n(1,2)\Omega^3\left\{F^1(1)F^1(2)F^1(3)\right\}U_{30}^{\dagger} \right]. \tag{36}$$

Furthermore, we insert on both sides of the F product the completeness relation in terms of unsymmetrized free three-particle states. We assume F^1 to have the Maxwell-Boltzmann form, diagonal in momentum and spin state. Splitting off a center-of-mass factor, we have

$$\langle \vec{P}'\vec{p}_i'\vec{q}_i'\alpha' \mid F^1(1)F^1(2)F^1(3) \mid \vec{P}\vec{p}_i\vec{q}_i\alpha \rangle$$
$$= N_H^3 \left[\frac{2\pi\hbar}{\mathcal{L}}\right]^{2d} F_{cm}(\vec{P}) F_{\alpha\alpha}(\vec{p}_i\vec{q}_i) \; \delta_{\vec{P}',\vec{P}} \; \delta_{\vec{p}_i'\vec{q}_i'\alpha' , \vec{p}_i\vec{q}_i\alpha}. \tag{37}$$

Here, $F_{\alpha\alpha}$ and F_{cm} are normalized according to

$$\sum_\alpha \sum_{\vec{p}_i\vec{q}_i} F_{\alpha\alpha}(\vec{p}_i\vec{q}_i) = \left[\frac{\mathcal{L}}{2\pi\hbar}\right]^{2d},$$
$$\sum_{\vec{P}} F_{cm}(\vec{P}) = 1. \tag{38}$$

The three-particle trace in Eq. (36) is written as a sum over $\vec{P}$, n and $\vec{q}_f$ in view of the operator $\mathscr{F}_n$. Using the fact that U_{30}, Ω^3 and $\mathscr{F}_n(1,2)$ operate only on relative degrees of freedom, we carry out the summation over $\vec{P}$ and use

$$\sum_n \mathscr{F}_n(1,2) \; \Omega^3 \mid \vec{p}_i\vec{q}_i\alpha \rangle = \frac{1}{E_{\vec{p}_i\vec{q}_i\alpha} + i\epsilon - H_3} U_{30} \mid \vec{p}_i\vec{q}_i\alpha \rangle. \tag{39}$$

We now take the limit $\mathcal{L} \to \infty$, making the replacements:

$$\sum_{\vec{P}} \to \left[\frac{\mathcal{L}}{2\pi\hbar}\right]^d \int d\vec{P},$$
$$\mid \vec{p} \rangle \to \left[\frac{2\pi\hbar}{\mathcal{L}}\right]^{d/2} \mid \vec{p} \rangle. \tag{40}$$

for each of the momenta. In the second substitution of (40) we replace

a momentum state normalized over the cube (square) by one with Dirac normalization. The final result

$$
L = \frac{\pi}{3\hbar} (2\pi\hbar)^{2d} \sum_n \int d\vec{q}_f \sum_\alpha \int d\vec{p}_i d\vec{q}_i \; F_{\alpha\alpha}(\vec{p}_i \vec{q}_i)
$$
$$
\times \; \delta(E_{\vec{p}_i \vec{q}_i \alpha} - E_{\vec{q}_f n}) \; \left| \langle \vec{q}_f n | U_{30} \sum_P P | \vec{p}_i \vec{q}_i \alpha \rangle \right|^2
\tag{41}
$$

is easily seen, using Eq. (34), to be identical with the result of Sec. II.

IV. DIPOLE RECOMBINATION

In the previous sections we derived general expressions for L, applying to both bulk and surface recombination, and to exchange as well as dipole recombination. We now derive more special expressions.

Starting with L_g in the 3D case we eliminate the energy conserving δ-function by carrying out the integration over $|\vec{q}_f|$, ending up with an angular integral over $\hat{q}_f = \vec{q}_f / |\vec{q}_f|$:

$$
L_g = (2\pi\hbar)^9 \frac{1}{4m_H} \langle \sum_n \sum_\alpha \int d\hat{q}_f \; q_f |f_{\vec{q}_f n, \vec{p}_i \vec{q}_i \alpha}|^2 \rangle_{thermal}
\tag{42}
$$

with the recombination amplitude

$$
f_{\vec{q}_f n, \vec{p}_i \vec{q}_i \alpha} = \frac{\frac{2}{3}m_H}{2\pi\hbar^2} \langle \vec{q}_f n | v^3 | \sum_P P \psi^{(+)}(\vec{p}_i \vec{q}_i \alpha) \rangle .
\tag{43}
$$

q_f being determined by energy conservation.

Continuing with the surface rate constant, we now split off from $\vec{q}_f$ the implicit total center-of-mass momentum P_z, obtaining

$$
L_s = (2\pi\hbar)^7 \frac{1}{4m_H} \langle \sum_n \sum_\alpha \int dP_z \int d\hat{q}_f \; q_f |f_{\vec{q}_f P_z n, \vec{p}_i \vec{q}_i \alpha}|^2 \rangle_{thermal}
\tag{44}
$$

with

$$f_{\vec{q}_f P_z n, \vec{p}_i \vec{q}_i \alpha} = \frac{\frac{2}{3} m_H}{2\pi\hbar^2} \langle \vec{q}_f P_z n | V^3 | \sum_P P \psi^{(+)}(\vec{p}_i \vec{q}_i \alpha) \rangle. \tag{45}$$

We stress that the final state $|\vec{q}_f P_z n\rangle$ contains in principle the full influence of the (inert) wall, both for the atom and for the molecule.

The previous derivations of expressions for L contain exact three–particle collision matrix elements. These form a suitable starting point for recombination processes which can take place via the strong central (singlet + triplet) interaction, such as a + a + b recombination. For the class of dipole recombination processes, with changing total spin projection ($\Delta M_F \neq 0$), the magnetic–dipole interaction is essential as a non–central interaction to transfer angular momentum from orbital to spin degrees of freedom. The relative weakness of this interaction enables us to approximate the exact three–particle transition amplitude f to first order in the dipole interaction. Neglecting the very small energy shift of the final singlet state to first order in the dipole interaction, which is in principle induced by the hyperfine interaction, it is easy to write down the first–order part of the V^3 matrix element in f. We separate V^3 and the bra and ket in a "central" part, due to the central interaction, and a first–order dipole part:

$$V^3 = V^{3,c} + V^{3,d},$$

$$|\vec{q}_f n\rangle = |\vec{q}_f n\rangle_c + \frac{1}{E_{\vec{q}_f n} - H_3^c}(1 - \mathscr{P}_n)V_3^d |\vec{q}_f n\rangle_c,$$

$$|\psi^{(+)}(\vec{p}_i \vec{q}_i \alpha)\rangle = |\psi^{(+)}(\vec{p}_i \vec{q}_i \alpha)\rangle_c \tag{46}$$

$$+ \frac{1}{E_{\vec{p}_i \vec{q}_i \alpha} + i\epsilon - H^c} V^d |\psi^{(+)}(\vec{p}_i \vec{q}_i \alpha)\rangle_c.$$

In view of the factor $1-\mathscr{P}_n$, we may add a term $-i\epsilon$ in the denominator of the second equation. We then use energy conservation, a Lippmann–Schwinger equation like Eq. (18) for the central interactions and the orthogonality of "free" atom states. We thus find, noting that the zeroth–order contribution vanishes in the special case of dipole recombination:

$$f_{\vec{q}_f n, \vec{P}_i \vec{q}_i \alpha} = \frac{\frac{2}{3}^m H}{2\pi \hbar^2} {}_c \langle \psi^{(-)}(\vec{q}_f n) | V^d \sum_P P | \psi^{(+)}(\vec{P}_i \vec{q}_i \alpha) \rangle_c . \qquad (47)$$

in which the eigenstate of H^c with ingoing scattered-wave character is given by

$$|\psi^{(-)}(\vec{q}_f n)\rangle_c = |\vec{q}_f n\rangle_c + \frac{1}{E_{\vec{q}_f n} - i\epsilon - H^c} V^{3,c} |\vec{q}_f n\rangle_c . \qquad (48)$$

In the following section we use Eq. (47) to calculate the dipole recombination rate. Note that it applies both to the volume and to the surface. We repeat that the right-hand sides of Eqs. (42) and (44) contain an unweighted sum over m_{s_3}. For comparison with experiment, however, we are interested in effective rates. In the following we therefore present either L_s^{eff} or its separate contributions $L_s^{\pm\frac{1}{2}}$.

V. CALCULATION OF $L_s^{\pm\frac{1}{2}}$

The model we use here is based on the Kagan dipole mechanism.[11] In this description of the recombination the electronic dipolar interactions induce a transition from a bbb incoming state to a final state, consisting of a bound pair of atoms (1 and 2) and atom 3, which does not interact with this pair. In view of this and the selection rule $s_{12}=1 \rightarrow s_{12}=1$, the dipolar interaction between 1 and 2 does not contribute. It was pointed out in Ref. 22 that such a contribution does arise when an additional exchange interaction of particle 3 with 1 or 2 in the final state is taken into account. This dipole-exchange mechanism and possible other more complicated higher-order processes are neglected in the present paper.

An attractive feature of the Kagan approach is that it admits a simple interpretation. The electronic spin of atom 3 causes a magnetic-dipole field at the positions of 1 and 2. The difference in magnetic field, experienced by 1 and 2, leads to different precessions of their electron spins. This induces a singlet component in the

54

wavefunction of the 1-2 system, offering the atoms the possibility to recombine subsequently. It is clear that the proton spins are not influenced during the process. Therefore we leave them out of consideration in the following.

This mechanism explains the fact that a third H atom is required, even in the presence of an abundance of third bodies provided by the He surface. As a result of the long range of the dipolar interaction, this third atom can be located at a large distance from the recombining pair.

Fig. 1 shows the geometry of the system. We use Jacobi coordinates $\vec{r}_{ij}$, $\vec{r}_{ij,k}$ and their projections $\vec{\rho}_{ij}$, $\vec{\rho}_{ij,k}$ on the surface.

To calculate f, we first consider the initial state $|\psi^{(+)}(\vec{P}_i\vec{q}_i\alpha)\rangle_c$ of Eq. (47). This represents a state of three non-interacting H atoms bound to the surface, i.e.
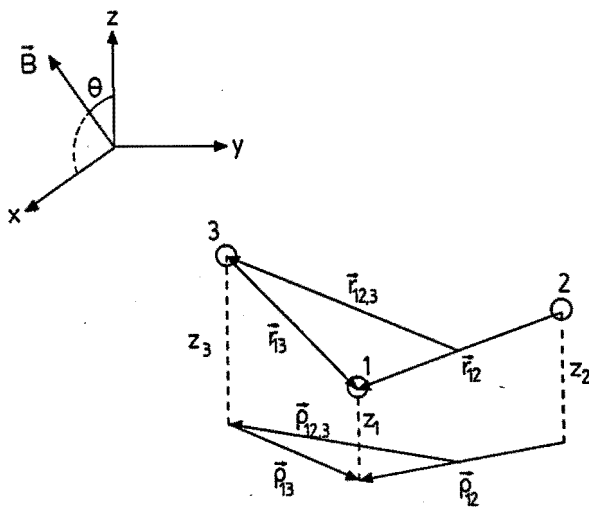

Fig. 1 Situation for three-body collisions on a ^{4}He film. Here, z_i denotes the distance of particle i from the surface. Furthermore, $\vec{r}_{ij}$, $\vec{r}_{ij,k}$ and $\vec{\rho}_{ij}$, $\vec{\rho}_{ij,k}$ are 3D and 2D Jacobi coordinates, and Θ is the angle between magnetic-field direction and surface normal.

$$|\vec{p}_1\vec{q}_1\alpha\rangle \hat{=}$$

$$\phi_0(z_1)\phi_0(z_2)\phi_0(z_3) \left\{ \frac{e^{i(\vec{p}_1\vec{\rho}_{12}+\vec{q}_1\vec{\rho}_{12,3})/\hbar}}{(2\pi\hbar)^2} \right\} \times_{S=\frac{3}{2},M_S=\frac{-3}{2}} (1,2,3), \tag{49}$$

of which the spatial part is distorted by the mutual triplet interactions. For this distortion we use the "2½-dimensional" model,[8-9] which has proved to be very succesful for the description of two-particle collisions along the surface. In this model the distortion affects only the factor between curly brackets in Eq. (49). It is replaced by a solution $u(\vec{\rho}_{12},\vec{\rho}_{12,3})$ of the 2-dimensional Schrödinger equation for three H atoms mutually interacting by means of triplet potentials $V^c_{s=1}$ averaged over the z-motion of the atoms:

$$\bar{V}^c_{s=1}(\rho_{ij}) = \int_{-\infty}^{\infty} dz_i \int_{-\infty}^{\infty} dz_j \, \phi_0^*(z_i)\phi_0^*(z_j)V^c_{s=1}(r_{ij})\phi_0(z_i)\phi_0(z_j). \tag{50}$$

In the spin part χ of Eq. (49) the magnetic quantum number refers to the magnetic field direction.

The calculation of $u(\vec{\rho}_{12},\vec{\rho}_{12,3})$ is a 2-dimensional three-atom problem. It could be obtained with the help of the Faddeev formalism[21,22] in 2 dimensions. Instead of this, however, we follow the method of Kagan et al.[11] We approximate $u(\vec{\rho}_{12},\vec{\rho}_{12,3})$ by only taking into account spatial correlations between the atoms of the recombining pair (1 and 2) and the pair (1-3 or 2-3) interacting via the dipolar interaction. We start with the symmetrized free state and replace the exponentials of the recombining pair and dipole pair by two-particle triplet scattering states. For instance for the $V^d(1,3)$-term of Eq. (47) we make the replacement

$$\sum_P P u \rightarrow \bar{u}(\vec{\rho}_{12},\vec{\rho}_{13}) = \left\{\psi_{t\vec{k}_{12}}(\vec{\rho}_{12}) + \psi_{t,-\vec{k}_{12}-\vec{k}_{13}}(\vec{\rho}_{12})\right\} \psi_{t\vec{k}_{13}}(\vec{\rho}_{13}) +$$

$$\left\{\psi_{t\vec{k}_{13}}(\vec{\rho}_{12}) + \psi_{t,-\vec{k}_{12}-\vec{k}_{13}}(\vec{\rho}_{12})\right\} \psi_{t\vec{k}_{12}}(\vec{\rho}_{13}) + \tag{51}$$

$$\left\{\psi_{t\vec{k}_{12}}(\vec{\rho}_{12}) + \psi_{t\vec{k}_{13}}(\vec{\rho}_{12})\right\} \psi_{t,-\vec{k}_{12}-\vec{k}_{13}}(\vec{\rho}_{13}) .$$

in which $\vec{k}_{12}' = (\vec{p}_1 + \frac{1}{2}\vec{q}_i)/\hbar$ and $\vec{k}_{13}' = -\vec{q}_i/\hbar$. Furthermore, $\psi_{t\vec{k}}(\vec{\rho})$ denotes a 2D two-particle relative scattering state, with $\exp(i\vec{k}.\vec{\rho})/(2\pi\hbar)$ as a plane-wave part. Note that this Kagan-like replacement destroys partly the symmetry of $\sum P$ u. Note furthermore that the combination of six terms in Eq. (51) describes correctly the asymptotic plane-wave part.

In the volume case the six terms are identical in the T=0 limit, leading to Kagan's results. We believe that Eq. (51) is a reasonable approximation, since the volume of configuration space in which particles 2 and 3 are closely together and thus correlated, is only a small fraction of the total volume contributing significantly to the dipole integral. For low temperatures the only significant contribution of $\psi_{t\vec{k}}(\vec{\rho})$ to the amplitude comes from the lowest partial wave m=0, which for low k separates further into ρ and k dependent factors[23]:

$$\psi_{t\vec{k}}(\vec{\rho}) \simeq g(k) \, v_t(\rho),$$ (52)

with

$$g(k) = \frac{-1}{\left\{\frac{\pi^2}{4} + [\gamma + \log(ka/2)]^2\right\}^{\frac{1}{2}}}$$ (53)

and

$$v_t(\rho) = \frac{\log(\rho/a)}{2\pi\hbar}$$ (54)

just outside the potential range. Here, γ is Euler's constant and a is the 2D scattering length, which has the value of 2.4 a_0 for the 2D potential given by Eq. (50), if we choose the Mantz-Edwards wavefunction[24] for $\phi_0(z)$. Note that $\psi_{t\vec{k}}(\vec{\rho})$ differs in normalization from the radial wavefunction in Ref. 23. A T=0 calculation, as for volume recombination, is now impossible, because of the logarithmic k-dependence in Eq. (53). These equations, however, still enable us to derive a low-T approximation, since the energy dependence in now contained in a separate factor. We will use this later to calculate the thermally averaged rate constants.

We now turn to the final state $|\psi^{(-)}(\vec{q}_f n)\rangle_c$ of Eq. (47). In the

previous section we defined it as an eigenstate of the Hamiltonian with central interactions between the atoms and atom-wall, molecule-wall interactions included. We now follow Kagan, however, in leaving out the atom-molecule interaction. Furthermore, in view of the rather high $H+H_2$ relative kinetic energy (~ 60 K for $B=10$ T, $v=14$, $j=3$ and $m_{s_3}=-\frac{1}{2}$), we neglect the attractive part of the surface potential (~ 4.5 K) and replace it by a perfectly reflecting rigid wall. As a first step, however, we will leave out the wall completely. An estimate of the effects neglected with this approximation is given in Sec. VIII.

On the basis of this the final state reduces to

$$
|\psi^{(-)}(\vec{q}_f\ n)\rangle_c \stackrel{\wedge}{=} \psi_{vjm}(\vec{r}_{12})
$$
$$
\times \frac{e^{iP_ZZ/\hbar}}{(2\pi\hbar)^{1/2}} \frac{e^{i\vec{q}_f\vec{r}_{12,3}/\hbar}}{(2\pi\hbar)^{3/2}} X_{s_{12}=0,m_{s_{12}}=0}(1,2)\ X_{\frac{1}{2},m_{s_3}}(3). \tag{55}
$$

In Eq. (55) Z is the center-of-mass position perpendicular to the surface and ψ_{vjm} is the molecular wavefunction (m relative to z). It turns out that only odd j final states are possible, since the $V^d(1,3)$- and $V^d(2,3)$-terms of f cancel for even j and are equal for odd j. Using Eqs. (49), (51) and (55) we obtain for the amplitude

$$
f = \frac{\frac{2}{3}^{m_H}}{2\pi\hbar^2}\frac{2\delta_{j,odd}}{(2\pi\hbar)^2} \int dZ \int d\vec{r}_{12} \int d\vec{r}_{13}\ e^{-i\vec{q}_f(\vec{r}_{12}/2-\vec{r}_{13})/\hbar}\ e^{-iP_ZZ/\hbar}\ \psi^*_{vjm}(\vec{r}_{12})
$$
$$
\times \langle X_{s_{12}=0,m_{s_{12}}=0}(1,2)\ X_{\frac{1}{2},m_{s_3}}(3) | V^d(1,3) | X_{S=\frac{3}{2},M_S=\frac{3}{2}}(1,2,3)\rangle \tag{56}
$$
$$
\times \bar{u}(\vec{\rho}_{12},\vec{\rho}_{13})\ \phi_0(z_1)\phi_0(z_2)\phi_0(z_3).
$$

To evaluate the integrals it is convenient to use cylindrical coordinates with the surface normal as a symmetry axis. The dipolar interaction can be written as a scalar product of rank-2 tensor operators $\Sigma^{(2)}$ and $Y^{(2)}$ in spin and coordinate space, respectively. Clearly, only the term

$$
\Sigma^{(2)}_{\frac{3}{2}+m_{s_3}}\ Y^{(2)}_{-\frac{3}{2}-m_{s_3}} \tag{57}
$$

of this scalar product contributes, when these operators have the magnetic-field direction as a quantization axis. The z-axis normal to the surface being the natural quantization axis for the spatial part of the problem, we express the $Y^{(2)}$ operator in terms of $Y^{(2)}$ operators with respect to the z-axis. Choosing x along the projection of $\vec{B}$ as in Fig. 1, the coefficients in this expression are reduced Wigner functions

$$d^{(2)}_{-\frac{3}{2}-m_{s_3},\mu}(\theta). \tag{58}$$

Here, θ is the angle between $\vec{B}$ and the surface normal and $\mu\hbar$ is the transfer of angular momentum from the spin system to the orbital system along the z-axis. The Wigner functions describe the field-orientation dependence of the amplitude. Furthermore, the P_Z-dependence of f is concentrated in the exponential $\exp(-iP_Z Z/\hbar)$ and in q_f by means of the energy-conservation relation

$$-3\epsilon_0 + \frac{P_i^2}{m_H} + \frac{3q_i^2}{4m_H} = \frac{P_Z^2}{6m_H} + \frac{3q_f^2}{4m_H} + E_{vj} + (\frac{3}{2} + m_{s_3})2\mu_B B, \tag{59}$$

where E_{vj} is the energy of the molecular state. In the first instance we neglect a possible energy transfer to the center of mass in the final state, i.e. the $P_Z^2/6m_H$ term in Eq. (59). In Sec. VIII we discuss also the effect of this approximation. This reduces the Z-integral in Eq. (56) to a more simple Fourier integral:

$$f = G(\vec{k}'_{12}, \vec{k}'_{13})$$
$$\times \sum_\mu d^{(2)}_{-\frac{3}{2}-m_{s_3},\mu}(\theta)\, (i)^{\mu-m}\, e^{i(\mu-m)\phi_q} \int_{-\infty}^{\infty} dZ\, e^{-iP_Z Z/\hbar}\, F_{m\mu}(\theta_q, Z), \tag{60}$$

where (θ_q, ϕ_q) are the polar angles of $\vec{q}_f$. Evaluating the two integrals over the azimuthal angles ϕ_{12} and ϕ_{13}, reduces the expression for $F_{m\mu}(\theta_q, Z)$ to a multiple integral over ρ_{12}, z_{12}, ρ_{13} and z_{13}. This is worked out in App. A. There we also give the expression for G in terms of the functions $g(k'_{12})$, $g(k'_{13})$ and $g(|-\vec{k}'_{12}-\vec{k}'_{13}|)$, defined in

Eq. (53). In the volume case, we would obtain two separable integrals over r_{12} and r_{13}. Now the 12 and 13 integrals are not completely separable because of the surface bound states in Eq. (56). The problem, however, is still manageable numerically.

We now turn to the calculation of the rate constants $L_s^{\pm\frac{1}{2}}$. By Parceval's theorem the integral over P_Z in Eq. (44) can be carried out analytically. Apparently, this is due to the present neglect of the $P_Z^2/6m_H$-term in Eq. (59). As we are only interested in low temperatures, the energy pertaining to the initial state is much smaller than that of the final state. Therefore, we neglect energy changes in the final state due to the thermal-averaging procedure. With the help of Eq. (53) it is now possible to determine the temperature-dependent factor of the rate constants $L_s^{\pm\frac{1}{2}}$:

$$\langle G^2 \rangle_T = \langle\, G^2(\vec{k}_{12},\vec{k}_{13})\,\rangle_{th} = \tag{61}$$
$$\frac{3}{16\pi^4}\lambda_{th}^4 \int d\vec{k}_{12}\int d\vec{k}_{13}\; e^{\left\{-(k_{12}^2+k_{13}^2+\vec{k}_{12}\cdot\vec{k}_{13})\hbar^2/m_H k_B T\right\}} G^2(\vec{k}_{12},\vec{k}_{13}).$$

We end up with $L_s^{\pm\frac{1}{2}}$ as a function of $\vec{B}$ and T:

$$L_s^{\pm\frac{1}{2}}(\vec{B},T) = \ell_s^{\pm\frac{1}{2}}(\vec{B})\,\langle G^2 \rangle_T. \tag{62}$$

where

$$\ell_s^{\pm\frac{1}{2}}(\vec{B}) = (2\pi\hbar)^8 \sum_{vj}\frac{2\pi q_f}{4m_H}\sum_{m\mu}\int_{-\infty}^{\infty}dZ\int_{-1}^{1}d(\cos\theta_q)\;|F_{m\mu}(\theta_q,Z)|^2$$
$$\times\left[d_{-\frac{3}{2}\mp\frac{1}{2},\mu}^{(2)}(\theta)\right]^2. \tag{63}$$

To exhibit more clearly the dependence on field orientation, we expand $L_s^{\pm\frac{1}{2}}$ in Legendre plynomials $P_n(\cos\theta)$, making use of Wigner 3j symbols:

$$\left[d_{\sigma,\mu}^{(2)}(\theta)\right]^2 = \sum_n (2n+1)\begin{pmatrix}2 & 2 & n\\ \sigma & -\sigma & 0\end{pmatrix}\begin{pmatrix}2 & 2 & n\\ \mu & -\mu & 0\end{pmatrix}P_n(\cos\theta). \tag{64}$$

The result is

$$L_s^{\pm\frac{1}{2}}(\vec{B},T) = \sum_{n=0,2,4} A_n^{\pm\frac{1}{2}}(B,T)\, P_n(\cos\theta). \tag{65}$$

Only even n values contribute because $F_{m\mu}$ turns out to be even in μ. Apparently, as in the volume case the double-spin-flip ($m_{s_3} = \frac{1}{2}$) and single-spin-flip ($m_{s_3} = -\frac{1}{2}$) contributions are related by

$$A_n^{+\frac{1}{2}}(B,T) \begin{bmatrix} 2 & 2 & n \\ -1 & 1 & 0 \end{bmatrix} = 4\, A_n^{-\frac{1}{2}}(2B,T) \begin{bmatrix} 2 & 2 & n \\ -2 & 2 & 0 \end{bmatrix}. \tag{66}$$

where the factor of 4 results from the spin matrix element of Eq. (56). Eq. (66) is the counterpart of a similar relation between $L_g^{+\frac{1}{2}}$ and $L_g^{-\frac{1}{2}}$ for the volume.

VI. RESULTS

As in the volume case, the most important molecular states appear to be the states close to the continuum. For fields below 10 Tesla 99% of the total contribution to the effective rates comes from the v=14,j=3 state, with a binding energy of 72 K, and the small remaining fraction from the v=14,j=1 state, with a binding energy of 183 K. This fraction becomes the dominant part for higher fields.

In the previous section we used the surface wavefunction $\phi_0(z)$ of Mantz and Edwards[24] to calculate the potentials $\overline{V}_{s=1}^c$ of Eq. (50). To keep the computation time within reasonable bounds, we prefer to use the form $\phi_0(z)=2\alpha^{3/2}z\,\exp(-\alpha z)$ for calculating f. For $\alpha=0.15a_0^{-1}$ ϕ_0 resembles rather closely the Mantz and Edwards wavefunction, while it resembles the wavefunction in a Stwalley-type potential reproducing the experimental adsorption energy[8] for $\alpha=0.20\,a_0^{-1}$. In most of the calculations we shall use the former value for α. The error bar in some of the results to be given corresponds with the change in the effective rate constant if this value for α is replaced by $\alpha=0.20\,a_0^{-1}$. It turns out that our values for the effective surface rate constants scale roughly with α^2, which would suggest the validity of the scaling prescription[15] (see, however, Sec. VII).
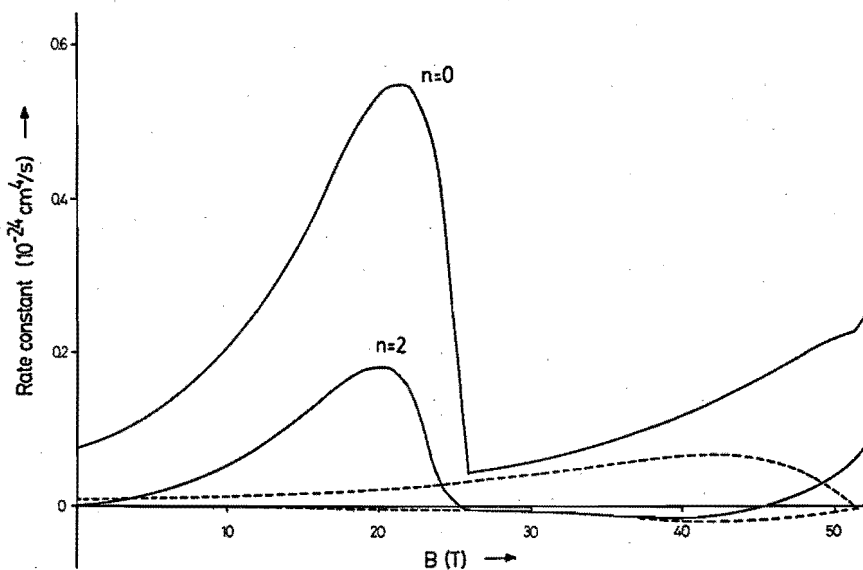
Fig. 2 *Partial contributions to* L_s^{eff} *as a function of B* ($\alpha=0.15$ a_0^{-1}, $T=0.4$ K).
Broken curves: single-spin-flip fractions $A_n^{-1/2}$.
Full curves: effective rate constant $A_n^{-1/2} + 2A_n^{+1/2}$.

In Fig. 2 we present the partial contributions $A_n^{-1/2}(n=0,2)$ to L_s^{eff} as a function of B at $T=0.4$ K (broken curves). We also present the partial effective rate constants $A_n^{-1/2} + 2A_n^{+1/2}$ for $n=0,2$ (solid curves). The double-spin-flip process is dominant. Furthermore, we observe a double-spin-flip cutoff at 25.6 T and a (less pronounced) single-spin-flip cutoff at 51.2 T. For fields B$>$25.6 T (51.2 T) the Zeeman energy needed to flip two (one) spins increases beyond the then available recombination energy $(-E_{v,j}-3\epsilon_0=69$ K for $v=14,j=3)$. The sharpness of the cuttof results from the low-energy approximation. For higher temperatures the uncertainty in the initial kinetic energy leads to a spread in the available recombination energy and thus in the field for which $q_f=0$. Another effect which tends to a smoother field dependence around 25.6 and 51.2 T is the transfer of z-momentum to the 3-atom center of mass, to be considered in Sec. VIII. Note that

in I we presented values for L_s instead of L_s^{eff}. The remaining differences between the results of I and Fig. 2 can be explained by the fact that we here use a H-H potential, which reproduces more accurately the experimental data on singlet boundstate energies. Therefore the potentials of Eq. (50) and the wavefunctions ψ_{vjm} and ψ_t are slightly changed. An important effect comes from the increase of the binding energy of the $v=14, j=3$ state by about 6 K, which results in a shift of the curves of the rate constant as a function of B.

The $n=0$ curves in Fig. 2 represent the rates averaged over all field orientations. The $n\neq0$ curves express the anisotropy as a function of the field direction. As we see in Fig. 2, the $n=2$ coefficients are small compared to the corresponding $n=0$ values. The $n=4$ part turns out to be negligible: $|A_4^{-\frac{1}{2}}+2A_4^{+\frac{1}{2}}| < 9.0\times10^{-27}$ cm^{4}sec^{-1}. Therefore we may conclude that the anisotropy is small, which is caused by the fact that all μ values in Eq. (63) give contributions of the same order of magnitude. This seems to be in agreement with experimental indications.[12,25]

Both the field dependence and absolute magnitude of the effective rate constant, however, are at variance with experiment. We find a rate which is growing with B by 70% from B=4 to 9 Tesla, whereas experiments show a slow decrease. For the field orientation normal to the surface we find $L_s^{eff}= 2.7(7)\times10^{-25}$ cm^{4}sec^{-1} at B=7.6 T and T=0.4 K, while the corresponding experimental values are $L_s^{eff}=1.5(2)\times10^{-24}$ cm^{4}sec^{-1} (Ref. 25) and $L_s^{eff}=1.8(4)\times10^{-24}$ cm^{4}sec^{-1} (Ref. 12). These values are a factor of 6 larger than our calculated value. In Ref. 15 it was noticed that a scaling prescription to convert the volume rate into a surface rate, leads to a correct order of magnitude for L_s^{eff}. (More precisely, the difference with experiment is a factor of 2). Objections against this scaling prescription will be presented in the following section.

In Fig. 3 we present the temperature dependence of the rate constant, governed by Eq. (61). As a reference temperature we use $T_0=0.4$ K and therefore we plotted $\langle G^2 \rangle_T / \langle G^2 \rangle_{T_0}$ as a function of T. Note that effective surface rate constant goes to zero logarithmically for T→0, illustrating again that a zero-temperature approximation as in three dimensions is not feasible.
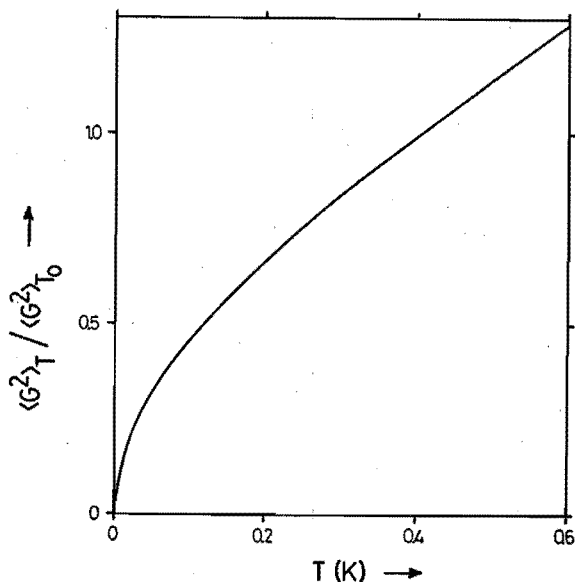
Fig. 3 The function $\langle G^2 \rangle_T / \langle G^2 \rangle_{T_0}$ as a function of T for $T_0 = 0.4$ K.

As can be seen from Eq. (63), the surface rate constant is essentially an incoherent sum or integral over m, μ, Z and θ_q of $|F_{m\mu}(Z, \theta_q)|^2$. To understand the underlying physics, we plot in Fig. 4 the $|F_{m\mu}(Z, \theta_q)|^2$ surfaces as a function of Z and $\sin\theta_q$ for various $|\mu|$, $|m|$ combinations. In Fig. 4 the maximum value of the m=μ=0 surface has arbitrarily been taken as 1. All surfaces have their maximum value for Z$\approx$7 a_0, which corresponds to the most probable location of the atoms from the wall in the ϕ_0 state. For $\sin\theta_q \to 1$ the dominant $|F|^2$ surfaces show a decrease which is due to the absence of high relative momenta along the surface in the initial state. A similar feature gives rise to the increase of L_s^{eff} with B at lower fields. The absence of high initial momenta along the surface is also responsible for the gradual shift of the maximum of the $|F|^2$ surface to larger $\sin\theta_q$ values for increasing $|m|$ and $|\mu|$: atom 3 can only gain high momentum $q_{\parallel} = q_f \sin\theta_q$ by the dipole interaction, say with atom 1. The strong xy-recoil of atom 1, however, enhances rapid rotation (large $|m|$) of atom 1 around atom 2, which has not been involved in

64

the dipole force. On the other hand, strong dipole forces along the
surface are correlated with high transfers $|\mu|$ of z-angular momentum
from the spin system to the spatial degrees of freedom. The above
picture also explains that the absolute value of the surfaces
decreases for increasing $|m|$ and $|\mu|$. Via Eq. (63) this would seem to
be inconsitent with the previously mentioned small anisotropy as a
function of Θ. It turns out, however, that the solid angle in which
atom 3 is emitted decreases for decreasing $|\mu|$. This leads to
comparable contributions of all $|\mu|$ values and thus a non-significant
anisotropy of the rate constant with respect to the magnetic-field
direction. It turns out that the summation over μ also washes out the
anisotropic structure as a function of $\sin\Theta_q$ implied by the individual
surfaces in Fig. 4.

VII. SCALING PRESCRIPTION

As has been pointed out in the previous section, the scaling
procedure, proposed by Kagan et al.[15] leads to surface rates which
differ by more than an order of magnitude from the values presented
here. Their results agree better with the experimental data. We
believe, however, that this scaling procedure is a bad approximation
in the present situation. To show this, let us analyze step by step
where the above-mentioned large difference with our L_s^{eff} value arises
from.

In Ref. 15 Kagan et al. claim that a state of adsorbed atoms can
be regarded as quasi three-dimensional, when the width of the one-atom
z wavefunction is much larger than the interaction range of the
particles. (In the case of polarized atomic hydrogen atoms the
interaction range $\sigma \simeq 6$ a_0 and the ^{4}He-H potential well has a width of
$d \simeq 10$-20 a_0). The initial state is considered to be a product of a 3D
relative three-atom state and three surface bound states. The autors
use the function $\widetilde{\phi}_0(z) = (2\widetilde{\alpha})^{1/2} \exp(-\widetilde{\alpha}z)$, with $\widetilde{\alpha}=\sqrt{2m_H\epsilon_0}/\hbar$, as a
boundstate. A choice of 0.9 K for the binding energy in the case of a
superfluid helium film leads to a value of 0.10 a_0^{-1} for $\widetilde{\alpha}$. Strictly
speaking, the exponential form is only assumed for large positive z.
The normalization factor implies a cutoff close to z=0. The simple
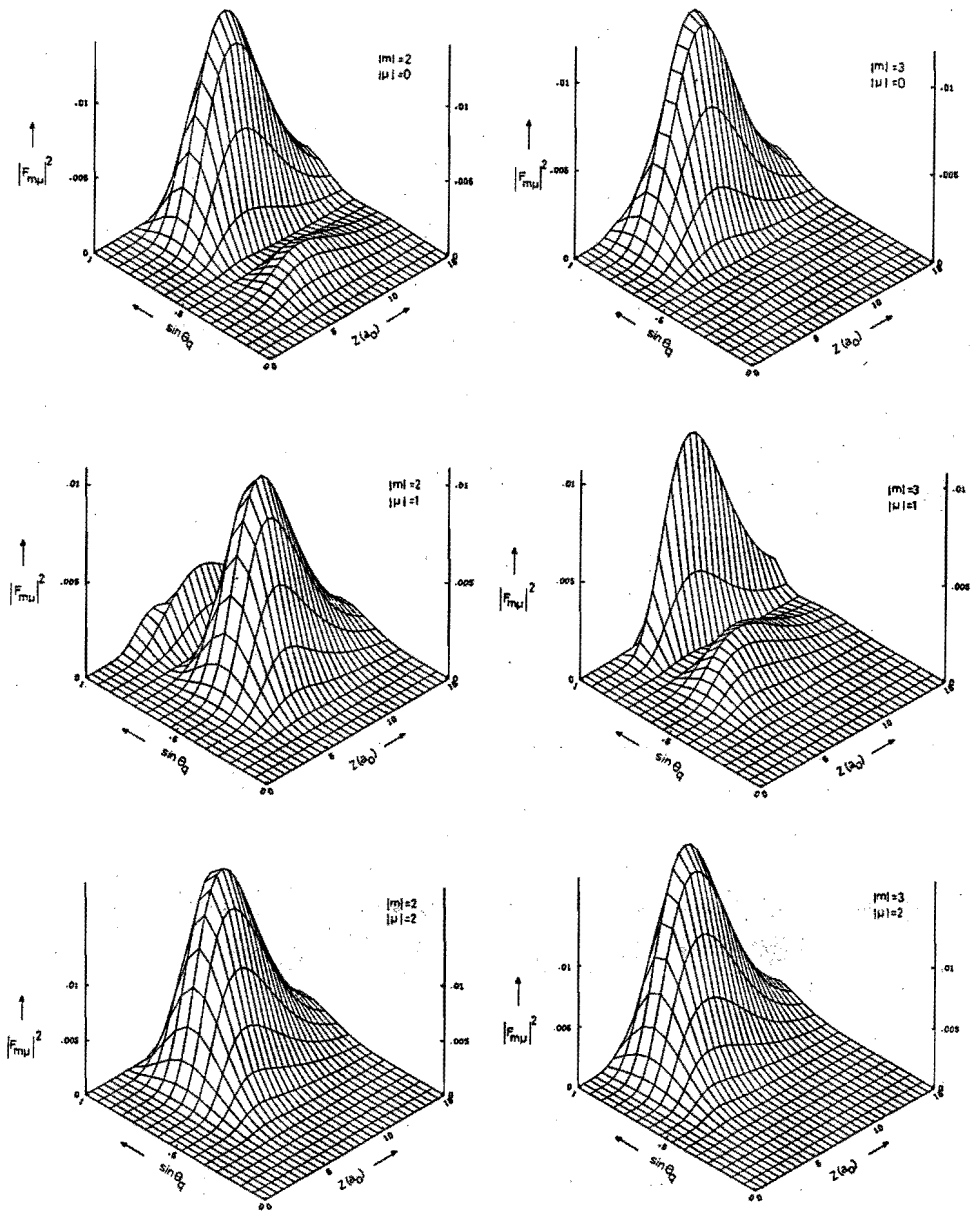exponential form introduces a simplification in that the product of
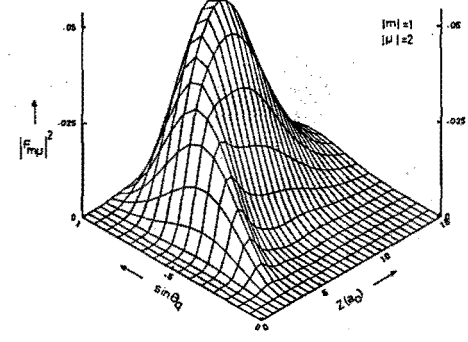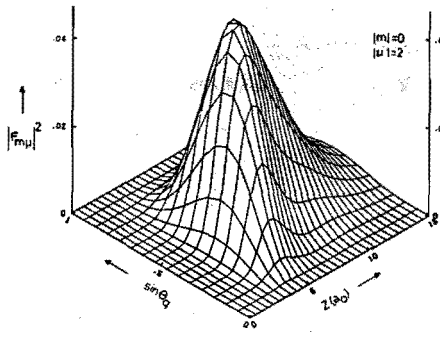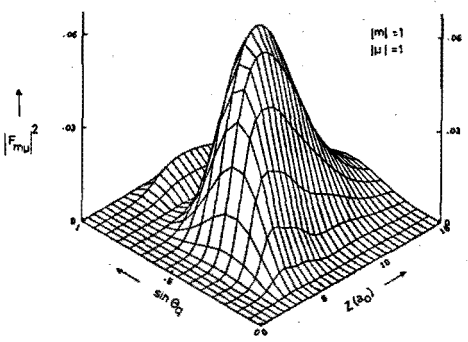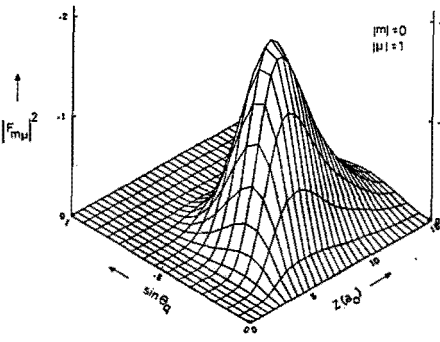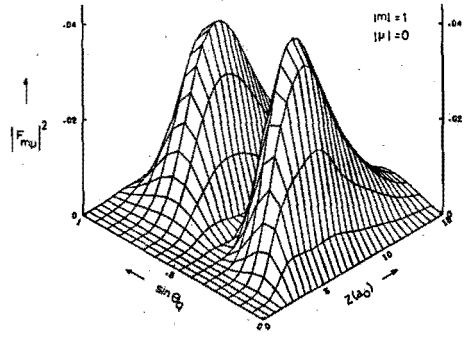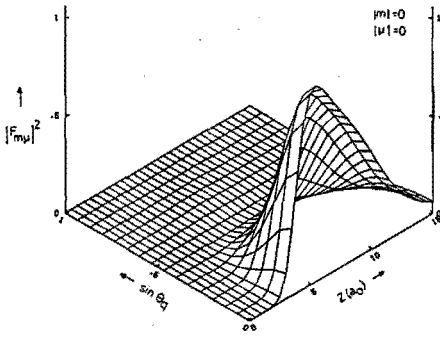
Fig. 4 Transition probability $|F_{m\mu}(Z,\theta_q)|^2$ as a function of Z, $\sin\theta_q$ for all $|m|$ (rotational angular momentum) and $|\mu|$ (angular momentum transfer) values. (B=7.6 T, α=0.15 a_0^{-1}, v=14, j=3, m_{s_3}=-½,). All surfaces are normalized relative to the maximum of the m=µ=0 surface.

bound states then depends only on Z. When the relative and center-of-mass motion are subsequently treated independently, this leads to a very simple relation between the surface and bulk rates

$$\tilde{L}_s^{eff} = \frac{4}{3}\tilde{\alpha}^2 L_g^{eff}. \tag{67}$$

At a field of 7.6 Tesla, where the Kagan dipole rate constant has the value $L_g^{eff}=6.8\times10^{-39}$ $cm^6 sec^{-1}$, this leads to $\tilde{L}_s^{eff} = 3.2\times10^{-24}$ $cm^4 sec^{-1}$ for the surface rate constant, which is a factor of 16 larger than our value $L_s^{eff} = 2.0\times10^{-25}$ $cm^4 sec^{-1}$ for B=7.6 T, $\theta=0$, T=0.4 K, $\alpha=0.15$ a_0^{-1} (and only a factor of 2 different from experiment).

We notice that the bound states ϕ_0 and $\tilde{\phi}_0$ of the two models are different. The widths Δz of the wavefunctions are comparable, however. To analyze the differences between the two models, we first try to find out how the result of our calculation is modified by replacing our ϕ_0 and α by $\tilde{\phi}_0$ and $\tilde{\alpha}$. This leads to an increase of L_s^{eff} by a factor 2.4, which indicates that the different choice of bound states is not the main reason for the large difference.

In the derivation of Eq. (67) by Kagan et al., the relative and center-of-mass motions are considered to be independent, which is not strictly justified, since all three-particle coordinates perpendicular to the surface should essentially be positive. This gives rise to restrictions in relative z coordinates, which have been taken into account correctly in our model, but not in the scaling procedure. If we introduce the same approximation in our calculation, this leads to another increase by a factor of 1.6. The remaining factor of 4.2 can only be accounted for by the two- and three-dimensional natures of the relative three-atom state, used in the two models.

As we already pointed out, Kagan et al. argue that the nature of this state should be three-dimensional when $d \gg \sigma$. However, a third length scale plays a crucial role: the wavelength λ. For $d \gg \lambda$ the well would indeed be wide enough to justify this approximation, especially near the interaction region. However, the actual situation is closer to the opposite limit: at 0.4 K the wavelength $\lambda \simeq 130$ a_0. In this situation the typical single-particle energy separation $\epsilon_0 = \hbar^2/(2m_H d^2)$ in the z-direction is larger than $4\pi^2\hbar^2/(m_H\lambda^2)$, the relative kinetic energy along the surface, thus impeding transitions in which the z-eigenstate ϕ_0 is changed. Freezing the ϕ_0 eigenstate in

the z-direction, however, is the basic assumption leading to the 2½D model. A 2½D approach therefore seems more appropriate than the limiting situation $\varepsilon_0 \ll (4\pi^2\hbar^2/(m_H\lambda^2)$ in which the atoms would behave unconfined also in the z-direction. This is also the main conclusion reached in previous more exact calculations[8-9] of b+b surface dipole relaxation.

To make the comparison of our surface recombination model with the scaling approach complete, we also replaced our 2D triplet functions in Eq. (56) by 3D ones. This indeed resolved the last factor of 4.2 discrepancy. It is of interest here to point to the radically different low-energy behaviors of 2D and 3D relative two-particle wavefunctions: 2D wavefunctions tend to zero logarithmically, as can be seen from Eq. (52), while 3D wavefunctions are finite in this limit. This feature expresses itself in the temperature dependence of $\langle G^2 \rangle_T$ (see Fig. 3) and thus represents a characteristic difference with the scaling result.

VIII. DISCUSSION OF SOME APPROXIMATIONS

In this section we estimate the errors introduced by some of the approximations in the previous sections. To begin with, we neglected the center-of-mass energy in the final state in Eq. (59). If we take it into account, it leads to a redistribution of the energy released by the recombination among the relative atom-molecule motion and the center-of-mass motion in the final state. As a result, we cannot use Parceval's theorem to simplify the calculation, but we have to use Eqs. (44) and (45) to calculate $L_s^{\pm\frac{1}{2}}$ and f. All equations presented in Sec. V remain valid, except for Eq. (63), which has to be replaced by

$$\ell_s^{\pm\frac{1}{2}}(\vec{B}) = (2\pi\hbar)^8 \sum_{vj} \frac{2\pi}{4m_H} \sum_{m\mu} \int_{-\infty}^{\infty} dP_Z \, q_f(P_Z) \int_{-1}^{1} d(\cos\theta_q)$$

$$\times \left| \int_{-\infty}^{\infty} dZ \frac{e^{-iP_Z Z/\hbar}}{(2\pi\hbar)^{1/2}} F_{m\mu}(\theta_q, Z) \right|^2 \left[d_{-\frac{3}{2} \mp \frac{1}{2}, \mu}^{(2)}(\theta) \right]^2. \tag{68}$$

keeping in mind that $F_{m\mu}$ also depends on P_Z through its dependence on $q_f(P_Z)$. Since the center of mass now absorbs part of the recombination energy, the average value of q_f decreases compared to the situation

before. Therefore the curve of the rate constant as a function of B, presented in Fig. 2, is expected to shift to lower field values. For B=7.6 T, T=0.4 K and field orientation perpendicular to the surface we now find $L_s^{eff} = 2.2 \times 10^{-25}$ cm^{4}sec^{-1}, which is a factor of 1.1 larger than the corresponding value given in Sec. VI. In Fig. 5 we present the effective rate constants averaged over field orientations as a function of B (full curve). Altogether we find a shift of the curve by about 1.5 Tesla, which corresponds to an average of 2.0 K for $P_Z^2/6m_H$. This is at least a factor of 20 smaller than $3q_f^2/4m_H$, the average relative kinetic energy. The expectation value of the kinetic energy $P_Z^2/6m_H$ in the initial state $\phi_0(z_1)\phi_0(z_2)\phi_0(z_3)$ is $\hbar^2\alpha^2/2m_H$ for the analytic choice of our bound state. This leads to a value of 2.0 K for the center-of-mass energy if $\alpha=0.15\ a_0^{-1}$, and is in agreement with the shift found here. Furthermore, the field dependence of the effective rate constant L_s^{eff} as a function of B found in Sec. VI, is
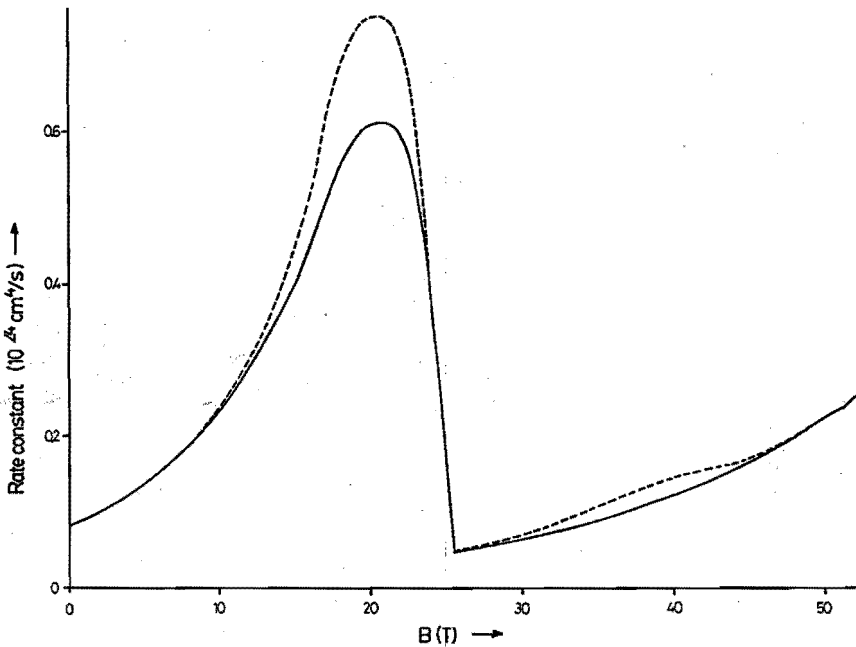
Fig. 5 *The field dependence of the effective rate constant averaged over field directions: Full curve: without wall, but center-of-mass energy in the z-direction taken into account. Broken curve: with rigid wall.*

hardly changed. The smallness of the effect is related to the small expectation value and spread in the center-of-mass energy compared to the relative kinetic energy.

The derivation of L_s and f in Secs. II and III included the inert wall in the final state. In Sec. V, however, the actual calculation was carried out without it. This might seem a very crude approximation, because the atom-wall interaction has a strong repulsive part for small distances. Therefore, we will now estimate the effect of this approximation. We improve the model described in Sec. V by assuming that the surface is a hard rigid wall. As we already explained, the shallow attractive part of the surface potential is neglected for the final state (but not for the initial state). The atom and molecule are now offered the possibility to reflect from this wall in the final state. In principle the molecule could be deexcited to states with higher binding energy by these collisions. This is not likely, however, because the additional energy released would give rise to higher final momenta, and a decreasing overlap with the initial state. Therefore we will only consider reflections of the center of mass of the molecule from the surface.

To compare with the case without a wall, we explicitly give the expressions for both models here. Without wall Eq. (44) can be rewritten as

$$L_s = (2\pi\hbar)^7 \frac{1}{4m_H} \sum_n \sum_\alpha \int d\varphi_q \int dp_{at,z} \int dp_{mol,z} \langle |f_{\vec{q}_f P_z n, \vec{P}_i \vec{q}_i \alpha}|^2 \rangle_{thermal}. \quad (69)$$

where the momenta perpendicular to the surface

$$
\begin{aligned}
P_{at,z} &= \frac{1}{3} P_Z + q_z \\
P_{mol,z} &= \frac{2}{3} P_Z - q_z
\end{aligned}
\quad (70)
$$

can be both positive and negative. The final state vector $|\psi^{(-)}(\vec{q}_f P_z n)\rangle_c$ in Eq. (47) for f is then given by Eq. (55), where the z-motion is described by

$$|P_{at,z}, P_{mol,z}\rangle \hat{=} \frac{e^{i p_{at,z} z_3/\hbar}}{(2\pi\hbar)^{1/2}} \frac{e^{i p_{mol,z} (z_1+z_2)/2\hbar}}{(2\pi\hbar)^{1/2}}. \quad (71)$$

In the case including the wall the integrals over $p_{at,z}$ and $p_{mol,z}$ in Eq. (69) run from 0 to ∞, because the particles can only move away from the surface. Furthermore, the plane-wave part Eq. (71) should be supplemented with "time-reversed" reflected waves of atom and molecule:

$$
\begin{aligned}
&|p_{at,z}, \; p_{mol,z}\rangle + |-p_{at,z}, \; -p_{mol,z}\rangle \\
&- |p_{at,z}, \; -p_{mol,z}\rangle - |-p_{at,z}, \; p_{mol,z}\rangle
\end{aligned}
\tag{72}
$$

For the following it is of importance to point out that we may now extend the ranges of integration of $p_{at,z}$ and $p_{mol,z}$ again to $(-\infty,\infty)$ if we multiply Eq. (69) by an additional factor ½. The total z wavefunction now vanishes for $z_3=0$ and for $\frac{1}{2}(z_1+z_2)=0$. We note that the integrals over z_3 and $\frac{1}{2}(z_1+z_2)$ in the expression for the amplitude F run over positive values only.

We were able to calculate the rate constant numerically for this case of a rigid wall. In Fig. 5 we plot the effective rate constant averaged over magnetic-field directions as a function of B at T=0.4 K for the case including the wall (broken curve). We see that the difference with the case without a wall is not significant. It is at most 20%. There is also no sign of change with respect to the field-orientation dependence. The similarity between these results can be explained as follows. In good approximation the four terms of Eq. (72) give rise to equal and non-interfering contributions to the transition probability, which add up to the original result. As a matter of fact, the main contribution of the terms comes from non-overlapping parts of the $(p_{at,z}, \; p_{mol,z})$-plane. As has been pointed out in the foregoing, small center-of-mass momenta in the z-direction are dominant. Therefore the dominant regions in the $(p_{at,z}, \; p_{mol,z})$-plane are the parts where $p_{at,z} \approx -p_{mol,z}$ $(p_{at,z}\rangle 0)$, $p_{at,z} \approx -p_{mol,z}$ $(p_{at,z}\langle 0)$, $p_{at,z} \approx p_{mol,z}$ $(p_{at,z}\rangle 0)$ and $p_{at,z} \approx p_{mol,z}$ $(p_{at,z}\langle 0)$ for the terms of Eq. (72), respectively. Because of the absence of high momenta along the surface, $p_{at,z}^2/2m_H + p_{mol,z}^2/4m_H$ is large for weaker fields. Consequently, the foregoing regions do not overlap, and do not interfere. For stronger fields this is no longer the case and the difference with the results without a wall is indeed observed to increase.

IX. CONCLUSION

In the foregoing we described a method, based on the Kagan dipole mechanism, for the calculation of the three-body dipolar recombination rate for atoms adsorbed on a ^{4}He film. The results can be summarized as follows: (1) At a field of 7.6 T and temperature of 0.4 K we obtained L_s^{eff}=2.7(7)×10^{-25} cm^{4}sec^{-1}, which is a about a factor of 6 smaller than the experimental value. (2) The field-orientation dependence of the effective rate constant is found to be weak, which agrees with experimental data. (3) We predict a strong increase of L_s^{eff} with increasing temperature between T=0.1 K and T=0.6 K. It might be interesting to include this in the analysis of the experiments. (4) The field dependence of L_g^{eff} calculated by Kagan and that of L_s^{eff} display a similar behavior and disagree both with the experimental B-dependence.

Although the model we presented here is far from exact, we believe that the essential features of the interaction of the particles with the wall are included. Some refinements to improve the model in connection with the influence of the inert wall have shown to be of minor importance. Part of the discrepancy with the experimental data may be ascribed to the dynamical role of the wall. However, since the magnetic-field dependence of the volume and surface rate constants display similar deviations, it is likely that the discrepancies in both cases are caused by the same mechanism. We have strong indications that the discrepancy in the volume case is caused by the neglect of interactions between the final state molecule and atom, in particular by the absence of exchange: a more rigorous calculation of volume recombination, in which all three-particle correlations are included except for exchange, lowers the rate constants to values a factor of 5 too small compared to the experimental data.[26] The physical picture underlying this correlation effect is the quenching of the dipole force at small distances due to repulsion. From the same physical picture we expect the above-mentioned factor of 6 surface discrepancy to show a further increase, when similar correlations would be taken into account. It seems probable that the dipole-exchange mechanism[22] is crucial to resolve the discrepancies for both volume and surface recombination. It remains to be seen,

however, whether a calculation including this mechanism would be feasible in the surface case, where a great part of the symmetry of the volume is lost.

ACKNOWLEDGEMENT

APPENDIX A

We here present a complete expression for the reduced amplitude $F_{m\mu}(\theta_q, Z)$ of Eq.(60) for fixed final state quantum numbers $\vec{q}_f$, v, j, m, m_{s_3}, and fixed μ, Z:

$$
\begin{aligned}
F_{m\mu}(\theta_q, Z) = {} & \frac{\frac{2}{3}m_H}{2\pi\hbar^2} \frac{2\delta_{j,\text{odd}}}{(2\pi\hbar)^2} (2\pi)^2 \frac{\mu_0\mu_B^2}{4\pi} \sqrt{\frac{12\pi}{5}} (1 - 3\delta_{m_{s_3}, \frac{1}{2}}) \\
& \times \int_{-3Z}^{3Z} dz_{12}\, e^{-iq_z z_{12}/2\hbar} \int_a^b dz_{13}\, e^{+iq_z z_{13}/\hbar}\, I_m(z_{12}, q_\parallel)\, K_\mu(z_{13}, q_\parallel) \qquad \text{(A1)} \\
& \times \phi_0(z_1)\phi_0(z_2)\phi_0(z_3).
\end{aligned}
$$

This includes the subsidiary conditions $z_1 \geq 0$ introduced in Sec. 4, which also lead to

$$
\begin{aligned}
a &= \min(-3Z - z_{12},\ -3Z + 2z_{12}), \\
b &= \frac{3}{2}Z + \frac{1}{2}z_{12}
\end{aligned}
\qquad \text{(A2)}
$$

Furthermore,

$$
\begin{aligned}
I_m(z_{12}, q_\parallel) &= \int_0^\infty d\rho_{12}\, \rho_{12}\, v_t(\rho_{12})\, J_m(q_\parallel \rho_{12}/2\hbar)\, \frac{\psi_{vj}(r_{12})}{r_{12}}\, Y_{jm}(\theta_{12}, 0), \\
K_\mu(z_{13}, q_\parallel) &= \int_0^\infty d\rho_{13}\, \rho_{13}\, v_t(\rho_{13})\, J_\mu(q_\parallel \rho_{13}/\hbar)\, \frac{Y_{2\mu}(\theta_{13}, 0)}{r_{13}^3}.
\end{aligned}
\qquad \text{(A3)}
$$

74

represent the uncoupled integrals along the surface, with $q_{\parallel} = q_f \sin\theta_q$ and $q_z = q_f \cos\theta_q$. The functions J_m are cylindrical Bessel functions and $\cos\theta_{ij} = z_{ij}/r_{ij}$. Finally, the energy-dependence in the f amplitude is concentrated in the function

$$G(\vec{k}'_{12}, \vec{k}'_{13}) = 2\left\{ g(k'_{12})g(k'_{13}) + g(k'_{13})g(|-\vec{k}'_{12}-\vec{k}'_{13}|) + g(k'_{12})g(|-\vec{k}'_{12}-\vec{k}'_{13}|)\right\}. \tag{A4}$$

REFERENCES

[1] F. London, *Superfluids* Vol. I (Dover, New York, 1961); Vol. II (Wiley, New York, 1954).

[2] T.J. Greytak and D. Kleppner, *New Trends in Atomic Physics*, Les Houches Summer School, 1982, Edited by G. Greenberg and R. Stora, (North-Holland, Amsterdam, 1984), p. 1125.

[3] I.F. Silvera and J.T.M. Walraven, *Progr. in Low Temp. Phys.*, edited by D.F. Brewer (North-Holland, Amsterdam, 1985) Vol. X, p. 139.

[4] B.W. Statt and A.J. Berlinsky, Phys. Rev. Lett. $\underline{45}$, 2105 (1980).

[5] A. Lagendijk, Phys. Rev. B $\underline{25}$, 2054 (1982).

[6] A.E. Ruckenstein and E.D. Siggia, Phys. Rev. B $\underline{25}$, 6031 (1982).

[7] B.W. Statt, Phys. Rev. B $\underline{25}$, 6035 (1982).

[8] R.M.C. Ahn, J.P.H.W. van den Eijnde, C.J. Reuver, B.J. Verhaar and I.F. Silvera, Phys. Rev. B $\underline{26}$, 452 (1982).

[9] J.P.H.W. van den Eijnde, C.J. Reuver, and B.J. Verhaar, Phys. Rev. B $\underline{28}$, 6309 (1983).

[10] M. Papoular, J. Phys. B: At. Mol. Phys. $\underline{18}$, L821 (1985).

[11] Yu. Kagan, I.A. Vartan'yants and G.V. Shlyapnikov, Zh. Eksp. Teor. Fiz. $\underline{81}$, 1113 (1981), [Sov. Phys. JETP $\underline{54}$, 590 (1981)].

[12] H.F. Hess, D.A. Bell, G.P. Kochanski, D. Kleppner, and T.J. Greytak, Phys. Rev. Lett. $\underline{52}$, 1520 (1984).

[13] M.W. Reynolds, I. Shinkoda, W.N. Hardy, A.J. Berlinsky, F. Bridges, and B.W. Statt, Phys. Rev. B $\underline{31}$, 7503 (1985); B.W. Statt, W.N. Hardy, A.J. Berlinsky, and E. Klein, J.L.T.P. $\underline{61}$, 471 (1985); B.W. Statt, A.J. Berlinsky, and W.N. Hardy, Phys. Rev. B $\underline{31}$, 3169 (1985).

[14] L.P.H. de Goey, J.P.J. Driessen, B.J. Verhaar, and J.T.M. Walraven, Phys. Rev. Lett. $\underline{53}$, 1919 (1984).

[15] Yu. Kagan, G.V. Shlyapnikov, I.A. Vartan'yants, and N.A. Glukhov, Zh. Eksp. Teor. Fiz. $\underline{81}$, 1131 (1981), [Sov. Phys. JETP Lett. $\underline{35}$, 477 (1982)].

[16] W. Glöckle, *The Quantum Mechanical Few-Body Problem* (Springer-Verlag, Berlin, 1983).

[17] S. Hess, Z. Naturforschung $\underline{22A}$, 1871 (1967).

[18] Y.L. Klimontovich and D. Kremp, Physica $\underline{109A}$, 517 (1981).

[19] J.A. McLennan, J. of Stat. Phys. **28**, 257 (1982).

[20] R. Goosen, Eindhoven University of Technology, Department of Physics, Internal Report (1985).

[21] L.D. Faddeev, Zh. Eksp. Teor. Fiz. **39**, 1459 (1961) [Sov. Phys. JETP **12**, 1014 (1961)].

[22] L.P.H. de Goey, T.H.M. v.d. Berg, N. Mulders, H.T.C. Stoof, B.J. Verhaar and W. Glöckle, Phys. Rev. B **34**, 6183 (1986) (Chapter 4).

[23] B.J. Verhaar, J.P.H.W. van den Eijnde, M.A.J. Voermans and M.M.J. Schaffrath, J. Phys. A **17**, 595 (1984); J.P.H.W. van den Eijnde, Ph. D. Thesis, Eindhoven University of Technology, 1984; B.J. Verhaar, L.P.H. de Goey, J.P.H.W. van den Eijnde and E.J.D. Vredenbregt, Phys. Rev. A **32**, 1424; 1430 (1985) (Chapters 7 and 8); B.J.Verhaar, L.P.H. de Goey, E.J.D. Vredenbregt and J.P.H.W. van den Eijnde, Phys. Lett. A **110**, 371 (1985) (Chapter 6).

[24] I.B. Mantz and D.O. Edwards, Phys. Rev. B **20**, 4518 (1979).

[25] R. Sprik, J.T.M. Walraven, G.H. v. Yperen, and I.F. Silvera, Phys. Rev. B **34**, 6172 (1986).

[26] L.P.H. de Goey, H.T.C. Stoof, B.J. Verhaar and W. Glöckle, submitted for publication (Chapter 5).

Three-body recombination in spin-polarized atomic hydrogen

L. P. H. de Goey, T. H. M. v. d. Berg, N. Mulders, H. T. C. Stoof, and B. J. Verhaar
Department of Physics, Eindhoven University of Technology, Eindhoven, The Netherlands

W. Glöckle
Institut für Theoretische Physik, Ruhr-Universität Bochum, Bochum, West Germany
(Received 4 March 1986)

In view of the failure of the Kagan dipole mechanism to explain the magnetic field dependence of the H+H+H recombination rate in spin-polarized atomic hydrogen, we consider an additional process, the so-called dipole-exchange mechanism. Two simple approaches to estimate its consequences turn out to be promising but the question of the role of different and higher-order processes remains open. We therefore turn to in principle, an exact approach to the three-body recombination, including all possible processes. The first numerical results of the approach are presented.

I. INTRODUCTION

In several laboratories experiments are being carried out with the ultimate aim of achieving Bose-Einstein condensation in spin-polarized atomic hydrogen (H↓). For these attempts to be successful, it is of vital importance to understand the decay mechanisms in H↓ samples. Former belief that the decay at low temperatures found in "precompression" experiments was due to two-body surface relaxation[1] led to large discrepancies between theory and experiment. Hess et al.[2] first came up with the interesting suggestion, that these discrepancies might be resolved, if three-body processes were taken into account. At high magnetic fields in the doubly polarized regime (both electron and proton spins polarized), where only b atoms (a,b,c,d are hyperfine levels of ground-state atomic hydrogen in order of increasing energy) are present, they found three-body rates of $L_g = 7.5(3) \times 10^{-39}$ cm^{6}s^{-1} in the volume, and $L_s = 2.0(6) \times 10^{-24}$ cm^{4}s^{-1} at the surface at $B = 7.6$ T, both decreasing slightly with magnetic field B.

Since it is now believed that this decay process represents the main obstacle on the way to achieve Bose-Einstein condensation, it seems worthwhile to find out by which mechanism(s) it takes place. In Sec. II the Kagan dipole mechanism,[3] the first mechanism proposed for a bbb three-body process is reviewed both for the volume[3] and for the surface.[4] The absolute magnitude of L_s is too small by an order of magnitude, and, more important, both L_g and L_s have a field dependence different from experiment. We therefore try to find an additional recombination mechanism both for the volume and the surface with a different B dependence, dominating the Kagan dipole mechanism for the volume and strongly dominating in the surface case. The most promising approach would be to first solve the volume discrepancy. Once that recombination process is understood, it may be easier to deal with the surface. In Sec. III we therefore introduce a new mechanism, the socalled dipole-exchange mechanism, by which we hope to resolve the discrepancy. We find, however, that a naive approach to calculate its contribution

leads to an overestimate by more than an order of magnitude. On the basis of this we then turn to an approach which treats the three-body aspects exactly. This is described in Sec. IV. In Sec. V the first numerical results of this approach are shown. A discussion follows in Sec. VI.

II. KAGAN DIPOLE MECHANISM

We consider the recombination of two H atoms in a three-body collision, taking place in a strong external magnetic field. As first discussed by Kagan et al.,[3] with all three atoms doubly polarized, this recombination is caused by an electron-electron magnetic dipole interaction. The idea is that the electron spins of two atoms precess in the magnetic dipole field of a third H atom, thus getting a total $S = 0$ component, whereafter recombination is possible. The proton spins are unaffected during the process. The third atom is not only needed for this socalled spin flip, but also for conservation of the energy released during the recombination:

$$\frac{q_f^2}{2(\tfrac{2}{3}m_H)} = -E_{vj} - 2\mu_B B \quad (T \to 0) . \tag{1}$$

Here $-E_{vj}$ is the binding energy of the molecule in the final state with vibrational and rotational quantum numbers v and j, $2\mu_B B$ is the Zeeman energy needed for a single spin-flip process, μ_B is the Bohr magneton and q_f is the relative momentum of atom (mass m_H) and molecule. We shall restrict ourselves to $T \to 0$ calculations. In Eq. (1) and in the following we restrict ourselves for simplicity to the socalled single spin-flip process. With some obvious changes, such as the replacement of $2\mu_B B$ by $4\mu_B B$, similar expressions hold for double spin flip.

The most appealing feature of the calculation of Kagan et al. is its simplicity. The starting point is the exact "post form,"

$$f^{\sigma}_{vjm}(\mathbf{q}_f) = \frac{m_H/9}{2\pi\hbar^2}\left\langle \phi_f \left| \sum_{k=2}^{3} V_k^d + \sum_{k=2}^{3} V_k^e \right| S\Psi_i^+ \right\rangle , \tag{2}$$

---

34   6183   ©1986 The American Physical Society

for the scattering amplitude, vjm being the molecular quantum numbers (m is the magnetic quantum number), while σ_f is the final spin projection of the atom along **B**. Here V_k^d and V_k^c are the dipole and central interactions between the atoms of pair k (particles m and n with $m \neq k$ and $n \neq k$). The initial state Ψ_i^+, symmetrized using the symmetrization operator S (sum over six permutations without normalization coefficient), is in the first instance an exact scattering state of the total system, describing three atoms approaching one another with momenta which are considered to be small. The plane-wave part of Ψ_i^+ is normalized as an exponential with coefficient $(2\pi\hbar)^{-3}$. In Eq. (2), ϕ_f describes the free motion of atom 1 and the molecule consisting of atoms 2 and 3. Again its plane-wave factor is the usual exponential with coefficient $(2\pi\hbar)^{-3/2}$.

In terms of the amplitudes (2) the rate constant L_g for volume recombination has the form

$$L_g = \left\langle \sum_{v,j,m\sigma_f} \frac{9q_f}{m_H} (2\pi\hbar)^9 \int d\hat{q}_f \, |f_{vjm}^{\sigma_f}(q_f)|^2 \right\rangle_{\text{thermal}} \quad (3)$$

where the integral is an angular integral over directions of q_f. The corresponding expression for surface recombination has been given in Ref. 4.

Starting from Eq. (2) we now introduce the approximations of Kagan *et al.* The amplitude is calculated to first order in the weak dipole interaction, which is only taken into account in the form of the operator connecting initial and final state. A far-reaching simplification for Ψ_i^+ would consist of replacing it by its exponential free part. Instead Kagan *et al.* introduce some of the distortions, but in such a way that the final expression can still be handled fairly easily. Insofar as the initial state is operated upon by V_2^d, they consider the distortions of the relative motion of atom pair 2 as essential, as well as the distortion of the pair 1, since this pair is bound as a molecule in the final state. With this in mind they write the free exponential as a product of two exponentials in the corresponding relative coordinates and subsequently replace the exponentials by the corresponding distorted waves Ψ_t. The term with V_3^d is handled similarly. The contributions of the two terms cancel for $j=$even and are equal for $j=$odd.

Using these approximations the amplitude separates into two spatial matrix elements:

$$f_{vjm}^{\sigma_f}(q_f) = C_j \langle \Psi_{vjm} \,| e^{iq_f \cdot r/2\hbar} | \Psi_t \rangle_1 \langle q_f | V_\sigma^d | \Psi_t \rangle_2 , \quad (4)$$

where V_σ^d represents the spatial part of the dipole interaction: $Y_{2,-1}(\hat{r})/r^3$ or $-2Y_{2,-2}(\hat{r})/r^3$ for $\sigma = -\frac{1}{2}$ or $\sigma = +\frac{1}{2}$, respectively, while

$$C_j = -\frac{1}{(15\pi^3)^{1/2}} \frac{\mu_0 \mu_B^2 m_H}{\hbar^2} \delta_{j,\text{odd}} . \quad (5)$$

The subscripts to the matrix elements in Eq. (4) indicate the particle pair to which each of the matrix elements applies. The second factor describes the action of the dipole interaction among particles 1 and 3 (1 and 2) giving rise to final momentum q_f. The free relative state $|q_f\rangle$ is again normalized as an exponential with coefficient $(2\pi\hbar)^{-3/2}$.
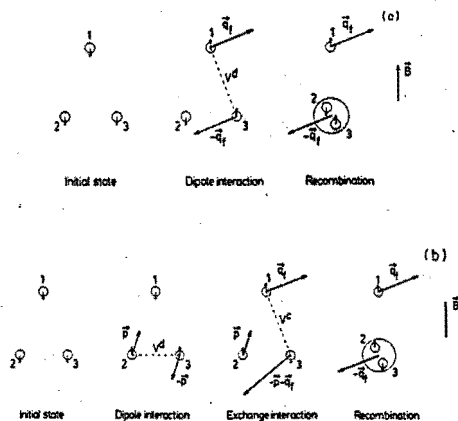

FIG. 1. (a) Graphical representation of the Kagan dipole process. The long arrows represent the momenta of the particles after the various stages of the process displayed. The short arrows represent spin angular momenta. (b) Graphical representation of the dipole-exchange process. Long arrows: momenta. Short arrows: spins.

The first factor describes the corresponding momentum change of particles 2 and 3 and the overlap with the final molecular state. A graphical representation of this so-called Kagan-mechanism is given in Fig. 1(a). Momenta are indicated by long arrows, spins by short arrows. In contrast to the equations in this paper, Figs. 1(a) and 1(b) illustrate double spin flip, which is somewhat easier to visualize.

The dipole interaction turns out to introduce only small momentum changes. Since q_f goes down with increasing B, the momentum mismatch decreases, leading the amplitude to increase in magnitude with B. The approach of Kagan *et al.* leads to a volume rate of $L_g = 8.5 \times 10^{-39}$ cm^{6}s^{-1} at $B=10$ T and $T=0$, increasing with B by a factor of 3 from 4–9 T.

The rate of this Kagan mechanism was also calculated for the surface case by de Goey *et al.*,[4] who found $L_s = 1.3 \times 10^{-25}$ cm^{6}s^{-1} at $B=7.6$ T and $T=0.4$ K, increasing by 70% from 4 to 9 T. The increase of these rates as a function of B, contrary to the experimental field dependence, has led us to investigate other mechanisms with non-negligible rate.

III. DIPOLE-EXCHANGE MECHANISM

An essential feature of the Kagan dipole mechanism is that the two particles, interacting via the dipole interaction cannot recombine, because this interaction only permits $S=1$ to $S=1$ transitions. The idea behind the dipole-exchange mechanism is that recombination between these particles is made possible, after that one parti-

cle has meanwhile changed its spin state by interaction with a third one via a strong exchange (triplet or singlet) interaction [see Fig. 1(b)].

We have estimated the rate for this process in two ways. The first one is a Kagan-like approach, the second one is an impulse-approximation-like calculation. We will discuss them in this order.

The idea of the first approach is to follow the approach of Kagan et al.[3] for exchange recombination, e.g., for aab scattering, but to consider dipole distorted states for the recombining atoms instead of hyperfine distorted states. We write the amplitude again as Eq. (2), but now we con-

sider the remaining part of the operator consisting of the central interactions. The initial state Ψ_i^+ is now approximated to first order in the dipole interaction. Following Kagan et al. we replace Ψ_i^+ by a product of two triplet wave functions. The triplet function describing the initial motion of the recombining particles, is distorted with a dipole interaction. This changes Ψ_t into Ψ_t^d and produces the necessary spin flip(s), but no change of S. The subsequent spin exchange due to the V_2^c and V_3^c operators enables atoms 2 and 3 to recombine.

The amplitude for single spin flip ($\sigma_f = -\frac{1}{2}$) can now be written as [cf. Ref. 3 and Eq. (4)]

$$f_{vjm}^{\sigma_f=-1/2}(q_f) = \frac{1}{2}C_j\langle\Psi_{vjm}|e^{iq_f\cdot r/2\hbar}|\Psi_t^d\rangle_1\langle q_f|V^c|\Psi_t\rangle_2$$

$$= \frac{1}{2}C_j\int dp\langle\Psi_{vjm}|\frac{1}{2}q_f+p\rangle_1\langle q_f|V^c|\Psi_t\rangle_2\frac{1}{(p^2/m_H)+2\mu_BB}\langle p|V_\sigma^d|\Psi_t\rangle_1. \qquad (6)$$

Here $\langle q_f|V^c|\Psi_t\rangle_2$ and $\langle p|V_\sigma^d|\Psi_t\rangle_1$ represent the action of central and dipole interactions, leading to final momenta q_f and p, respectively. Furthermore, $\langle\Psi_{vjm}|\frac{1}{2}q_f+p\rangle_1$ is the overlap of the resulting state with momentum $\frac{1}{2}q_f+p$ of the recombining atom pair with the final molecular state. The energy denominator represents the free propagation in between the interactions. Figure 1(b) illustrates this approach, except for the p contribution to the momenta of the atoms 2 and 3, which for the time being is left out in the V^c matrix element. In a way, therefore, the present approach deals with the dipole and exchange interaction as parallel processes in sofar as the spatial degrees of freedom are concerned. For the spin degrees of freedom the order of the processes is as indicated in Fig. 1(b). Results for L_g are given in Fig. 2(a).

To introduce the second approach we first note that the V^c matrix element in Eq. (6) can be written as

$$\langle q_f|V^c|\Psi_t\rangle_2 = \langle q_f|t^c|0\rangle_2 \quad (T\to0). \qquad (7)$$

Writing it in such a way it indeed becomes clear that the momentum change of particle 3 in the dipole process is not taken into account in the subsequent exchange process. With this in mind we replace the t^c matrix element by $\langle q_f+\frac{1}{2}p|t^c|\frac{1}{2}p\rangle_2$:

$$f_{vjm}^{\sigma_f=-1/2}(q_f) = \frac{1}{2}C_j\int dp\langle\Psi_{vjm}|\frac{1}{2}q_f+p\rangle_1$$

$$\times\langle q_f+\frac{1}{2}p|t^c|\frac{1}{2}p\rangle_2$$

$$\times\frac{1}{(p^2/m_H)+2\mu_BB}\langle p|V_\sigma^d|\Psi_t\rangle_1. \qquad (8)$$

The replacement of $|0\rangle$ by $|\frac{1}{2}p\rangle$ introduces higher partial waves. For even (odd) partial waves contained in $|\frac{1}{2}p\rangle$, t^c is effectively a triplet (singlet) t matrix. As we shall see in Sec. IV this expression (8), with $|\Psi_t\rangle$ replaced by the free state $|0\rangle$ in the V^d matrix element, would be

obtained as one of the first-order terms in the expansion for the exact transition amplitude in powers of t^c. However, we do not base our analysis on such an expression, since replacing $|\Psi_t\rangle$ by $|0\rangle$ would lead to a strong unphysical increase of the amplitude: the triplet repulsion does no longer damp the small-distance $1/r^3$ dependence of V^d. Figure 1(b), now with the p contributions included, is a graphical representation of this second approach (8) for the dipole-exchange mechanism. The resulting L_g is presented in Fig. 2(b). The field range in this case has been restricted to 0—10 T. Note that the energy argument of the t^c matrix in Eq. (8) is the energy $-2\mu_BB-p^2/2m_H$ of the free intermediate state for pair 2, whereas in the first approach it has value 0. It thus becomes clear that the exchange process in the first approach does not take advantage of the relative momentum $\frac{1}{2}p$ acquired by the atoms 1 and 3 through the dipole interaction. As a consequence only the s-wave part of the relative pair 2 wave function participates in the exchange process. In addition the Zeeman energy for the spin flip(s) is produced by the dipole pair only, contrary to the second approach, where it is produced by all three particles.

These differences explain the much higher rate for the second approach. At a field of 8 T we find $L_g = 2.8\times10^{-40}$ cm^{6}s^{-1} and $L_g = 4.0\times10^{-38}$ cm^{6}s^{-1} for the first and second approach, respectively.

Turning from the absolute magnitude to the field dependence, we repeat that the dipole interaction can induce only small momentum changes. Therefore the integrals in Eqs. (6) and (8) are restricted to small p. Because of this we expect the rates to decrease with the field, mostly due to the denominator of the free propagator in Eqs. (6) and (8). This indeed appears to be the case. However, this field dependence is distorted in the first calculation by an additional zero of the exchange matrix element at $B=6$ T for the double spin-flip process and at $B=12$ T for the single spin-flip process [see Figs. 2(a) and 2(b)].

81

nothing happens with the other one, before the dipole interaction takes place. But this is very unlikely, especially for small q_f. The atom collides most probably with the molecule as a whole. In other words, rescattering processes, which are higher order in the t^c matrix, are important.

The shortcomings of the simple approaches (one underestimating the rate, caused by the approximations involved, the other giving rise to an overestimated rate, pointing to the fact that higher-order rescattering effects are important) force us to conclude that we are in need for a more exact three-body calculation, with all mechanisms and higher-order terms included. On the other hand, the field dependence found here gives us hope that the exact calculation will also give rise to a decreasing field dependence (higher-order rescatterings give rise to more free propagators with field B in the denominator). Such an approach is discussed in the remaining sections.

IV. EXACT THREE-BODY CALCULATION

In this section we describe a method for carrying out a three-body calculation of the *bbb* dipolar recombination process based on the Faddeev formalism,[6] in which the three-body aspects are dealt with exactly. In this calculation we take into account the strong central (singlet and triplet) interactions to all orders. The dipole interaction, however, only to first order. This is a very good approximation, because of the weakness of this interaction.[7]

Doing this, we can write the transition amplitude as

$$f^{\sigma_f}_{vjm}(\mathbf{q}_f) = \frac{m_H/54}{2\pi\hbar^2}\left\langle S\Psi_f^- \left| \sum_{k=1}^{3} V_k^d \right| S\Psi_i^+ \right\rangle . \quad (9)$$

Here, $|\Psi_i^+\rangle$ and $|\Psi_f^-\rangle$ are the initial and final states of the process, with central interactions taken into account to all orders, normalized as in the previous sections. We define the Faddeev components $|X_j\rangle$ as

$$G_0(E)V_j^c(1+P)|\Psi\rangle , \quad j=1,2,3 ,$$

where

$$|\Psi\rangle = (1+P_{23})|\Psi_i^+\rangle$$

for the initial state and

$$|\Psi\rangle = (1+P_{23})|\Psi_f^-\rangle$$

for the final state, P_{jk} standing for a permutation of particles j and k and P for $P_{12}P_{23}+P_{13}P_{23}$ (see Ref. 8). Also, $G_0(E) = 1/(E-H_0)$ is the free propagator, H_0 being the free Hamiltonian, and E the total energy, both including Zeeman energy. The states $|X_j\rangle$ obey the Faddeev equations. For identical particles these equations reduce to equations, identical for all components. For $|X\rangle = |X_j\rangle$ this equation reads

$$|X\rangle = |\phi\rangle + G_0(E)t_1^c(E)P|X\rangle , \quad (10)$$

$t_1^c(E)$ being the central interaction t operator for pair 1. The driving term $|\phi\rangle = (1+P_{23})|\Psi_{vjm}\mathbf{q}_f\sigma_f\rangle_1$ describes the free motion of the molecule (pair 1) and atom 1 in spin state σ_f with relative momentum $\mathbf{q}_f$, when Eq. (10) is the Faddeev equation of the final state. For
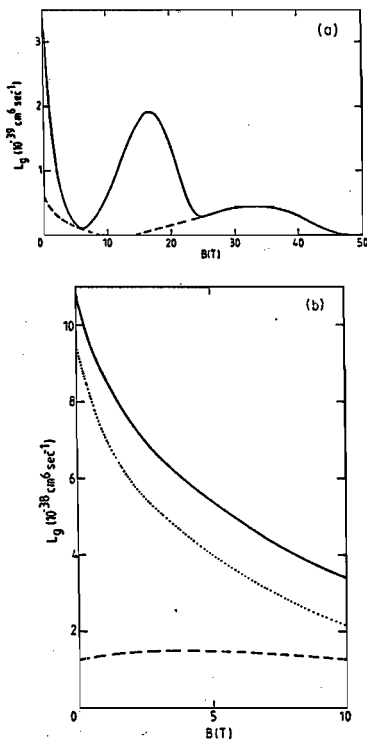

FIG. 2. (a) Three-body recombination rate L_g as a function of magnetic field B for the Kagan-like approach of the dipole-exchange process. The dashed curve represents the single spin-flip contribution, the full curve the sum of single and double spin-flip contributions. (b) Three-body recombination rate L_g as a function of B for the impulse-approximation-like approach of the dipole-exchange process. The dashed and dotted curves represent the contributions of the $v=14$, $j=3$ and $v=14$, $j=1$ final states to the total rate, respectively. The total rate is displayed by the full curve.

It may seem surprising that the rate of the second calculation is so large, roughly a factor of 5 larger than that of the Kagan dipole calculation. (This factor of 5 even increases to a factor of 20 if also other dipole-exchange terms are taken into account where the dipole interaction takes place between pair 2 if exchange occurs between pair 3 and vice versa.) Such large discrepancies seem to be common for calculations based on the impulse approximation.[5] This can be understood as follows. Considering the time-inversed process, i.e., the break-up process of a molecule colliding with an atom with relative momentum $-\mathbf{q}_f$, our impulse-like approximation means that the atom collides only with one atom of the molecule, while

the Faddeev equation of the initial state $|\phi\rangle$ $=(1+P_{23})|p_0^+q_0bbb\rangle_1$, describing pair 1 to be in a central interaction scattering state with momentum p_0 and atom 1 moving freely with momentum q_0 relative to pair 1. As usual the $+$ sign describes outgoing wave boundary conditions at infinity. For $T\rightarrow 0$, the momenta p_0 and q_0 go to zero. The symmetrized states $S|\Psi_i^+\rangle$ and $S|\Psi_f^-\rangle$ in Eq. (9) can finally be found from the corresponding Faddeev components by operating with $1+P$.

To solve the above-mentioned two versions of Eq. (10) it is useful to introduce the angular-momentum basis[8] $|pq\alpha\rangle_j=|pq(l\lambda)LM_L(s\frac{1}{2})SM_S\rangle_j$, where p represents the magnitude of the relative momentum p of pair j, l their relative angular momentum quantum number, s their total spin quantum number, q the absolute magnitude of the relative momentum q of particle j with respect to pair j and λ the associated angular momentum quantum number, while LM_LSM_S stand for orbital and spin quantum numbers of the total system. Unless stated otherwise, this basis will be used with j equal to 1. For simplicity we therefore in general suppress the subscript 1.

In this basis the t operator for pair 1 in the three-particle space becomes

$$\langle pq\alpha|t_1^c(E)|p'q'\alpha'\rangle$$

$$=t_{\check{s}}^{\xi}\left[p,p',E-\frac{3q^2}{4m_H}-2\mu_BBM_S\right]\frac{\delta(q-q')}{q^2}\delta_{\alpha\alpha'},$$

$$\tag{11}$$

where $t_{\check{s}}^{\xi}(p,p',z)$ is the t matrix in the two-particle space:

$$\langle plm_lsm_s|t^c(z)|p'l'm_l's'm_s'\rangle$$

$$=\delta_{ll'}\delta_{m_lm_l'}\delta_{ss'}\delta_{m_sm_s'}t_{ls}^{\xi}(p,p',z). \tag{12}$$

The basis $\{|plm_lsm_s\rangle\}$ with m_l and m_s denoting orbital and spin magnetic quantum numbers, is normalized according to

$$\langle plm_lsm_s|p'l'm_l's'm_s'\rangle=\frac{\delta(p-p')}{p^2}\delta_{ll'}\delta_{m_lm_l'}\delta_{ss'}\delta_{m_sm_s'}.$$

$$\tag{13}$$

The functions t_{ls}^{ξ} can be calculated with the Lippmann-Schwinger equation

$$t_{ls}^{\xi}(p,p',z)=V_{ls}^{\xi}(p,p')+\int_0^{\infty}dp''\frac{(p'')^2}{z-(p'')^2/m_H}$$

$$\times V_{ls}^{\xi}(p,p'')t_{ls}^{\xi}(p'',p',z), \tag{14}$$

V_{ls}^{ξ} being the "Fourier transform" of the singlet or triplet interactions normalized according to an equation analogous to Eq. (12). For energies $z\leq 0$, which are the only values appearing in the Faddeev equations for our initial and final states ($T\rightarrow 0$), the integral in Eq. (14) is regular and causes no problems. This one-dimensional integral equation can be solved by matrix inversion. When the energy $z=E-(3q^2/4m_H)-2\mu_BBM_S$ equals the energy E_{vl} of a two-particle bound state $v,j=l$, the t matrix has a pole in the singlet case $(s=0)$. We come back to this problem shortly.

In the angular-momentum basis the particle permutation operator P in Eq. (10) has the representation[8]

$$\langle pq\alpha|P|p'q'\alpha'\rangle={}_1\langle pq\alpha|p'q'\alpha'\rangle_2+{}_1\langle pq\alpha|p'q'\alpha'\rangle_3=\int_{-1}^{1}dx\frac{\delta(\pi_1-p)}{p^{l+2}}\frac{\delta(\pi_2-p')}{(p')^{l'+2}}G_{\alpha\alpha'}(q,q',x), \tag{15}$$

with $\pi_1=[(q')^2+(q^2/4)+qq'x]^{1/2}$, $\pi_2=[q^2+[(q')^2/4]+qq'x]^{1/2}$, and

$$G_{\alpha\alpha'}(q,q',x)=\sum_{k=0}^{\infty}P_k(x)\sum_{l_1+l_2=l}\sum_{l_1'+l_2'=l'}q^{l_2+l_1'}q'^{l_1+l_2'}g_{\alpha\alpha'}^{kl_1l_2l_1'l_2'}. \tag{16}$$

The functions $P_k(x)$ are Legendre polynomials of the cosine x of the angle between q and q' and $g_{\alpha\alpha'}^{kl_1l_2l_1'l_2'}$ is the so-called geometrical factor, a complicated expression in terms of 3-j and 6-j symbols, for which we refer to Glöckle's monograph[8].

The remaining operator $G_0(E)$ in Eq. (10) has a simple form in the basis $|pq\alpha\rangle$:

$$\langle pq\alpha|G_0(E)|p'q'a'\rangle=\left[E-\frac{p^2}{m_H}-\frac{3q^2}{4m_H}-2\mu_BBM_S\right]^{-1}\frac{\delta(p-p')}{p^2}\frac{\delta(q-q')}{q^2}\delta_{\alpha\alpha'}. \tag{17}$$

For low temperatures, the energy $E=(p_0^2/m_H)+(3q_0^2/4m_H)-3\mu_BB<0$ approaches the energy for three polarized electron spins. Therefore for the final state, where $M_S=\pm\frac{1}{2}$, the energy factor in large parentheses in Eq. (17) is nonvanishing. For the initial state, on the other hand, the denominator vanishes when $p^2+3q^2/4=p_0^2+3q_0^2/4$. This leads to singularities[9] in the kernel of the Faddeev equation (10). For $T\rightarrow 0$, however, the contribution of the singularities goes to zero continuously. We will come back to this problem shortly.

Equation (10) is a two-dimensional integral equation. The dimension of the kernel $G_0t_1^cP$ is too large to solve the equation by matrix inversion. Instead, we solve it by iteration (if the Neumann-series diverges, it is summed using Padé's method[10]). The successive terms in the series build in scattering correlations between the particles. Note that the final state $|\phi_f\rangle$ in our previous discussion of the Kagan dipole mechanism [see Eq. (2)] is just the driving term $|\phi\rangle$ of the Faddeev equation for the final state. The first iterated term $G_0t_1^cP|\phi\rangle$ is the state on

the left-hand side of the dipole interaction in the treatment of the dipole-exchange mechanism (Sec. III).

The advantage of the Faddeev equation is that its kernel is compact so that it has a unique solution.[11] The driving term $|\phi\rangle$, however, in general contains δ functions, which one cannot discretize. Therefore, instead of working with $|X\rangle$ we use another state $|\widetilde{X}\rangle$. For the final state we write $|\widetilde{X}\rangle = |X\rangle - |\phi\rangle$, which obeys

$$|\widetilde{X}\rangle = G_0 t_1^c P |\phi\rangle + G_0 t_1^c P |\widetilde{X}\rangle . \qquad (18)$$

The driving term in this equation no longer contains δ functions. The driving term of the Faddeev equation of the initial state may be written as

$$|\phi\rangle = (1 + G_0 t_1^c)(1 + P_{23}) |\phi_0\rangle$$

$$= (1 + G_0 t_1^c)(1 + P_{23}) |p_0 q_0 bbb\rangle , \qquad (19)$$

where $|\phi_0\rangle$ describes the free motion of three polarized atoms. We now define $|\widetilde{X}\rangle$ as $|X\rangle - (1 + P_{23}) |\phi_0\rangle$ $- G_0 t_1^c S |\phi_0\rangle$ and find $|\widetilde{X}\rangle$ to obey the Faddeev equation

$$|\widetilde{X}\rangle = G_0 t_1^c P G_0 t_1^c S |\phi_0\rangle + G_0 t_1^c P |\widetilde{X}\rangle . \qquad (20)$$

Once again δ functions have been eliminated from the driving term.

In Eqs. (18)–(20), G_0 and t_1^c have energy arguments E. Because of the poles of the t matrix (11) for $l=j$ at $(3q^2/4m_H) = E - E_{vl} - 2\mu_B BM_S$, the kernel of the Faddeev equation (18) for the final state is irregular. These poles also occur in the solution $|\widetilde{X}\rangle$. The physical meaning of these poles in the solution is that they are associated with waves extending to infinity in all open (elastic and inelastic) channels corresponding to the possible molecular states vj. The poles are handled in the following way. We define a new state $|\widehat{X}\rangle$ by splitting off the pole factor from $|\widetilde{X}\rangle$:

$$\langle pq\alpha | \widehat{X}\rangle = \langle pq\alpha | \widetilde{X}\rangle$$

$$\times \prod_p \left[E - \frac{3q^2}{4m_H} - E_{vl} - 2\mu_B BM_S - i\epsilon \right], \quad (21)$$

in which the product runs over all bound states with energy $E_{vl} < E - 2\mu_B BM_S$ for a certain angular momentum l. The poles in the driving term of Eq. (18) are eliminated in this way, but those in the kernel in the new integral equation for $|\widehat{X}\rangle$ are not. The latter, however, can be handled by writing its kernel as a sum over individual pole terms and subsequently dealing with a pole at a specific q value q' by means of the following equation:

$$\int_0^\infty dq \frac{f(q)}{q^2 - (q')^2 - i\epsilon} = \int_0^\infty dq \frac{f(q) - f(q')}{q^2 - (q')^2}$$

$$+ f(q') \int_0^\infty dq \frac{1}{q^2 - (q')^2 - i\epsilon} \qquad (22)$$

for some regular function $f(q)$. Here the integrand of the first integral in the *rhs* is regular and the second term is easily calculated to be $-f(q')\pi i/2q'$.

The propagator G_0 in the initial state equation (20) gives rise to a singular behavior. Therefore we introduce a state $|\widehat{X}\rangle = (E - H_0) |\widetilde{X}\rangle$ for which we finally have the

following Faddeev equation

$$|\widehat{X}\rangle = t_1^c P G_0 t_1^c S |\phi_0\rangle + t_1^c P G_0 |\widehat{X}\rangle . \qquad (23)$$

For $T \to 0$, the well-known singularity lines[9] in the kernel of this equation disappear.

V. FIRST NUMERICAL RESULTS

In this section we present the first results of an approach based on the method described in the preceding section. These calculations have been carried out by means of the local Eindhoven computer, with some exceptions for which we turned to the Cyber vector-array com-

(a)

(b)
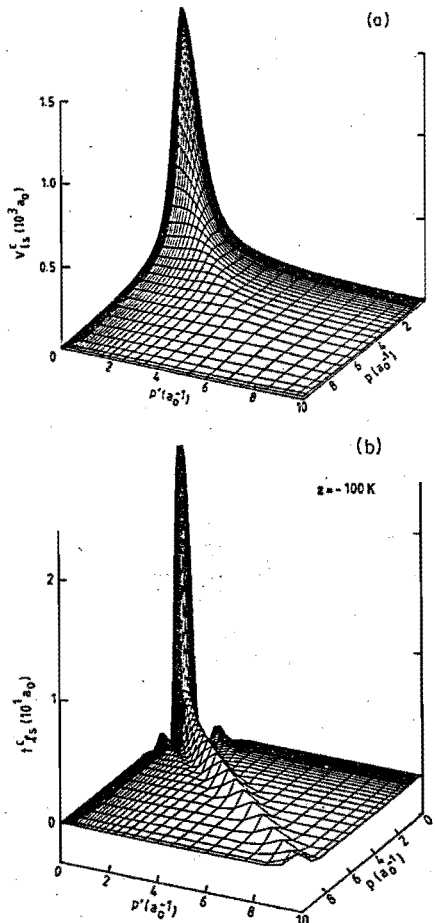
$z = -100$ K

FIG. 3. (a) "Fourier transform" of the $l=0$ triplet potential $V_0^c(p,p')$ as a function of final and initial momenta p and p'; (b) $l=0$ triplet t matrix $t_0^c(p,p',z)$ as a function of p and p' for energy $z = -100$ K.
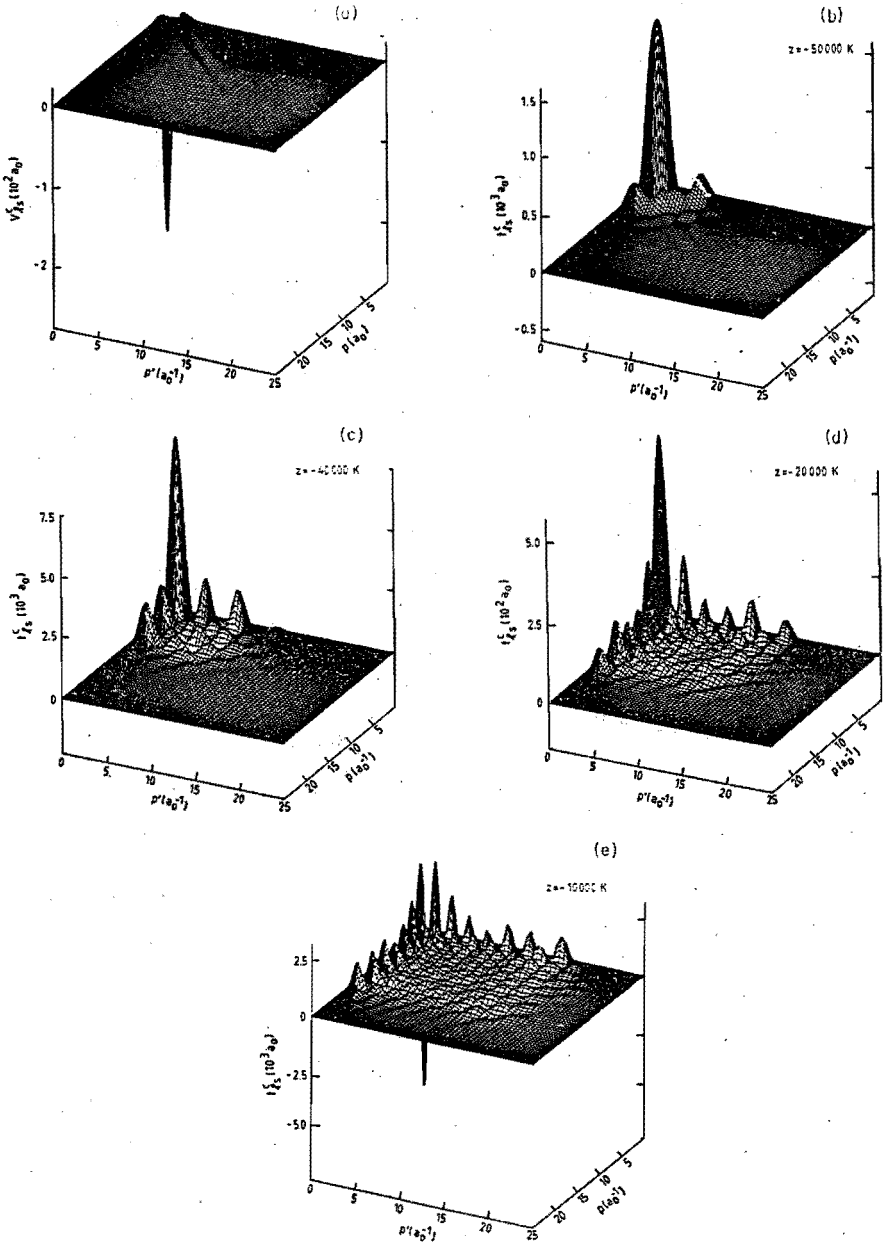
FIG. 4. (a) "Fourier transform" of the $l=1$ singlet potential $V_s^1(p,p')$ as a function of p and p'; (b) $l=1$ singlet t matrix $t_s^1(p,p',z)$ for energy $z=-50000$ K; (c) $l=1$ singlet t matrix $t_s^1(p,p',z)$ for $z=-40000$ K; (d) $l=1$ singlet t matrix $t_s^1(p,p',z)$ for $z=-20000$ K; (e) $l=1$ singlet t matrix $t_s^1(p,p',z)$ for $z=-10000$ K.

85

puter of SARA in Amsterdam. The first step is the calculation of the functions $V_b^c(p,p')$, the "Fourier transform" of the triplet and singlet potentials. These are shown in Fig. 3(a) for $s=1$, $l=0$ and in Fig. 4(a) for $s=0$, $l=1$. The second step is to calculate the t matrix with Eq. (14) by matrix inversion. As grid points we used Gauss-Legendre points. For the triplet case 75 grid points were sufficient. For the singlet case we used 121 points. A maximum momentum value of 35 a_0^{-1} turned out to be necessary. For the triplet potential, a value of 10 a_0^{-1} appeared to be sufficient. Special care has to be devoted to the choice of the "central" Gauss-Legendre point in the singlet case, due to the more complicated structure. As can be seen in Figs. 3(b)-4(e), where we present t_b^c matrices for $s=1$, $l=0$ and $s=0$, $l=1$, respectively, we need more points for the singlet case, again because of the oscillations as a function of p and p'. For very low energies the oscillations disappear and less points are sufficient. However, energies near $z=0$ are likely to be more important for the solution of the Faddeev equations. We also calculated the residues $\hat{t}_b^c(p,p',E_{vl})$ of the $t_b^c(p,p',z)$ functions at the pole energies with the help of an additional equation:

$$\hat{t}_{b=0}^c(p,p',E_{vl}) = \langle plm_l | V^c | \Psi_{vlm_l} \rangle \langle \Psi_{vlm_l} | V^c | p'lm_l \rangle ,$$

(24)

$|plm_l\rangle$ being the orbital part of the states $|plm_ls m_s\rangle$ with normalization corresponding to Eq. (13). The results of this calculation were in accordance with results from matrix inversion.

As a check on our program for solving the Faddeev equations we calculated the phase shift of elastic neutron-deuteron scattering at an energy $E_{lab}=3.26$ MeV for a single α channel ($l=0$, $\lambda=0$, $L=0$, $s=1$, $S=\frac{3}{2}$, $M_S=\frac{3}{2}$, and isospin quantum numbers for pair 1 $t=0$ and total system $T=\frac{1}{2}$). We took this nuclear physics example, since similar calculations for atomic hydrogen are not available in the literature. The results were in accordance with results presented previously.[9]

To start with we did a one-channel calculation for the initial-state Faddeev equation (23), for which we needed 40×40 (p,q) grid points and found convergence after 20 iterations with Padé's method. We chose the most important $l=\lambda=L=0$, $S=\frac{3}{2}$, $M_S=-\frac{3}{2}$ channel. Because of the $1/q^2$ behavior of the driving term of Eq. (23), the solution $\hat{X}_\alpha(p,q)=\langle pq\alpha|\hat{X}\rangle$ also displays a $1/q^2$ dependence. This $1/q^2$ factor is cancelled by the q^2 phase-space factor of the matrix element in Eq. (9). For this reason and to see the underlying structure we plotted $q^2\hat{X}_\alpha(p,q)$ as a function of p and q in Fig. 5. This function is purely real, because of the disappearance of the singularities for $T\rightarrow0$, and obeys the "one channel" Schrödinger equation. We indeed checked that it fulfills that equation.

Furthermore, we did a preliminary one-channel calculation of the final state with 40×50 (p,q) points, in which we included eight poles of the kind mentioned in Eq. (21). We found convergence with Padé's method after 25 iterations. Clearly, the first results given in this section show
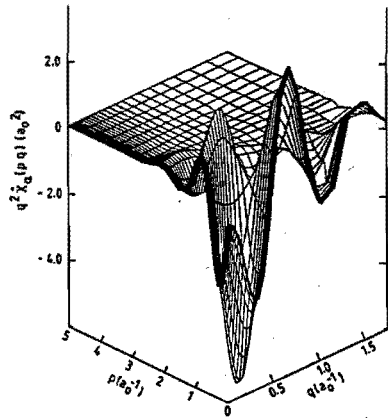

FIG. 5. Solution of the Faddeev equation (23) for the initial state, multiplied by q^2, i.e., $q^2\hat{X}_\alpha(p,q)$ as a function of p and q for channel $\alpha=\{l=\lambda=L=0$, $S=\frac{3}{2}$, $M_S=-\frac{3}{2}\}$.

the basic correctness of our method and also its feasibility when applied to atomic hydrogen.

VI. DISCUSSION

Anticipating a more complete approach extending the previous one-channel calculation, we now present some general considerations regarding the number of α channels to be taken into account. For the Faddeev equation of the initial state for $T\rightarrow0$, we have $s=1$, $S=\frac{3}{2}$, $M_S=-\frac{3}{2}$, $L=0$, and $l=\lambda$; so if l values ranging from 0 to l_{max} are to be included, we need about $l_{max}/2$ channels (see Table I), because only even l values are possible. This is because of the fact that pairs of ground-state hydrogen atoms should have even $l+s+i$ for identical-particle reasons, where i is the total nuclear spin. With three b atoms in the initial state, $i=1$ for each atom pair. In our recombination process proton spins are unaffected.

For the final state the Faddeev equation is not as easy to solve, because we need a far greater number of channels. In Table I we see the number of channels needed as a function of the maximum l value l_{max}. We now have both singlet and triplet channels. From the denominator of the propagator, the energy argument of the t matrix and the fact that the geometrical factor is independent of M_S, it can be concluded that the transition amplitude for the $M_S=+\frac{1}{2}$ channel ($\sigma_f=+\frac{1}{2}$) can be obtained from the $M_S=-\frac{1}{2}$ ($\sigma_f=-\frac{1}{2}$) channel by doubling the magnetic field B. We have an additional factor of -2 from the spin matrix element of the dipole interaction in Eq. (9):

$$f_{vjm}^{\sigma_f=+1/2}(B) = -2f_{vjm}^{\sigma_f=-1/2}(2B) .$$

(25)

As a consequence there is no need to calculate the field dependence for both M_S channels. In interpreting Table I it is of importance to point out that even and odd $l+\lambda$

TABLE I. Number of coupled channels as a function of the maximum angular momentum l_{max} for the initial- and final-state Faddeev equations.

$l_{max} =$ State	0	1	2	3	4	5	$\cdots$	l_{max}
Initial	1	1	2	2	3	3	$\cdots$	$[l_{max}/2]+1$
Final	1	3	6	9	12	15	$\cdots$	$3l_{max}$

channels are uncoupled. This simplification of our three-particle problem follows from the diagonality of t^c and G_0 with respect to l and λ and from the fact that the geometrical factor does not couple even and odd $l+\lambda$. Furthermore, the initial state has even angular momentum quantum numbers $l=\lambda$ (otherwise not understandable) and the dipole interaction couples triplet channels only. As a consequence, only the $l+\lambda$ even channels are possible both for the initial and final states. From the conservation of total angular momentum $J=L+S$, we would have both $L=1$ (i.e., $|l-1| \leq \lambda \leq l+1$) and $L=2$ (i.e., $|l-2| \leq \lambda \leq l+2$) channels. However, the dipole interaction transferring angular momentum $|\Delta L| = |\Delta S| = 2\hbar$ from spin to spatial degrees of freedom, only $L=2$ is allowed. These considerations lead to the dimensions of independent sets of coupled channels given in Table I.

From the considerations in Sec. III we may conclude that our so-called dipole-exchange mechanism is a potential candidate for solving the existing discrepancies of present theory and experimental recombination kinetics. In Sec. IV devoted to the principles of an exact approach, we have demonstrated that the building blocks of the Faddeev scheme, the potentials and t matrices with their complicated structure (see Fig. 4), can be controlled numerically. We have also shown that Faddeev equations can be solved under simplifying assumptions. The exploration of the rich content of physics contained in the process of recombination of three H atoms, including more and more channels, is under way using a vector-array computer. This should also answer the question whether three-body recombination is sufficiently suppressed at fields larger than about 25 T to allow Bose-Einstein condensation to be achieved in a compression experiment.

ACKNOWLEDGMENTS

[1]R. M. C. Ahn, J. P. H. W. van den Eijnde, C. J. Reuver, B. J. Verhaar, and I. F. Silvera, Phys. Rev. B 26, 452 (1982); J. P. H. W. van den Eijnde, C. J. Reuver, and B. J. Verhaar, ibid. 28, 6309 (1983).

[2]H. F. Hess, D. A. Bell, G. P. Kochanski, D. Kleppner, and T. J. Greytak, Phys. Rev. Lett. 52, 1520 (1984).

[3]Yu. Kagan, I. A. Vartan'yants, and G. V. Shlyapnikov, Zh. Eksp. Teor. Fiz. 81, 1113 (1981) [Sov. Phys.—JETP 54, 590 (1981)].

[4]L. P. H. de Goey, J. P. J. Driessen, B. J. Verhaar, and J. T. M. Walraven, Phys. Rev. Lett. 53, 1919 (1984).

[5]M. I. Haftel and T. K. Lim (unpublished).

[6]L. D. Faddeev, Zh. Eksp. Teor. Fiz. 39, 1459 (1961) [Sov. Phys.—JETP 12, 1014 (1961)].

[7]R. M. C. Ahn, J. P. H. W. van den Eijnde, and B. J. Verhaar, Phys. Rev. B 27, 5424 (1983).

[8]W. Glöckle, The Quantum Mechanical Few-Body Problem (Springer-Verlag, Berlin, Heidelberg, 1983), and references herein.

[9]W. M. Kloet and J. A. Tjon, Ann. Phys. (N.Y.) 79, 407 (1973).

[10]G. A. Baker, Essentials of Padé Approximants (Academic, New York, 1975).

[11]F. Smithies, Integral Equations (Cambridge University Press, New York, 1958).

CHAPTER 5

THE ROLE OF THREE-BODY CORRELATIONS IN RECOMBINATION OF
SPIN-POLARIZED ATOMIC HYDROGEN

L.P.H. de Goey, H.T.C. Stoof and B.J. Verhaar

Department of Physics, Eindhoven University of Technology,
5600 MB Eindhoven, The Netherlands

W. Glöckle

Institut für Theoretische Physik, Ruhr-Universität Bochum
Bochum, West Germany

ABSTRACT

We present results of a calculation of the volume rate constant L_g^{eff}
of dipole recombination in $H\downarrow\uparrow$, in which the bbb incoming state is
determined exactly by means of the Faddeev formalism. Inclusion of all
three-particle correlations in the initial state does not resolve the
discrepancies between Kagan's approach and experiment. As a first step
towards an exact determination of the outgoing atom-molecule state, we
present a calculation, in which all three-particle collision aspects
are taken into account, except for rearrangement. This leads to values
for L_g^{eff}, which are a factor 5 smaller than experiment, while the
B-dependence of the rate constant still shows a slowly increasing
behavior. On the basis of this state-of-the-art calculation we thus
localize the cause for the existing discrepancies in rearrangement
processes.

I. INTRODUCTION

In the last decade, a dramatic progress has been made in the creation and stabilization of gas samples of spin-polarized atomic hydrogen.[1,2] The interest in this field has been stimulated by the realization that spin-polarized atomic hydrogen is the only substance that remains in gaseous form even at the absolute zero of temperature. This would imply that a phase transition to the Bose-Einstein condensed state will thus be observable in a weakly interacting Bose gas. Furthermore, the simple structure of the hydrogen atom and the well-known interatomic interactions allow for a first-principles approach to describe the physical properties of this gas. Therefore, atomic hydrogen is an ideal medium to test quantum statistical theories. Beyond this, the experimental work has already led to numerous interesting applications.

In 1980 Silvera et al.[3] created the first long-lived sample of atomic hydrogen by polarizing the electron spins in a strong magnetic field using ^{4}He-coated cells. This leads to a population of only the two low-lying a and b hyperfine states (a,b,c,d are the hyperfine levels of the 1s ground state of atomic hydrogen labeled in order of increasing energy). Statt et al.[4] realized that a subsequent depopulation of the a state with its admixed electron $\uparrow$ state, by means of preferential recombination of the a atoms, would lead to a much more stable doubly-polarized gas of b atoms. This was first observed by Cline et al.,[5] who found lifetimes orders of magnitude larger than before. The next step towards Bose-Einstein condensation consisted of compression of the doubly-polarized gas to higher densities.[6] The occurrence of a rapid decay of the gas in these experiments has retarded further developments to reach the degeneracy regime at high densities. Explanations, restricted to two-body bulk and surface processes,[7] were found to be incapable to account for the experimentally observed rapid decay. This led to the suggestion that a three-body dipolar recombination process could provide for the dominant decay mode of the gas sample.[8] Inclusion of a three-body term in the rate equation immediately resolved the previous discrepancies between experiment and theory concerning the two-body contributions. Up to now, simple approaches to describe the three-body part[9,10] have

90

failed to reproduce the experimentally observed magnetic-field dependence of the volume and surface rate constants. There exists an additional discrepancy with respect to the absolute magnitude of the rate constants: for surface recombination the theoretical value is roughly a factor of 6 too small.[10,11]

A better understanding of the three-body dipolar recombination mechanism is thus crucial to remove the obstacles on the way to the degeneracy regime in compression experiments. Therefore, it seems important to perform a calculation, based on the Faddeev formalism,[12,13] in which the three-body collision aspects are taken into account exactly. Furthermore, the use of the Faddeev formalism, which has been succesfully applied in nuclear physics, is of interest in its own right, because it opens possibilities for further applications of exact three-body calculations in atomic physics. It turns out that, compared to the case of Yukawa-type potentials among nucleons, central (singlet and triplet) interatomic interactions present more difficulties. This expresses itself most clearly in the case of the singlet potential with its numerous bound states. Obviously, this situation has no counterpart in the few-nucleon problem.

In Ref. 13 (further referred to as I) we started an exact treatment of the three-body recombination process in the bulk. Here, further developments are presented. In Sec. II we review the method we use to calculate the effective volume rate constant L_g^{eff} in terms of the transition amplitude f, which describes the transition from the incoming bbb state to the outgoing atom-molecule state, induced by the electron-electron magnetic-dipole interaction. In the present paper we calculate the initial state rigorously, by means of the Faddeev equation. In Sec. III this equation is introduced, as well as our method for solving it. With respect to the final state we follow two approaches. In the first one all atom-molecule correlations are neglected. Despite the rigorous treatment of the initial state this does not resolve the discrepancies with experiment. The relation with an initial wavefunction previously used by Kagan et al.[9] is discussed in Sec. IV, where also a simple, more accurate approximation of the exact wavefunction is presented. As we already mentioned in I, solving the Faddeev equation for the final state is an even more difficult problem than the determination of the initial state. In Sec. V we

present an approach to calculate the final state, in which all three-particle correlation aspects are taken into account, except for rearrangement. We show that this leads to a rate constant, which displays a less strong field dependence than in Sec. III. It is, however, still increasing with B, and more importantly, the absolute magnitude of L_g^{eff} now turns out to be a factor of 5 smaller than the corresponding experimental value. In Sec. VI we therefore come to the conclusion that rearrangement (the dipole-exchange mechanism, introduced in I) must be the dominant decay channnel.

II. DIPOLE RECOMBINATION

The rate of decay of doubly-polarized atomic hydrogen can be described effectively by means of the rate equation

$$\frac{dn_H}{dt} = -C^{eff} n_H^2 - L^{eff} n_H^3,$$ (1)

where n_H is the atomic density, and C^{eff} and L^{eff} are the effective two- and three-body rate constants. The two-body term describes the decay of the gas due to bb→ab relaxation, in which the transition is induced by the weak electron-proton and the stronger electron-electron magnetic-dipole interactions. Both interactions give rise to comparable contributions, because the electron-electron dipole interaction only contributes in combination with the hyperfine interaction. Under normal circumstances, the density of the sample is so low that the probability of collisions of an increasing number of particles strongly decreases. This explains the fact that higher order terms in Eq. (1) can be neglected. However, the three-body part, which describes the decay due to dipole recombination, is still important, because the transition is caused purely by the electron-electron dipole interaction. As we already pointed out in Sec. I the three-body term even dominates for higher densities in compression experiments. The rate constant L^{eff} can be written as a sum of bulk and surface contributions

$$L^{eff} = L_g^{eff} + L_s^{eff} \left\{ \frac{A}{V} \lambda^3 \exp(3\epsilon_0/kT) \right\}.$$ (2)

In Eq. (2). A/V is the surface to volume ratio. λ the thermal de Broglie wavelength and ϵ_0 the adsorption energy of an atom on the surface.

Up to now, simple models have not succeeded to explain the experimental behavior of L_g^{eff} and L_s^{eff}. The discrepancies are probably in both cases caused by the same mechanism, due to their similar features. Therefore, it seems reasonable to concentrate first on the easier case of volume recombination. We can distinguish between contributions due to single- and double-spin-flip processes, for which the total final electron-spin projection M_S is $-\frac{1}{2}$ or $+\frac{1}{2}$, respectively:

$$L_g^{eff} = L_g^{-\frac{1}{2}} + 2L_g^{+\frac{1}{2}}. \tag{3}$$

Here the factor 2 results from the fact that the final c-atom in the double-spin-flip process recombines immediately on the surface, removing an additional pair of particles from the sample. A weight factor somewhat different from 2 is also sometimes used in experimental analyses. Furthermore, $L_g^{-\frac{1}{2}}$ and $L_g^{+\frac{1}{2}}$ are related by[13]

$$L_g^{+\frac{1}{2}}(B) = 4L_g^{-\frac{1}{2}}(2B). \tag{4}$$

In I we concentrated on

$$L_g = L_g^{+\frac{1}{2}} + L_g^{-\frac{1}{2}}, \tag{5}$$

the rate constant representing the pure bbb$\rightarrow$H$_2$+H decay, instead of the effective rate constant, which is more important experimentally.

We assume that the final molecule consists of particles 2 and 3 (pair 1). Furthermore, we introduce the Jacobi momenta $\vec{p}$ and $\vec{q}$, $\vec{p}$ being the relative momentum of pair 1 and $\vec{q}$ the momentum of particle 1 relative to pair 1. As we have shown in Ref. 11

$$L_g^{\pm\frac{1}{2}} = \frac{(2\pi\hbar)^9}{4m_H} \langle \sum_{v\ell m} \int d\hat{q}_f \, q_f \, |f_{\vec{q}_f v\ell m M_S=\pm\frac{1}{2},\vec{p}_0\vec{q}_0}|^2 \rangle_{thermal}. \tag{6}$$

which is essentially the transition probability, described by $|f|^2$, summed over all possible final state quantum numbers v, ℓ, m and

$\vec{q}_f$ and averaged over all initial momenta $\vec{p}_0$ and $\vec{q}_0$. In Eq. (6) m_H is the mass of the hydrogen atom, $v\ell m$ are the vibrational and rotational quantum numbers of the molecule and $\vec{q}_f$ is the relative atom-molecule momentum. The integral over this final momentum has reduced to an angular integral over $\hat{q}_f$, due to energy conservation

$$E = \frac{p_0^2}{m_H} + \frac{3q_0^2}{4m_H} - 3\mu_B B = \frac{3q_f^2}{4m_H} + E_{v\ell} + 2M_S\mu_B B. \tag{7}$$

In Eq. (7) $-E_{v\ell}$ is the binding energy of the molecule and $2(M_S + \frac{3}{2})\mu_B B$ the Zeeman energy needed to flip one or two electron spins, μ_B being the Bohr magneton. Furthermore, $p_0^2/m_H + 3q_0^2/4m_H$ is the small relative kinetic energy of the three particles before the collision.

The dipole recombination amplitude f can be described very accurately by means of a DWBA-approach,[11] in which the extremely weak dipole interaction is treated in first order. The amplitude f, which is essentially a matrix element of the summed dipole interactions V_k^d (the pair k is denoted by the spectator particle) then reduces to:

$$f_{\vec{q}_f v\ell m M_S, \vec{p}_0\vec{q}_0} = \frac{\frac{2}{3}m_H}{2\pi\hbar^2} \langle \psi_f^{(-)} | \sum_{k=1}^{3} V_k^d \, S | \psi_i^{(+)} \rangle. \tag{8}$$

Here, S is the unnormalized symmetrization operator

$$S = (1+P_{23})(1+P) \tag{9}$$

where

$$P = P_{12}P_{23} + P_{13}P_{23}. \tag{10}$$

P_{ij} being a permutation operator of particles i and j.

In the fully symmetrized initial three-atom state $S|\psi_i^{(+)}\rangle$ and final atom-molecule state $|\psi_f^{(-)}\rangle$ of Eq. (8), the central interactions in principle have to be taken into account to all orders. The (+) and (−) superscripts denote outgoing and incoming asymptotic boundary conditions, respectively. Since three hydrogen atoms consist of three electrons and three protons, we have to solve six-particle

94

Schrödinger equations. As in the two-atom case,[14] however, we reformulate these as three-atom Schrödinger equations[15] by the introduction of effective interactions, which are essentially the Coulomb interactions averaged over the electron motions. These effective central potentials consist of direct parts and contributions representing the exchange of two or three electrons. Since there exists no completely anti-symmetric spin state of three electrons, there is always at least one repulsive hydrogen pair. Moreover, for our polarized initial state the three subsystems are repulsive, which prohibits the particles to approach each other closely. Therefore, a three-body force, describing the exchange of three electrons, can be neglected. Throughout this paper we describe the central interactions by a sum of pair (singlet and triplet) interactions.

III. EXACT bbb INCOMING STATE

In this section we determine the wavefunction of the bbb incoming state. The method we use is based on the Faddeev formalism, which we introduced in I. We start with a recollection of the main results of I and continue the discussion started there.

The state $S|\psi_1^{(+)}\rangle$ can be regarded to develop out of the free state

$$|\phi_0\rangle = |\vec{p}_0\vec{q}_0\rangle \, |bbb\rangle. \tag{11}$$

by successive pair collisions. This introduces all three-particle correlations. The orbital part of the free state is normalized as a product of two Dirac δ-functions in momentum space. The multiple-scattering series is generated by the Faddeev equation

$$|\hat{\chi}\rangle = t_1^c(E)PG_0^{(+)}(E)t_1^c(E)S|\phi_0\rangle + t_1^c(E)PG_0^{(+)}(E)|\hat{\chi}\rangle. \tag{12}$$

where the amplitude $|\hat{\chi}\rangle$ contains all terms of second and higher order in t_1^c:

$$S|\psi_1^{(+)}\rangle = S|\phi_0\rangle + (1+P)G_0^{(+)}(E)t_1^c(E)S|\phi_0\rangle + (1+P)G_0^{(+)}(E)|\hat{x}\rangle. \quad (13)$$

Here, $G_0^{(+)}(E) = (E+i0-H_0)^{-1}$ is the outgoing-wave free propagator, H_0 being the free Hamiltonian including the Zeeman energy and E the total energy. Furthermore, $t_1^c(E)$ is the t operator of pair 1 operating in three-particle space, which obeys the Lippmann-Schwinger equation

$$t_1^c(E) = V_1^c + V_1^c G_0^{(+)}(E) t_1^c(E). \quad (14)$$

Since we are only interested in recombination at very low temperatures, we perform our calculations for T=0. This simplifies the calculations significantly, because the initial momenta $\vec{p}_0$ and $\vec{q}_0$ are zero in this case, leading to a trivial thermal averaging procedure. At the same time, the denominator of the free propagator in momentum representation is: $E-p^2/m_H-3q^2/4m_H+3\mu_B B = -p^2/m_H-3q^2/4m_H$, leading to harmless singularities at p=q=0 (see I).

To solve Eq. (12), we introduce the angular momentum basis[16]

$$|pq\alpha\rangle = |pq\ (\ell\lambda)LM_L\ (s\tfrac{1}{2})SM_S\rangle. \quad (15)$$

which is normalized according to

$$\langle p'q'\alpha'|pq\alpha\rangle = \frac{\delta(p-p')}{p^2}\frac{\delta(q-q')}{q^2}\delta_{\alpha\alpha'}. \quad (16)$$

In Eq. (15) ℓ,s are the orbital and spin angular momenta of pair 1, λ is the orbital angular momentum of particle 1 relative to pair 1 and LM_L,SM_S are the total three-particle orbital and spin angular momenta. Note that the proton spins are left out of consideration in Eq. (15). They remain polarized during the process and do not influence the dynamics of the recombination. For the polarized initial state the spin angular momenta are restricted to s=1, S=3/2 and $M_S=-3/2$. Furthermore, only the total orbital angular momentum L=0 contributes, due to the T=0 limit. This restricts the number of α channels to be taken into account to a few even $\ell=\lambda$ values.

With the help of the representation of the various operators in the angular momentum basis, as discussed in I, Eq. (12) is a coupled

two-dimensional integral equation. In discretized form, using spline techniques to express the functions in the values at the grid points,[17] this equation can be transformed to a matrix equation

$$\underline{y}_1 = \underline{a}_1 + \mu \, \underline{\underline{K}}_{11} \, \underline{y}_1 . \tag{17}$$

where the vectors $\underline{y}_1$ and $\underline{a}_1$ represent $|\hat{\chi}\rangle$ and $t_1^c P G_0^{(+)} t_1^c S |\phi_0\rangle$, the Faddeev component and driving term of Eq. (12), respectively. The matrix $\underline{\underline{K}}_{11}$ stands for the kernel $t_1^c P G_0^{(+)}$ of Eq. (12). Furthermore, we added the strength parameter μ, for which we will finally substitute the value 1.

Due to the oscillating behavior of the t operator and consequently also of the solution as a function of momenta, we need at least 40 p and 40 q Gauss-Legendre grid points to describe $\underline{y}_1$. The kernel $\underline{\underline{K}}_{11}$ is therefore too large to solve Eq. (17) by matrix inversion, even for a few α channels. Instead we solve it by iteration. Furthermore, we use Padé's method,[18] because the Neumann series diverges for the physical value $\mu=1$, as a result of the strength of the triplet potential. The iteration series converges for complex μ values with $|\mu| < 1/|\lambda_{max}|$, where $\lambda_{max} \simeq -2.0$ is the eigenvalue of $\underline{\underline{K}}_{11}$ with the largest absolute magnitude. Because of the compactness of $1 - \underline{\underline{K}}_{11}$ it is possible, to construct an analytic continuation of $\underline{y}_1(\mu)$ into the complete complex μ-plane in the form of a meromorphic function, i.e. a ratio of two regular analytic functions. In our case the application of this Padé method to the iteration series generated by Eq. (17) leads to a non-uniformly converging behavior of the solution: for small p and q values $\underline{y}_1$ converges rapidly, but for larger p and q values we find no stable solution, at least within a reasonable number of iterations. To solve this problem we make use of a variant of the Nyström method.[19] In addition to Eq. (17), with μ replaced by 1, we introduce the equation

$$\underline{y}_2 = \underline{a}_2 + \underline{\underline{K}}_{21} \, \underline{y}_1 \tag{18}$$

which links the solution $\underline{y}_1$ based on the initial set of grid points to that based on an alternative set, denoted by the subscript 2. The number of points of this last set is supposed to be only a fraction of the initial set. With Eqs. (17) and (18) we subsequently formulate an

equation for $\underline{Y}$, the direct sum of $\underline{y}_1$ and $\underline{y}_2$:

$$\underline{Y} = \underline{A} + \underline{\underline{K}}\, \underline{Y}, \tag{19}$$

where

$$\underline{A} = \begin{bmatrix} \underline{a}_1 + \underline{\underline{K}}_{12}\, \underline{\underline{C}}_{22}\, \underline{a}_2 \\ \underline{\underline{C}}_{22}\, \underline{a}_2 \end{bmatrix} \tag{20}$$

and

$$\underline{\underline{K}} = \begin{bmatrix} \underline{\underline{K}}_{11} + \underline{\underline{K}}_{12}\, \underline{\underline{C}}_{22}\, \underline{\underline{K}}_{21} & -\underline{\underline{K}}_{12}\underline{\underline{C}}_{22} \\ \underline{\underline{C}}_{22}\underline{\underline{K}}_{21} & -\underline{\underline{C}}_{22}\underline{\underline{K}}_{22} \end{bmatrix}. \tag{21}$$

In Eqs. (20) and (21) we used $\underline{\underline{C}}_{22}$ for $(\underline{\underline{1}}-\underline{\underline{K}}_{22})^{-1}$. It can be checked that the eigenvalues of the new kernel $\underline{\underline{K}}$ of Eq. (19) become arbitrarily small, when the set of points denoted by 2 approaches that denoted by 1. In this limit the matrix $\underline{\underline{K}}$ becomes singular, its upper submatrices approaching the lower ones. If the sets of points are different, one can systematically improve the vector $\underline{A}$ by iteration of Eq. (19). That convergent procedure leads in the upper component of $\underline{Y}$ to the desired solution $\underline{y}_1$. To solve Eq. (19), the dimension of $\underline{\underline{K}}_{22}$ should be small enough to be able to calculate the inverse $\underline{\underline{C}}_{22}$, and on the other hand it should be large enough in order to obtain small eigenvalues of $\underline{\underline{K}}$, i.e. in order for $\underline{\underline{C}}_{22}\, \underline{a}_2$ to describe the most essential correlations. A choice of 15 p and 15 q points fulfills both demands, leading to a spectrum of eigenvalues of $\underline{\underline{K}}$, with $|\lambda_{max}|\simeq 0.15$. Therefore, we now find convergence after about 10 iterations.

We solved Eq. (19) with various numbers of channels. The four lowest partial waves up to $\ell=\lambda=6$ are sufficient to describe the wavefunction of the initial state and to find a converged transition amplitude. Furthermore, the $\ell=\lambda=0$ partial wave appears to be dominant.

As we already pointed out here and in I, the wavefunction in momentum space displays a lot of structure and is not useful for a clear physical picture. To understand the underlying physics, we therefore performed a Fourier transformation of the various terms of Eq. (13) to configuration space, by means of

$$\psi_\alpha(r,R) = \langle rR\alpha | S\psi_i^{(+)} \rangle =$$

$$\frac{2}{\pi\hbar^3} i^{\ell+\lambda} \int_0^\infty p^2 dp \; j_\ell(pr/\hbar) \int_0^\infty q^2 dq \; j_\lambda(qR/\hbar) \; \psi_\alpha(p,q), \tag{22}$$

where $\psi_\alpha(p,q) = \langle pq\alpha | S\psi_i^{(+)} \rangle$ is the orbital part of the symmetrized initial state in the angular momentum basis. In our special case of $|\alpha\rangle = |(\ell\ell)00 \; (1\frac{1}{2}) \frac{3}{2} \frac{-3}{2}\rangle$, it is possible to write $S|\psi_1^{(+)}\rangle$ as a function of r, R and θ:

$$\psi(r,R,\theta) = \frac{1}{4\pi} \sum_\ell (-1)^\ell \sqrt{2\ell+1} \; P_\ell(\cos\theta) \; \psi_\alpha(r,R), \tag{23}$$

where θ is the angle between the Jacobi coordinates $\vec{r}$ and $\vec{R}$ (see Fig. 1). Note that the free part $S|\phi_0\rangle$ in Eq. (13) contributes only an $\ell=\lambda=0$ partial wave. This is also the case for the term $C_0^{(+)} t_1^c S|\phi_0\rangle$, while the remaining parts contain in principle all even $\ell=\lambda$ partial waves. In Figs. 2a-2c we plotted $\psi(r,R,\theta)$ as a function of r and R for $\theta=0,\pi/4$ and $\pi/2$. The wavefunction is symmetric under a permutation of particles 2 and 3, leading to symmetry of $\psi(r,R,\theta)$ with respect to the interchange of θ and $\pi-\theta$ due to the evenness of ℓ and λ. In each of the figures we observe that the wavefunction vanishes for $r\lesssim6$ a_0, which is caused by the strongly repulsive triplet interaction for small distances between particles 2 and 3. This effect also plays a role in Fig. 2a for $\theta=0$, when the distance between particles 1 and 2 $|\vec{R}-\frac{1}{2}\vec{r}|\lesssim6$ a_0. In Figs. 2b and 2c we see that $\psi(r,R,\theta)$
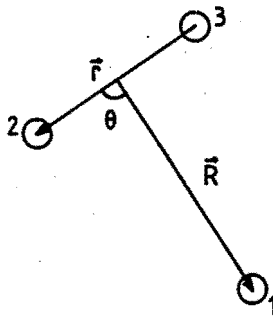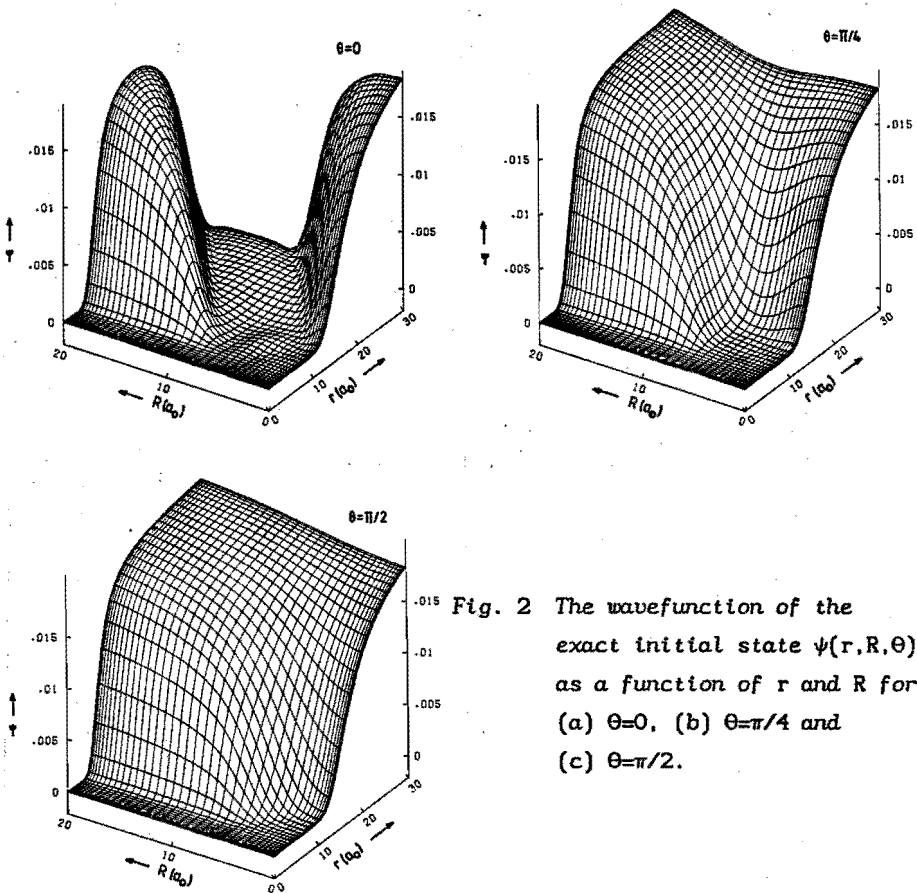

Fig. 1 *The Jacobi vectors $\vec{r}$ and $\vec{R}$.*

θ=0

θ=π/4

θ=π/2

Fig. 2 *The wavefunction of the exact initial state $\psi(r,R,\theta)$ as a function of r and R for (a) $\theta=0$, (b) $\theta=\pi/4$ and (c) $\theta=\pi/2$.*

behaves for large R essentially as the zero-temperature two-particle triplet wavefunction $\psi_t(r)$. For small R values, however, ψ approaches $\psi_t(\frac{1}{2}r)$, because the distance between particles 2 or 3 from particle 1 is only $\frac{1}{2}r$ in this case. Furthermore, $\psi(r,R,\theta)$ approaches the free wavefunction $\langle \vec{r}\,\vec{R}|\langle(s\frac{1}{2})SM_S|S\phi_0\rangle = 6/(2\pi\hbar)^3$ for large distances r and R.

It is of interest in this connection to point out the role of the various terms in Eq. (13). It turns out that the $(1+P)G_0^{(+)}|\hat{\chi}\rangle$ term contributes only in that part of configuration space where all three particles are closely together. Similarly, a $G_0^{(+)}t_i^c S|\phi_0\rangle$ term contributes only when the distance between the atoms of pair i is small. Note that $PG_0^{(+)}t_1^c$ is effectively equal to $G_0^{(+)}(t_2^c+t_3^c)$. Taking

100

particle i apart, the non-zero part $(1+G_0^{(+)}t_i^c)S|\phi_0\rangle$ of Eq. (13) converts a free three-particle state into a state in which the pair i wavefunction is distorted to a triplet scattering state.

We now turn to the calculation of the effective rate constant with the help of Eqs. (6) and (8). It turns out that the expansion of $\psi_t(|\pm\vec{R}-\frac{1}{2}\vec{r}|)$ in partial waves $\ell=\lambda$ converges very slowly, due to the fact that $\psi_t(r)\simeq0$ for $r\lesssim6$ a_0. Therefore, the contribution of the term $PG_0^{(+)}t_i^cS|\phi_0\rangle$ of Eq. (13) to $\psi(r,R,\theta)$ and to the dipole matrix element cannot be calculated in the angular momentum basis. We calculated it in the momentum basis $|\vec{p}\vec{q}\rangle|(s\frac{1}{2})$ $SM_S\rangle$.

Another numerical problem arises from the strong increase of the dipole interaction at small r. The fully correlated initial state gives rise to a suppression of the small r contribution to the $1/r^3$ magnetic-dipole integral. It turns out, however, that the separate terms in Eq. (13) lead to large (but finite) contributions of the order of a "free" matrix element, which cancel when added. The ensuing loss of accuracy is easily avoided. The magnetic-dipole interaction has an artificial $1/r^3$ dependence only as a result of the Shizgal approximation,[20] according to which the electronic magnetic-dipole moment of the H atom is located at the position of the proton. This is a good approximation, except for small distances, where the dipole interaction should rapidly decrease to negligible values. We therefore multiply it by a function g(r) which damps its $1/r^3$ behavior near the origin and which is equal to 1 for distances $r\gtrsim6$ a_0. Clearly, apart from this restriction, the precise form of g(r) is unimportant. This is confirmed by numerical results.

We now turn to the evaluation of the effective rate constant. In a previous calculation of Kagan et al.[9] both the exact initial and final state wavefunctions were replaced by simple approximations. As a first step we now follow the same procedure for the final state: we neglect all atom-molecule correlations. In this case, the dipole interaction V_k^d for k=1 does not contribute to the transition probability, because it can cause no transition from s=1 to s=0. Furthermore, the results presented here do not include any contribution of the dipole-exchange mechanism, as a result of the neglect of all atom-molecule interactions. The calculation can be regarded as an improvement of the original evaluation of the Kagan dipole mechanism.[9]

As in previous calculations, the major contribution to f turns out to be supplied by the $v=14,\ell=3$ molecular state, while the small remaining fraction comes from the $v=14,\ell=1$ state. In Fig. 3 we present the separate contributions $L_g^{+\frac{1}{2}}$ and $L_g^{-\frac{1}{2}}$ to the effective rate constant, evaluated with the help of the exact initial state, as a function of magnetic field B Ccurves 1 and 3). In Fig. 4 we also plot the total effective rate constant L_g^{eff} as a function of B (curve 2). For comparison we also give the results of the calculation of Kagan et al. (curve 1). The difference between the curves is small, both in
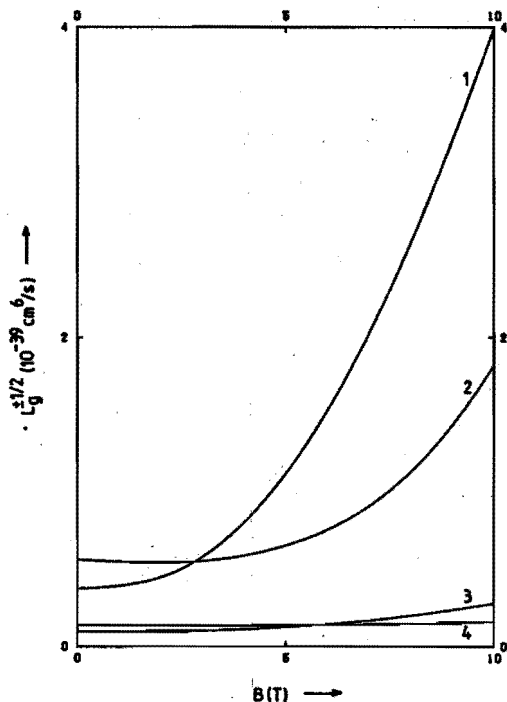

Fig. 3 The single- and double-spin-flip contributions $L_g^{-\frac{1}{2}}$ and $L_g^{+\frac{1}{2}}$ to the rate constant as a function of magnetic field B.

curve 1: $M_S=+\frac{1}{2}$, exact initial state, undistorted final state.

curve 2: $M_S=+\frac{1}{2}$, exact initial state, (in)elastically distorted final state.

curve 3: $M_S=-\frac{1}{2}$, exact initial state, undistorted final state.

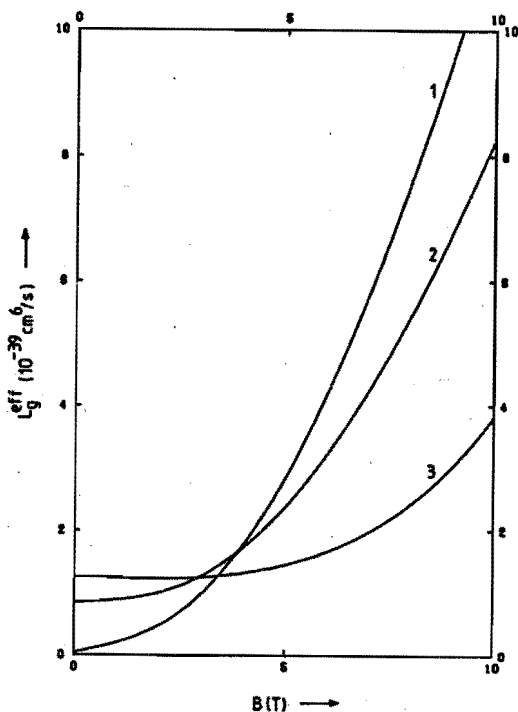curve 4: $M_S=-\frac{1}{2}$, exact initial state, (in)elastically distorted final state.

Fig. 4 The effective rate constant L_g^{eff} as a function of B.
   curve 1: Kagan's result.
   curve 2: exact initial state, undistorted final state.
   curve 3: exact initial state, (in)elastically distorted
        final state.

absolute magnitude and in B-dependence. We will come back to this
remarkable resemblance in the following section, where we compare the
initial states of both calculations.

Since the results are still not in agreement with experimental
data, we come to the important conclusion that the poor treatment of
the final state is the cause of the discrepancies. A better treatment
of the final state, which was also the aim of our earlier calculation
of the dipole-exchange mechanism in I, will be discussed in Sec. V.

IV. COMPARISON WITH THE CALCULATION OF KAGAN

As we pointed out in the previous section, the approach of Kagan et al.[9] leads to an effective rate constant L_g^{eff}, which displays a similar behavior as a function of B, as the results obtained in Sec. III. We here investigate the reason for this resemblance. In both approaches the correlations between the final atom and molecule are neglected. Therefore, the only difference between the calculations is the character of the initial state. We first analyze the features of Kagan's incoming state and subsequently discuss their effect on the transition probability.

In the initial state of Kagan, only the correlations between the recombining atoms (pair 1) and among the particles interacting via the dipole interaction (pair 2 or 3) are taken into account in the form of a product of two pair wavefuntions. For instance, in the V_2^d term of Eq. (8):

$$\langle \vec{r}\, \vec{R} | S | \psi_1^{(+)} \rangle \rightarrow 6 \, \psi_t(r) \, \psi_t(|-\vec{R}-\tfrac{1}{2}\vec{r}|) \, |bbb\rangle. \tag{24}$$

For the contribution of V_3^d, $\psi_t(|-\vec{R}-\tfrac{1}{2}\vec{r}|)$ is replaced by $\psi_t(|\vec{R}-\tfrac{1}{2}\vec{r}|)$. As in the previous section, the zero-temperature wavefuntion $\psi_t(r)$ is normalized as $(2\pi\hbar)^{-3/2}$ for larger r values.

The spin part of the initial state is symmetric under all particle permutations. Because of the boson character of H atoms, the orbital part of the wavefunction should also be completely symmetric. However, because of the fact that not all particle pairs are distorted by the triplet interaction, Eq. (24) is only symmetric under a permutation of particles 1 and 2, and not under an exchange of other atoms. Therefore, an expansion of Eq. (24) in partial waves ℓ, describing the dependence on the angle Θ between the Jacobi vectors $\vec{r}$ and $\vec{R}$, shows that unphysical odd ℓ values contribute to the wavefunction and the transition amplitude. Moreover, the contribution of the odd partial waves to f is essential in Kagan's model in order to obtain reasonable results: odd ℓ values have to be included to obtain a vanishing wavefunction for small distances between the particles 1 and 3, interacting by the dipole force V_2^d.
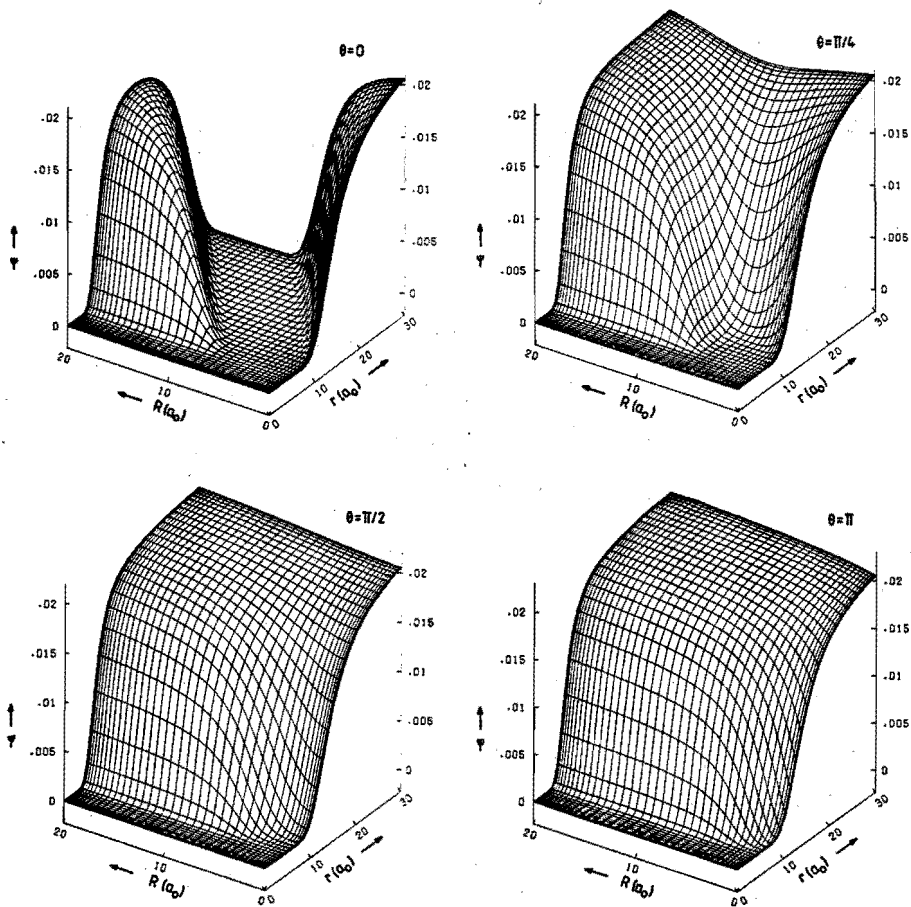
Fig. 5 Kagan's approximation to the initial state $\psi(r,R,\theta)$ as a function of r and R for (a) $\theta=0$, (b) $\theta=\pi/4$, (c) $\theta=\pi/2$ and (d) $\theta=\pi$.

To compare Kagan's wavefunction Eq. (24) with our exact initial state, we plotted the spatial part of Eq. (24) as a function of r and R in Figs. 5a-5d for $\theta=0,\pi/4,\pi/2$ and π. Notice that the figures for $\theta=0,\pi/4$ and $\pi/2$ look very similar to the corresponding surfaces for the exact wavefuntion, presented in Fig. 2. In spite of the lack of symmetry of Kagan's wavefunction, it possesses the essential elements of the exact initial state. For $\theta\to\pi$, however, the difference between

the wavefunctions becomes significant, as can be seen by comparing
Fig. 5d with Fig. 2a. This results from the neglect of correlations
between particles 1 and 2, which is of importance for $\theta \approx \pi$. The
asymmetry of the wavefunction with respect to the exchange of θ and
$\pi-\theta$, which can be observed by comparing the surfaces for $\theta=0$ and $\theta=\pi$,
demonstrates again that Eq. (24) contains odd ℓ values.

An essential element in understanding the effectiveness of
Kagan's approach can be found in the zero-temperature approximation.
This causes the wavefunctions to "heal" within distances of roughly
10 a_0. In a way the atoms behave as transparent objects, except for
smaller distances. Therefore, the wavefunction of Kagan is a good
approximation of the exact initial state for the complete
three-particle configuration space, except for the part where the
distance $|\vec{R}-\tfrac{1}{2}\vec{r}|$ between particles 1 and 2 is less than 10 a_0.
Apparently, the contribution from this forbidden region is of minor
importance for dipole recombination.

The relative error, due to the contribution to f from small
$|\vec{R}-\tfrac{1}{2}\vec{r}|$ values is roughly proportional to $1/r_b^3$, i.e. to the average
strength of the dipole interaction between atoms 1 and 3, when
particles 1 and 2 are within the forbidden region. Here, r_b is the
most probable distance between the bound particles, directly after the
recombination. Obviously, the error in $|f|^2$ increases for more
strongly bound states. For the dominant $v=14$, $\ell=3$ state, the error
turns out to be roughly 20%. For the $v=14$, $\ell=1$ state it has already
increased to a factor of 2. Therefore, we conclude that the
applicability of Kagan's approach decreases, when the contribution of
stronger bound molecular states increases. We come back to this
shortly (Sec. V).

Guided by the success of Kagan's approximation for the initial
state, an obvious improvement to Eq. (24) would be a Jastrow-like
expression:

$$S|\psi_i^{(+)}\rangle \rightarrow 6 \ \psi_t(r_1) \ \psi_t(r_2) \ \psi_t(r_3) \ (2\pi\hbar)^{3/2} \ |bbb\rangle, \qquad (25)$$

with $\vec{r}_1 \equiv \vec{r}$, $\vec{r}_2 = -\vec{R}-\tfrac{1}{2}\vec{r}$ and $\vec{r}_3 = \vec{R}-\tfrac{1}{2}\vec{r}$. This wavefunction contains the pair
correlations in a completely symmetric way. Furthermore, Eq. (25)
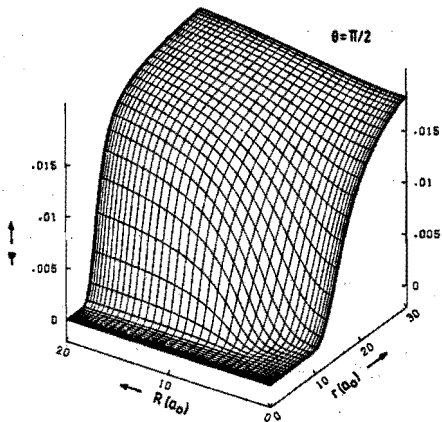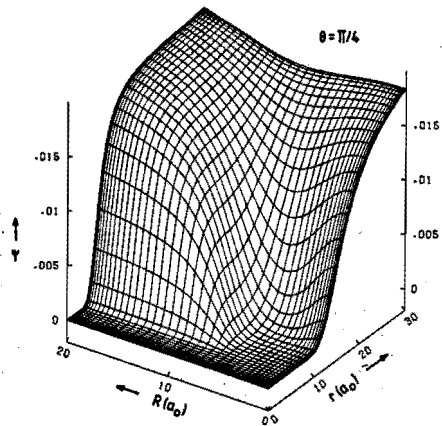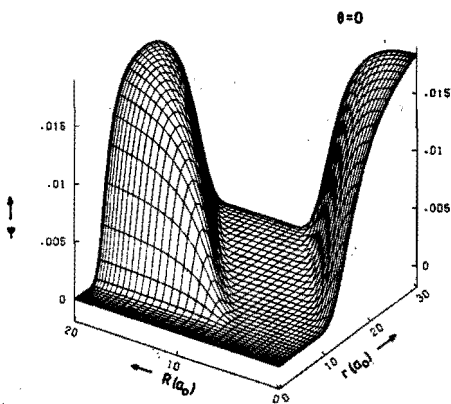describes correctly the behavior of the initial state, in the case

Fig. 6   *The wavefunction* $\psi(r,R,\theta)$
of Eq. (25) as a function
of r and R for (a) $\theta=0$, *(b)*
$\theta=\pi/4$ *and (c)* $\theta=\pi/2$.

that one of the particles is separated from the others. In Figs. 6a–6c
we plot Eq. (25) as a function of r and R for $\theta=0, \pi/4$ and $\pi/2$,
respectively. The difference with the exact wavefunction (Figs. 2a–2c)
is hardly observable. Only when all three atoms are located close to
the forbidden region, there are small deviations. We conclude that Eq.
(25) provides for a simple and accurate approximation of the T=0 bbb
incoming state, also for more strongly bound molecular states.

V. THE FINAL STATE

A calculation of the outgoing atom-molecule scattering state based on the Faddeev formalism is in principle possible. However, as we already pointed out in I, the solution of this problem is even more difficult than the determination of the initial state, because of the rapidly oscillating character of the singlet t matrix and the numerous bound states, which enter into the calculation. Furthermore, the number of α channels which have to be taken into account is at least a factor of 6 larger, and the solution now depends on the strength of the applied magnetic field. Therefore, we present as a first step a calculation of $|\psi_f^{(-)}\rangle$, in which atom-molecule (in)elastic scattering is included. The only approximation left is the neglect of rearrangement processes.

Our starting point is the three-particle Lippmann-Schwinger equation[16]

$$|\psi_f^{(-)}\rangle = (1+P_{23}) |\phi_1\rangle + G_1^{(-)}(E) (V_2^c + V_3^c) |\psi_f^{(-)}\rangle. \qquad (26)$$

The channel resolvent operator $G_1^{(-)}(E)$ of pair 1 is given by

$$G_1^{(-)}(E) = (E - i0 - H_0 - V_1^c)^{-1}, \qquad (27)$$

where

$$H_0 = p^2/m_H + 3q^2/4m_H + 2\mu_B B S_z \qquad (28)$$

is the free three-particle Hamilton operator, including the Zeeman energy. The driving term $|\phi_1\rangle$ of the Lippmann-Schwinger equation (26) was used in Sec. III instead of the exact final state $|\psi_f^{(-)}\rangle$ to calculate the rate constant. It is an undistorted wavefunction, in which pair 1 is bound with vibrational and rotational quantum numbers v and ℓ, while atom 1 is free. In the angular momentum basis it can be expressed as follows:

$$|\phi_1\rangle = |\psi_{v\ell m} \, \vec{q}_f\rangle \, |(0\tfrac{1}{2}) \, \tfrac{1}{2}M_S\rangle =$$

$$\sum_{\lambda\mu} (\ell m \, \lambda\mu | LM_L) \, Y^*_{\lambda\mu}(\hat{q}_f) \, |\psi_{v\ell} \, q_f\lambda\rangle \, |(0\tfrac{1}{2}) \, \tfrac{1}{2}M_S\rangle, \tag{29}$$

where the spherical harmonics $Y_{\lambda\mu}$ describe the angular dependence of $|\phi_1\rangle$ and $(\ell m \, \lambda\mu | LM_L)$ is a Clebsch–Gordan coefficient. For reasons of linearity we can replace $|\phi_1\rangle$ in Eq. (26) by the vector

$$|\psi_{v\ell} \, q_f\lambda\rangle \, |(0\tfrac{1}{2}) \, \tfrac{1}{2}M_S\rangle = \int_0^\infty p^2 dp \, \psi_{v\ell}(p) \, |p \, q_f \, (\ell\lambda) \, LM_L\rangle \, |(0\tfrac{1}{2}) \, \tfrac{1}{2}M_S\rangle, \tag{30}$$

and solve Eq. (26) for such a vector separately.

Taking into account the possibility that the molecule changes its vibrational and rotational quantum numbers during the collision with the atom, but excluding rearrangement of atoms leads to the following expression for the final state:

$$|\psi_f^{(-)}\rangle = \sum_{v''\ell''\lambda''} \int_0^\infty p''^2 dp'' \int_0^\infty q''^2 dq'' \, \psi_{v''\ell''}(p'') \, \eta_{v''\ell''\lambda''}(q'')$$

$$\times |p''q'' \, (\ell''\lambda'')LM_L\rangle \, |(0\tfrac{1}{2}) \, \tfrac{1}{2} \, M_S\rangle. \tag{31}$$

The function $\eta_{v''\ell''\lambda''}(q'')$ describes the motion of the atom in the channel denoted by the quantum numbers v'', ℓ'' and λ''. The vibrational quantum number v'' runs over all possible bound states, belonging to a specific angular momentum ℓ'' of pair 1. Furthermore, ℓ'' is limited to odd values, due to the singlet character of the subsystem. In connection with the fact that $\ell''+\lambda''=$even (see I), this restricts λ'' to odd values, which obey the triangular rule $|\ell''-L|\leq\lambda''\leq\ell''+L$. Note that Eq. (31) does not include a sum over L, M_L and M_S due to the fact that the central interactions conserve these angular momenta.

The solution of the Lippmann–Schwinger equation (26) is in principle not defined uniquely,[16] because the two states $P_{12}P_{23}|\psi_f^{(-)}\rangle$ and $P_{13}P_{23}|\psi_f^{(-)}\rangle$ for which pair 2 or 3 is bound, respectively, obey the homogeneous equation and can be admixed arbitrarily. However, our special choice Eq. (31) for $|\psi_f^{(-)}\rangle$, in which

rearrangement terms are excluded, prevents the appearance of these undesired solutions.

Substitution of Eqs. (30) and (31) in the Lippmann–Schwinger equation (26) and a subsequent projection of the equation on $|\psi_{v'\ell'},q'\lambda'\rangle|(0\tfrac{1}{2})\,\tfrac{1}{2}M_S\rangle$ leads to a set of coupled one–dimensional integral equations:

$$
\eta_{v'\ell'\lambda'}(q') = \delta_{v'v}\delta_{\ell'\ell}\delta_{\lambda'\lambda}\frac{\delta(q'-q_f)}{q'^2} + \frac{1}{E_{v\ell}-E_{v'\ell'}+3q_f^2/4m_H-3q'^2/4m_H-i0}
$$

$$
\times \sum_{v''\ell''\lambda''}\int_0^\infty q''^2 dq''\, V_{v'\ell'\lambda',v''\ell''\lambda''}(q',q'')\,\eta_{v''\ell''\lambda''}(q''),
\tag{32}
$$

where we used the energy–conservation relation (7) to rewrite the energy denominator. The coupling matrix of Eq. (32) is given by

$$
V_{v'\ell'\lambda',v''\ell''\lambda''}(q',q'') = \int_0^\infty p'^2 dp'\,\psi_{v'\ell'}(p') \int_0^\infty p''^2 dp''\,\psi_{v''\ell''}(p'')
$$

$$
\times \langle p'q'\ (\ell'\lambda')LM_L|\langle(0\tfrac{1}{2})\,\tfrac{1}{2}M_S|\ (V_2^C + V_3^C)\ |(0\tfrac{1}{2})\,\tfrac{1}{2}M_S\rangle|p''q''\ (\ell''\lambda'')\ LM_L\rangle.
\tag{33}
$$

In our notation we suppressed the label L of the coupling matrix, since this has the unique value 2. This results from the fact that the dipole interaction, being a tensor operator of rank 2 in orbital space, causes transitions from L=0 in the initial state to L=2 in the final state. Eq. (33) is essentially the Fourier transform of a matrix element of the non–spherical atom–molecule interaction

$$
V_{v'\ell',v''\ell''}(R,\theta) = \sum_\kappa \frac{(2\kappa+1)}{2}\,V^\kappa_{v'\ell',v''\ell''}(R)\,P_\kappa(\cos\theta),
\tag{34}
$$

resulting from the average of the central interactions $V_2^C+V_3^C$ weighted by the product of the radial wavefunctions of the initial and final molecular states:

110

$$V^{\kappa}_{v'\ell',v''\ell''}(R) = \int_0^{\infty} r^2 dr \, \psi_{v'\ell'}(r) \, \psi_{v''\ell''}(r)$$

$$\times \int_{-1}^{1} d(\cos\theta) \, P_{\kappa}(\cos\theta) \left[V_{direct}(|\vec{R}+\tfrac{1}{2}\vec{r}|) + V_{direct}(|\vec{R}-\tfrac{1}{2}\vec{r}|) \right]. \tag{35}$$

The direct interaction is the sum of triplet and singlet interactions, $V_{direct} = \frac{3}{4}V^c_{s=1} + \frac{1}{4}V^c_{s=0}$, which has a strongly repulsive character. Only even κ values, which obey the triangular inequality $|\ell'-\ell''| \leq \kappa \leq \ell'+\ell''$, contribute. In Fig. 7 we present the potential surface $V_{v'\ell',v'\ell'}(R,\theta)$ as a function of $x'=R\sin\theta$ and $z'=R\cos\theta$, describing the elastic interaction of the atom and the molecule with quantum numbers $v'=14$, $\ell'=3$. Note that the potential is extremely repulsive for $x'\simeq 0$ and $z'\simeq\pm 2.7$ a_0, avoiding a close approach of atom 1 and one of the bound atoms, when the bound particles of the subsystem 1 have their most probable distance $r\simeq 5.4$ a_0.

Eq. (32) cannot be solved numerically as it stands, due to the presence of the Dirac δ function and the singular energy denominator. Instead, we solve the equation for the corresponding half-shell t matrix
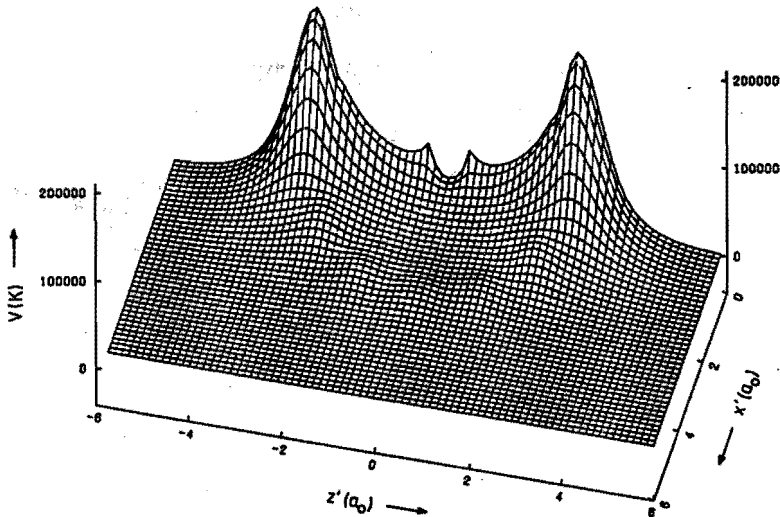

Fig. 7 *The diagonal potential* $V_{v'\ell',v'\ell'}$ *as a function of* $x'=R\sin\theta$
and $z'=R\cos\theta$ *for* $v'=14$, $\ell'=3$.

111

$$T_{v'\ell'\lambda',v\ell\lambda}(q',q_f,E_{v\ell}+3q_f^2/4m_H) =$$

$$\sum_{v''\ell''\lambda''} \int_0^\infty q''^2 dq'' \, V_{v'\ell'\lambda',v''\ell''\lambda''}(q',q'') \, \eta_{v''\ell''\lambda''}(q''). \tag{36}$$

The Lippmann-Schwinger equation for T contains no δ functions anymore and the poles in the integral kernel of the equation, related to the presence of additional incoming waves in the open channels, can now be handled without problems (see I).

We now turn to results for T, η and subsequently for $L_g^{\pm\frac12}$, L_g^{eff}. We solved the equation for T for various outgoing states v,ℓ,λ. It turns out that only the $|\psi_f^{(-)}\rangle$ states corresponding to $v=14,\ell=3$ and $v=14,\ell=1$ contribute significantly to the recombination rate, as was the case in Sec. III. However, within each of these $|\psi_f^{(-)}\rangle$ states the coupling to other loosely bound states with quantum numbers v' and ℓ' has to be taken into account. Scattering in the elastic channel appears to be dominant, while the contribution of other states decreases strongly with an increasing energy separation $E_{v'\ell'}-E_{v\ell}$ from the elastic channel. Inclusion of the six possible levels with $v'=13$, $\ell'=1,3,5,7$ and $v'=14$, $\ell'=1,3$ is found to be sufficient to solve the problem. Including the corresponding λ' values, the coupling within a total number of 16 channels is taken into account for each $|\psi_f^{(-)}\rangle$ state. Furthermore, we have to use roughly a number of 20 q grid points to find a converged solution. This leads to a matrix equation, of which the dimension is small enough to solve by matrix inversion.

From T we calculate η by making use of Eqs. (32) and (36). The wavefunction in coordinate space can subsequently be evaluated by means of a Fourier transformation

$$\eta_{v'\ell'\lambda'}(R) = i^{\lambda'} \left[\frac{2}{\pi}\right]^{\frac12} \int_0^\infty q'^2 dq' \, \eta_{v'\ell'\lambda'}(q') \, J_{\lambda'}(q'R). \tag{37}$$

In Figs. 8a-8c we plot the real and imaginary parts of these functions for $\lambda'=1,3,5$ and $v'=14,\ell'=3$, while the final channel has the quantum numbers $v=14,\ell=3,\lambda=3$. Note that $\eta_{v'\ell'\lambda'}(R)$ vanishes for small R values as a result of the repulsive character of V. Scattering within the

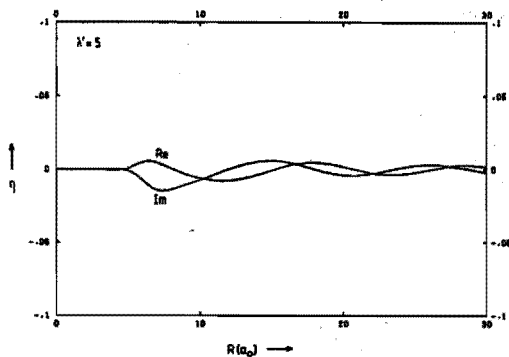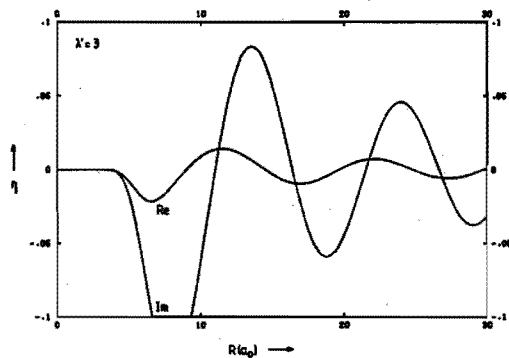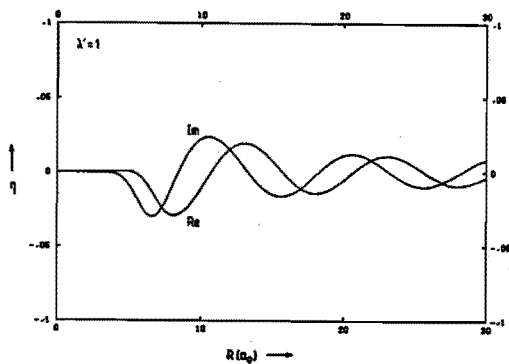Fig. 8 The relative atom-molecule motion $\eta_{v'\ell'\lambda'}(R)$ in the channel
$v'=v=14$, $\ell'=\ell=3$, for (a) $\lambda'=1$, (b) $\lambda'=3$ and (c) $\lambda'=5$. The
final channel is $v=14,\ell=3,\lambda=3$.

elastic channel $\lambda'=\lambda=3$ is observed to be dominant. The coupling to v',ℓ' states, except for $v'=14,\ell'=1$ and $\ell'=3$, is so weak that the solution in these channels would be hardly visible on the scale of Fig. 8.

With the help of the final state presented here, we calculate the effective rate constant, as well as the partial contributions $L_g^{\pm\frac{1}{2}}$, as a funtion of B. The results are presented in Fig. 4 (curve 3) and Fig. 3 (curves 2 and 4), respectively. Although the magnetic-field dependence is now less strong, L_g^{eff} is still increasing in the range 6-8 T where experimental data are available. Furthermore, the magnitude of the effective rate constant L_g^{eff} is roughly a factor of 5 too small in this range. Therefore, we are led to the important conclusion that rearrangement (the dipole-exchange mechanism of I) is an essential ingredient of the decay mechanism, and should be included in any future attempt to give a realistic description of volume recombination.

Compared to the case of the undistorted final state, the contribution to the dipole matrix element is largely suppressed for small atom-molecule distances R due to the repulsive character of the non-spherical interaction, especially for small angular momenta λ of atom 1. This is the reason for the smaller absolute magnitude of L_g^{eff}. The incorporation of three-particle correlations in the initial and final states explains the weaker field dependence of the effective rate constant L_g^{eff}. In the calculation of Kagan, the final momentum $\vec{q}_f$ of atom 1 relative to the molecule is to be induced by the dipole interaction. This momentum transfer decreases for increasing magnetic-field strengths, leading to a strongly increasing B-dependence of the rate constant (Fig. 4: curve 1). Part of this momentum change can be provided by the additional triplet interactions, taken into account in the exact $S|\psi_i^{(+)}\rangle$. This gives rise to a first sign of a weaker B-dependence (curve 2). The effect is further amplified by the incorporation of the final atom-molecule interactions, because the effective repulsive interactions can cause large momentum changes of the particles (curve 3).

We end this section with an important remark concerning the approach of Kagan et al.[9] In Sec. IV we explained that Kagan's approximation with respect to the initial state is excellent, as long

as the contributions to L_g^{eff} are dominated by extended bound states. The relative contribution of the $v=14,\ell=1$ state increases due to the inclusion of the final state interactions. A replacement of our exact initial state by the approximation Eq. (24) indeed turns out to be disastrous: the absolute magnitude of L_g^{eff} increases by roughly a factor of 2 in a Kagan-like calculation, due to the over-estimate of the $v=14, \ell=1$ contribution.

VI. CONCLUSIONS

We presented a calculation of the effective bulk rate constant L_g^{eff} in which all three-particle collision aspects are included, except for rearrangement. Kagan's approximation with respect to the initial state appears to be excellent, as long as the contribution to the transition probability is dominated by extended bound states, like the $v=14,\ell=3$ state. Inclusion of the initial state correlations gives rise to a weaker B-dependence of L_g^{eff}. The dependence on the magnetic-field strength becomes even weaker due to the incorporation of (in)elastic atom-molecule scattering in the final state. The absolute magnitude of L_g^{eff} is now roughly a factor of 5 too small. We therefore conclude that rearrangement (the dipole-exchange mechanism), is very important. Furthermore, it seems probable that the dipole-exchange mechanism is also essential to resolve the disagreement with experiment in the case of surface recombination.

ACKNOWLEDGEMENT

REFERENCES

[1] T.J. Greytak and D. Kleppner, *New Trends in Atomic Physics*, Les Houches Summer School, 1982, G. Greenberg and R. Stora, Eds. (North-Holland, Amsterdam, 1984), p. 1125.

[2] I.F. Silvera and J.T.M. Walraven, *Progr. in Low Temp. Phys.*, edited by D.F. Brewer (North-Holland, Amsterdam, 1985) Vol. X p. 139.

[3] I.F. Silvera and J.T.M. Walraven, Phys. Rev. Lett. 44, 164 (1980)

[4] B.W. Statt and A.J. Berlinsky, Phys. Rev. Lett. 45, 2105 (1980).

[5] R.W. Cline, T.J. Greytak and D. Kleppner, Phys. Rev. Lett. 47, 1195 (1981).

[6] R. Sprik, J.T.M. Walraven and I.F. Silvera, Phys. Rev. Lett. 51, 479 (1983); H.F. Hess, D.A. Bell, G.P. Kochanski, R.W. Cline, D. Kleppner and T.J. Greytak, Phys. Rev. Lett. 51, 483 (1983).

[7] A.E. Ruckenstein and E.D. Siggia, Phys. Rev. B 25, 6031 (1982); B.W. Statt, Phys. Rev. B 25, 6035 (1982); R.M.C. Ahn, J.P.H.W. van den Eijnde, C.J. Reuver, B.J. Verhaar and I.F. Silvera, Phys. Rev. B 26, 452 (1982).

[8] H.F. Hess, D.A. Bell, G.P. Kochanski, D. Kleppner and T.J. Greytak, Phys. Rev. Lett. 52, 1520 (1984)

[9] Yu. Kagan, I.A. Vartan'yants and G.V. Shlyapnikov, Zh. Eksp. Teor. Fiz. 81, 1113 (1981), [Sov. Phys. JETP 54, 590 (1981)].

[10] L.P.H. de Goey, J.P.J. Driessen, B.J. Verhaar, and J.T.M. Walraven, Phys. Rev. Lett. 53, 1919 (1984).

[11] L.P.H. de Goey, H.T.C. Stoof, J.M.V.A. Koelman, B.J. Verhaar and J.T.M. Walraven, to be published.

[12] L.D. Faddeev, Zh. Eksp. Teor. Fiz. 39, 1459 (1961) [Sov. Phys. JETP 12, 1014 (1961)].

[13] L.P.H. de Goey, T.H.M. v.d. Berg, N. Mulders, H.T.C. Stoof, B.J. Verhaar and W. Glöckle, Phys. Rev. B 34, 6183 (1986).

[14] W. Kolos and L. Wolniewicz, J. Chem. Phys. 43, 2429 (1965).

[15] R.N. Porter and M. Karplus, J. Chem. Phys. 40, 1105 (1964).

[16] W. Glöckle, *The Quantum Mechanical Few Body Problem* (Springer-Verlag, Berlin, 1983).

[17] W. Glöckle, G. Hasberg and A.R. Neghabian, Z. Phyz. A — Atoms and Nuclei, 305, 217 (1982).

[18]G.A. Baker, *Essentials of Padé Approximants* (Academic, New York, 1975).

[19]K.E. Atkinson, Numer. Math. $\underline{22}$, 17 (1973).

[20]B. Shizgal, J. Chem. Phys. $\underline{58}$, 3424 (1973).

SCATTERING LENGTH AND EFFECTIVE RANGE FOR SCATTERING IN A PLANE AND IN HIGHER DIMENSIONS

B.J. VERHAAR, L.P.H. DE GOEY, E.J.D. VREDENBREGT and J.P.H.W. VAN DEN EIJNDE

Department of Physics, Eindhoven University of Technology, P.O. Box 513, 5600 MB Eindhoven, The Netherlands

The concepts of scattering length and effective range for low-energy scattering are introduced for general dimension n in such a way that previously encountered dimensional and discontinuity problems are avoided. The theory is applied to two-body scattering in two-dimensional atomic hydrogen gas adsorbed to a superfluid helium film.

1. Introduction. The study of two-dimensional gases adsorbed to a superfluid helium surface or helium interface [1] has strongly stimulated the development of theories of two-dimensional (2D) systems. In view of such applications we introduced [2] scattering length and effective range parameters for scattering in a plane, in analogy with the commonly used corresponding concepts in three dimensions. Applications to 2D atomic hydrogen gas in the same paper and a subsequent one [3] showed the usefulness of the concepts introduced. Our discussion was based on potentials which vanish beyond a certain range, an approximation which for all practical purposes is valid for H + H scattering, even at low energies. A publication by Bollé and Gesztesy [4] reconsidered the same topic for potentials which need not satisfy this requirement, including in particular a possible γ/r potential. Such a generalization might have important applications in connection with 2D electron and ion gases [1]. In addition the $n = 2$ result was shown to be a natural extension of the well-known $n = 3$ formalism in the sense that both turned out to be special cases of formulae for general n. This work, however, led to a concept of scattering length in two dimensions with the property that it is discontinuous for $\gamma \to 0$ and even changes from a dimensionless quantity for $\gamma \neq 0$ into one with the inappropriate dimension of $1/\log(\text{length})$ at $\gamma = 0$. In the present contribution it is our aim to generalize the discussion of ref. [2] to more general potentials and to general dimension. We also find our $n = 2$ effective-range formula to be a special case of that for general n without, however, meeting with the discontinuity and dimensional difficulties inherent in ref. [4].

2. Local scattering length. The radial Schrödinger equation for scattering of the lowest partial wave in n dimensions from a potential $V(r) + \gamma/r$ is given by

$$[-d^2/dr^2 + V(r) + \gamma/r + l(l+1)/r^2 - k^2] u(r, k, \gamma) = 0, \tag{1}$$

in which $l = \frac{1}{2}(n-3)$ and a factor $2\mu/\hbar^2$ is absorbed in V (μ = mass or reduced mass). For $V \equiv 0$ we have the basis solutions

$$F(r, k, \gamma) = k^{-1/2} F_l(\rho, \eta), \quad G(r, k, \gamma) = -k^{-1/2} G_l(\rho, \eta), \tag{2}$$

with wronskian equal to 1, in terms of regular and irregular Coulomb functions F_l and G_l for integer and half-integer l-values $l \geqslant -\frac{1}{2}$, in conventional notation [5,6].

The regular solution $u(r, k, \gamma)$ of eq. (1) is chosen with normalization such that it satisfies the energy-independent and γ-independent boundary condition

$$\lim_{r \to 0} r^{-l-1} u = 1. \tag{3}$$

Then by Poincaré's theorem [7] both u and its radial derivative $u' := \partial u/\partial r$ are known to be entire functions of k^2 and γ for any fixed value of r. This is true under rather general conditions for the behavior of V. Splitting off $c_l(\eta)k^{l+1/2}$, in conventional notation, from F the same is true for that function.

We consider effective-range formulae for the phase-shift $\delta(k,\gamma,r)$ with V cut off [8] at r. We have

$$\cot\delta(k,\gamma,r) = (G'u - Gu')/(F'u - Fu')|_r. \tag{4}$$

Inserting the low-energy behavior [6] of G and that of u and F, as well as their derivatives, we recover our 2D effective-range formula [2]

$$\cot\delta = (2/\pi)(C + \log\tfrac{1}{2}ka) + O(k^2), \tag{5}$$

for $n = 2, \gamma = 0$, and furthermore

$$k^{2l+1}\cot\delta = -[\Gamma(l + 3/2)]^2 2^{2l+1}/\pi(l + \tfrac{1}{2})\, a^{2l+1} + O(k^2) \quad (n > 2, \gamma = 0), \tag{6}$$

$$\cot\delta = -(2/\pi)[e^{2\pi i} - (-1)^{2l}] [K_{2l+1}(2\sqrt{\gamma a})/I_{2l+1}(2\sqrt{\gamma a}) + O(k^2)] \quad (\gamma \neq 0). \tag{7}$$

We left out arguments r, k, γ of δ and r, γ of a. We denote Euler's constant 0.577215.... by C instead of γ to avoid confusion with the $1/r$ strength parameter. In Terms of $u_0 := u(r,0,\gamma)$ and $U_0 := (2l + 2)u_0 - 2ru_0'$ the "local" scattering length a in (5)–(7) is defined by

$$a = r\exp(2u_0/U_0) \quad (n = 2, \gamma = 0), \tag{8}$$

$$a = r[1 + (2l + 1)2u_0/U_0]^{1/(2l+1)} \quad (n > 2, \gamma = 0), \tag{9}$$

$$\frac{K_{2l+1}(2\sqrt{\gamma a})}{I_{2l+1}(2\sqrt{\gamma a})} = \frac{K_{2l+1}(2\sqrt{\gamma r})U_0 - 2\sqrt{\gamma r}\,K_{2l+2}(2\sqrt{\gamma r})u_0}{I_{2l+1}(2\sqrt{\gamma r})U_0 + 2\sqrt{\gamma r}\,I_{2l+2}(2\sqrt{\gamma r})u_0} \quad (\gamma \neq 0), \tag{10}$$

where K and I represent modified Bessel functions [5]. For three dimensions and $\gamma \neq 0$ the definition of a differs from the usual one. It has the advantage that it behaves smoothly as $\gamma \to 0$ also for $n = 2$. In addition it has the physical significance of an equivalent hard-sphere radius. The expression for $n = 2$ is the limit for $n \to 2$ of the $n > 2$ formula.

To obtain effective-range formulae for $r \to \infty$ we generalize $a(r,\gamma)$ to an equivalent hard-sphere radius $a(r,k,\gamma)$ for $k \neq 0$:

$$\cot\delta(k,r,\gamma) = G(a(r,k,\gamma),k,\gamma)/F(a(r,k,\gamma),k,\gamma). \tag{11}$$

This defines $a(r,k,\gamma)$ uniquely, if we require it to go continuously to $a(r,\gamma)$ for $k \to 0$. It satisfies the radial differential equation

$$a' = V(r)[F(a,k,\gamma)G(r,k,\gamma) - F(r,k,\gamma)G(a,k,\gamma)]^2. \tag{12}$$

An analogous equation for $a = a(r,\gamma)$ follows by the limit $k \to 0$ or by differentiation of (8)–(10):

$$a' = V(r)\,ar[\log(r/a)]^2 \quad (n = 2, \gamma = 0), \tag{13}$$

$$a' = V(r)\,ar\{(2l + 1)^{-1}[(r/a)^{l+1/2} - (a/r)^{l+1/2}]\}^2 \quad (n > 2, \gamma = 0), \tag{14}$$

$$a' = 4ar\,V(r)[K_{2l+1}(2\sqrt{\gamma a})I_{2l+1}(2\sqrt{\gamma r}) - I_{2l+1}(2\sqrt{\gamma a})K_{2l+1}(2\sqrt{\gamma r})]^2 \quad (n \geq 2, \gamma \neq 0). \tag{15}$$

We now equate (4) and (11) and multiply by $c_l^2 k^{2l+1}$:

$$T(a,r,k^2,\gamma) \equiv \frac{u(r)u'_{HS}(r) - u'(r)u_{HS}(r)}{F(a)[F(r)u'(r) - F'(r)u(r)]/[c_l^2 k^{2l+1}]} = 0. \tag{16}$$

372

120

In the second member of this equation we left out the arguments k and γ, while $u_{HS}(r) = F(a)G(r) - G(a)F(r)$ represents a (extrapolated) wave function for scattering from a hard sphere with radius a. From the analyticity properties of the functions in (16), following from Poincaré's theorem, we find by the implicit function theorem of complex function theory that $a(r, k, \gamma)$ is analytic in k^2 near $k = 0$ and in γ near $\gamma = 0$. The same properties can then be derived for $a(r = \infty, k, \gamma)$ by considering eqs. (12)–(15) for a potential V which decreases exponentially at infinity. This condition can be relaxed to a certain extent if continuity properties for a and a number of its k^2 and γ derivatives are desired. Such properties as a function of k^2 enable us to write down effective-range formulae (5)–(7) for $r \to \infty$ as asymptotic expressions with any desired number of k^2 powers. The resulting scattering length $a(\gamma)$ has for all n the dimension of length, the physical significance of an equivalent hard-sphere radius and the property of smoothness for $\gamma \to 0$. Upon comparing with ref. [4] we have

$$K_{2l+1}(2\sqrt{\gamma a})/I_{2l+1}(2\sqrt{\gamma a}) = [(2l+1)!]^2/2\gamma^{2l+1}a_B \quad (\gamma \neq 0), \tag{17}$$

$$a_B = -1/\log a \quad (n = 2, \gamma = 0), \qquad a_B = (n-2)a^{n-2} \quad (n > 2, \gamma = 0), \tag{18,19}$$

denoting the scattering length introduced by Bollé and Gesztesy by a_B. It is interesting to compare a and a_B for small non-vanishing γ. Approximating the K/I ratio for small argument we recover (19) for $n > 2$ and find $a_B = -1/(2C + \log \gamma a)$ for $n = 2$. Contrary to the continuity of a_B for $\gamma \to 0$ if $n > 2$, we thus find the two-dimensional a_B to tend to 0 for $\gamma \to 0$, whereas at $\gamma = 0$ it assumes a non-vanishing value. Apparently, a_B is even discontinuous with respect to physical dimension. Essentially, these problems are connected with the difficulties arising from the interchange of the $k \to 0$ and $\gamma \to 0$ limits. This contrasts with the smooth charge-dependence of our scattering length for all $n \geqslant 2$ under rather general conditions on V, making it possible to take into account the effect of charges on the neutral scattering length not only for $n = 3$ as in ref. [4], but for any n. We confirmed the above-mentioned behavior of a and a_B with γ by means of numerical calculations.

3. *Applications.* Scattering from an (attractive) square well with radius r is an analytically solvable illustration. From (8) and (9) we find

$$a(r) = r \exp[J_0(Kr)/KrJ_1(Kr)] \quad (n = 2), \tag{20}$$

$$a(r) = r/[1 - (2l+1)J_{l+1/2}(Kr)/KrJ_{l+3/2}(Kr)]^{1/(2l+1)} \quad (n > 2). \tag{21}$$

The $k = 0$ wave number within the well is denoted by K. The ratio of the oscillating Bessel functions leads to a cot Kr-like behavior. Again, the expression for $n = 2$ is the limit for $n \to 2$ of the $n > 2$ formula.
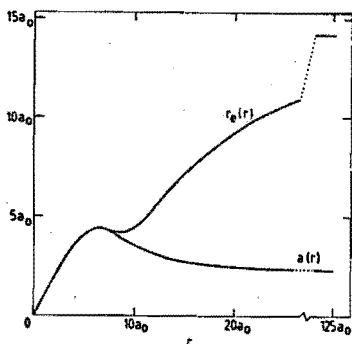

Fig. 1. Local scattering length $a(r)$ and effective range $r_e(r)$ for triplet scattering of H-atoms adsorbed at a superfluid helium film. The horizontal scale has been interrupted to indicate the asymptotic values at $125a_0$.

373

For the scattering of adsorbed H-atoms we show in fig. 1 how $a(r)$ and $r_e(r)$ build up as a function of r starting from 0 at the origin. We describe the scattering as a 2D phenomenon, accounting [9] for the spatial extent of the bound states of the H-atoms by averaging the H—H interaction potential with a gaussian weight-function (maximum value [10] equal to $0.050\, a_0^{-1}$) of the relative vertical distance. For small r $a(r)$ and $r_e(r)$ are both seen to be almost equal to r. This is due to the extreme hardness of the inner repulsive part of the potential. At about $7a_0$ the curves start to diverge; $a(r)$ continues to decrease due to the attractive part of the potential. Note that $r_e(r)$ converges more slowly than $a(r)$. The asymptotic values are found to be: $a = 2.3a_0$ and $r_e = 14.3a_0$. These parameter values can be used for the analysis of low-energy H—H scattering at a superfluid ^{4}He surface. To give some feeling for the influence of the width of the relative vertical probability distribution we here present the corresponding values for a truly 2D gas (i.e. no averaging): $a = 2.0a_0$ and $r_e = 17.4a_0$.

References

[1] J.T.M. Walraven, Physica 126B (1984) 176;
    P. Leiderer, Physica 126B (1984) 92.
[2] B.J. Verhaar, J.P.H.W. van den Eijnde, M.A.J. Voermans and M.M.J. Schaffrath, J. Phys. A17 (1984) 595.
[3] L.P.H. de Goey, J.P.J. Driessen, B.J. Verhaar and J.T.M. Walraven, Phys. Rev. Lett. 53 (1984) 1919.
[4] D. Bollé and F. Gesztesy, Phys. Rev. Lett. 52 (1984) 1469; Phys. Rev. A30 (1984) 1279.
[5] M. Abramowitz and I.A. Stegun, Handbook of mathematical functions (Dover, New York, 1968).
[6] F.S. Ham, Quart. Appl. Math. 15 (1957) 31.
[7] H. Poincaré, Acta Math. 4 (1884) 201;
    R.G. Newton, Scattering theory of waves and particles, 2nd Ed. (New York, 1982) p. 334.
[8] F. Calogero, Variable phase approach to potential scattering (Academic Press, New York, 1967).
[9] J.P.H.W. van den Eijnde, C.J. Reuver and B.J. Verhaar, Phys. Rev. B28 (1983) 6309.
[10] D.O. Edwards and I.B. Mantz, J. de Phys. (Paris) C7 (1980) 257.

Scattering length and effective range for scattering in a plane and in higher dimensions

B. J. Verhaar, L. P. H. de Goey, J. P. H. W. van den Eijnde, and E. J. D. Vredenbregt

Department of Physics, Eindhoven University of Technology, Postbus 513, 5600 MB, Eindhoven, The Netherlands

(Received 9 November 1984)

It is shown how the concepts of scattering length and effective range, previously introduced for low-energy scattering from a potential $V(r)$ in a plane, correspond to the well-known parameters in three dimensions. This is done by considering low-energy scattering in a general dimension $n \geq 2$ and subsequently showing that both the $n = 2$ and $n = 3$ cases fit naturally in such a generalized treatment. Furthermore, our previous work is extended to long-range potentials, decreasing faster than $1/r^{n+1}$. The method used is based on the properties of a local scattering length $a(r)$ for the potential $V(r)$ cut off at radius r and an equivalent hard-sphere radius $a(r,k)$ for $k \neq 0$. Some applications and illustrative examples are given.

I. INTRODUCTION

In this paper we present a generalized effective-range theory for low-energy quantum scattering in n dimensions. Earlier we introduced[1] for the first time the scattering length and effective-range parameters for scattering in a plane, in analogy with the commonly used corresponding concepts in three dimensions. Applications to scattering of spin-polarized H atoms adsorbed at a superfluid helium film in the same paper and a subsequent one[2] showed the usefulness of the concepts of scattering length and effective range introduced. Our discussion was based on potentials which vanish beyond a certain range, an approximation which for all practical purposes is valid for H + H scattering, even at low energies.

In the present contribution it is our aim to generalize the discussion of Ref. 1 to more general potentials, using a variable-phase approach,[3] and to show that our scattering length fits naturally in a concept of scattering length for general dimension. In particular we shall show how the two-dimensional scattering length a builds up from the origin to infinity as the limit of a local value $a(r)$, defined for the (spherically symmetric) potential V cut off at r. Differential equation for $a(r)$ will be presented. These make clear that $a(r)$ tends to $a(\infty) = a$ under rather weak conditions for V, satisfied in particular by the H + H system. Our derivation also applies to the case where a $1/r$ potential is added to $V(r)$. In principle, this would make it possible to apply the method to electron-electron scattering in a two-dimensional electron system in the vicinity of a superfluid helium film. In view of our more immediate interest in two-dimensional neutral gases like spin-polarized atomic hydrogen, however, we confine the discussion to the case where a $1/r$ potential is absent.

Section II of this paper will be devoted to the introduction of a "local scattering length" $a(r)$, the introduction of an "equivalent hard-sphere radius" $a(r,k)$ for $k \neq 0$, as well as to the derivation of equations for these quantities. In Sec. III we derive from the properties of $a(r,k)$ the effective-range expansion for $r \to \infty$. Also, we compare our results to those of Bollé and Gesztesy,[4] who introduce a different concept of scattering length for both neutral

and charged scattering and for general dimension $n \geq 2$. In Sec. IV some applications and illustrative examples are given: scattering from a square well and scattering of H atoms adsorbed at a superfluid helium film.

II. LOCAL SCATTERING LENGTH FOR DIMENSIONS $n \geq 2$

The radial Schrödinger equation for scattering of the lowest partial wave in n dimensions from a potential $V(r)$ is given by

$$\left[-\frac{d^2}{dr^2} + V(r) + \frac{m^2 - \frac{1}{4}}{r^2} - k^2 \right] u(r,k) = 0 , \qquad (1)$$

in which $m = \frac{1}{2}n - 1$ and a factor $2\mu/\hbar^2$ is absorbed in V (μ is the mass or reduced mass). We consider the local phase shift[3] $\delta(k,r)$ for this potential V cut off at r. According to Ref. 1 its low-energy behavior is described, for $n = 2$, by

$$\cot\delta(k,r) = \frac{2}{\pi}[\gamma + \ln\tfrac{1}{2}ka(r)] + O(k^2) , \qquad (2)$$

$\gamma = 0.577\,215\,665\ldots$ representing Euler's constant. For any dimension $n \geq 2$, Eq. (2) may be generalized by using the equation

$$\cot\delta(k,r) = \frac{G'u - Gu'}{F'u - Fu'} . \qquad (3)$$

Here $u = u(r,k)$ is a regular solution of the radial equation including V. If its normalization is chosen to be such that it satisfies the energy-independent boundary condition

$$\lim_{r \to 0} r^{-(n-1)/2} u = 1 , \qquad (4)$$

both $u(r,k)$ and its radial derivative $u'(r,k) \equiv \partial u / \partial r$ are known to be entire functions of k^2 for any fixed value of r. In Eq. (3), $F(r,k)$ is a regular solution

$$F = \left[\frac{\pi r}{2} \right]^{1/2} J_m(kr) \qquad (5)$$

without V, while $G(r,k)$ is an irregular solution without V given by

$$G = \left[\frac{\pi r}{2}\right]^{1/2} N_m(kr) . \qquad (6)$$

The expressions for the function F and G in terms of the Bessel and Neumann functions[5] have been chosen so as to make the Wronskian equal to unity.

The analyticity properties of u, u', and the Bessel and Neumann functions in Eq. (3) and their behavior for small arguments then lead to Eq. (2) for $n = 2$ and

$$k^{2m}\cot\delta(k,r) = -\frac{[\Gamma(m+1)]^2 2^{2m}}{\pi m}\frac{1}{[a(r)]^{2m}} + O(k^2) \qquad (7)$$

for any $n > 2$. Here, for $m = 0$ the local scattering length[3] $a(r)$ is given by

$$a(r) = r \exp(2u_0/U_0) , \qquad (8)$$

whereas for $m > 0$,

$$a(r) = r/[1 - 2m(2u_0/U_0)]^{1/2m} , \qquad (9)$$

with

$$u_0 = u(r,0) , \qquad (10)$$

$$U_0 = u_0 - 2ru_0' + 2mu_0 . \qquad (11)$$

For $m = \frac{1}{2}$ Eq. (7) is the well-known three-dimensional effective-range formula

$$k\cot\delta(k,r) = -1/a(r) + O(k^2) . \qquad (12)$$

The three-dimensional scattering length and that introduced in Ref. 1 for $n = 2$ are thus seen to fit naturally in a definition for general $n \geq 2$, contrary to the suggestion in Ref. 4 (p. 1288). Note that the right-hand side of Eq. (9) tends to that of Eq. (8) for $m \rightarrow 0$.

As in three dimensions the local scattering length $a(r)$ can be interpreted as an equivalent hard-sphere radius: if the local solution of the wave equation including V, characterized by u_0 and u_0', is extrapolated by means of the wave equation for $k = 0$ without V, a node is found precisely at $a(r)$. This follows directly from Eqs. (8) and (9). It is well-known that for three-dimensional scattering the scattering length may become negative, which already generalizes the concept of an equivalent hard-sphere radius to unphysical values. This is related to the fact that in such a case the extrapolated local wave function cuts the axis beyond the origin. The same is true for all other odd dimensions. For these dimensions we choose $a(r)$ to be positive or negative, although in principle also $2m - 1 = n - 3$ equivalent complex roots exist. Similarly, for all even dimensions $n > 2$ it follows for Eq. (9) that complex values for $a(r)$ are unavoidable, corresponding to the absence of a zero of the curved extrapolated radial wave function in that case. From the $2m$ equivalent choices for $a(r)$ we choose that with the smallest phase in the complex plane (positive real if $1 - 4mu_0/U_0$ is positive). For dimension $n = 2$ an extrapolated zero always occurs in the interval from 0 to ∞. This exceptional role
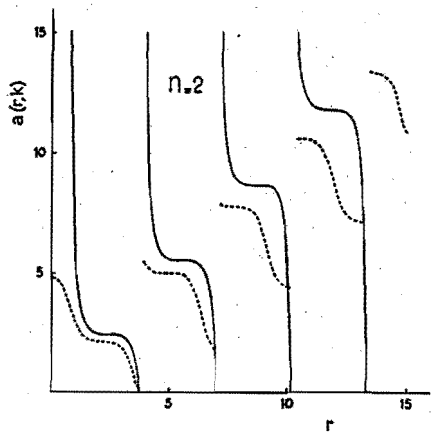

FIG. 1. Behavior of $a(r)$ for a square well of radius r in two dimensions (solid curve) and of $a(r,k)$ with $k=0.5$ (dashed curve).

of $n = 2$ may be related to the fact that for that dimension the "centrifugal" potential of the lowest partial wave is negative, so that the wave function bends more strongly towards the axis.

We point out that in dimension $n = 2$ the values $a = 0$ and ∞ are equivalent in the sense that δ changes continuously in going from the one value of a to the other. In all other dimensions the infinite a values are equivalent. See Figs. 1–3.

In the foregoing $a(r)$ has been defined so that the leading term in the long-wavelength energy dependence of $\cot\delta(k,r)$ is identical to that for scattering from a hard sphere with radius $d = a(r)$:
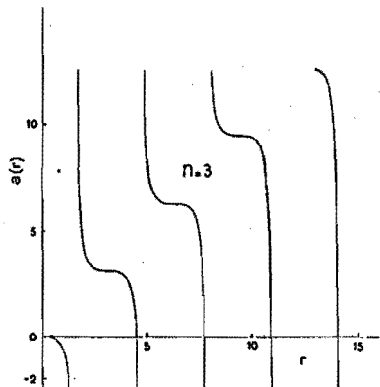

FIG. 2. Scattering length $a(r)$ for square well of radius r in three dimensions.
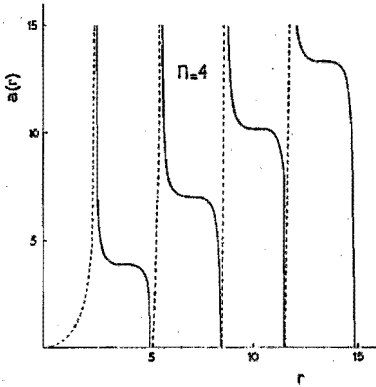
FIG. 3. Scattering length $a(r)$ for square well of radius r in four dimensions. Solid parts, $a(r)$ positive real. Dashed parts, $a(r)$ positive imaginary.

$$k^{2m}\cot\delta_{\mathrm{HS}}(k,d)=k^{2m}\frac{G(k,d)}{F(k,d)}$$

$$=\begin{vmatrix}\dfrac{2}{\pi}(\gamma+\ln\tfrac{1}{2}kd)+O(k^2)\ , & n=2\\[2mm]-\dfrac{[\Gamma(m+1)]^2 2^{2m}}{\pi m}\dfrac{1}{d^{2m}}+O(k^2)\ ,\\[2mm]\hspace{4cm} n>2\ .\end{vmatrix}\quad(13)$$

As explained previously, we are interested in the possibility of writing down equations such as (2) and (7) for long-range potentials, decreasing at infinity, for instance, as $1/r^6$ in the case of the two-dimensional scattering of (hydrogen) atoms. To that end we want to relate the low-energy behavior of $\cot\delta(k,\infty)$ to $a(\infty)=a$. This is not a trivial problem mathematically, since the interchange of two limits $(r\to\infty$ and $k\to0)$ is involved. To discuss this point properly we introduce an equivalent hard-sphere radius $a(r,k)$ also for $k\neq0$, i.e., in the spirit of Eq. (13),

$$\cot\delta(k,r)=\frac{G(k,a(r,k))}{F(k,a(r,k))}\ .\qquad(14)$$

Taken by itself Eq. (14) does not define $a(r,k)$ uniquely, since any radial node of the oscillating extrapolated radial wave function is an equivalent hard-sphere radius in this sense. However, for small k, $a(r,k)$ is uniquely defined, if we require it to approach $a(r)$ for $k\to0$. This is discussed in more detail in Sec. III.

A radial differential equation for $a(r,k)$ can be derived by differentiating both Eqs. (14) and (3) with respect to r:

$$\frac{d}{dr}\cot\delta(k,r)=\frac{a'}{F^2(k,a)}\ ,\qquad(15)$$

$$\frac{d}{dr}\cot\delta(k,r)=V(r)\left[\frac{u}{Fu'-F'u}\right]^2\ ,\qquad(16)$$

where we made use of the Wronskian relation of F and G. In Eq. (16) we omitted the arguments k,r of all functions within the large parentheses. Equating Eqs. (15) and (16) we find

$$\frac{a'}{F^2(a,k)}=V(r)\left[\frac{u}{Fu'-F'u}\right]^2\ ,\quad a=a(r,k)\ .\qquad(17)$$

A second useful equation for a' is obtained from Eq. (17) by expressing u'/u in terms of $\cot\delta(k,r)$ by means of Eq. (3) and replacing the latter quantity by the right-hand side of Eq. (14). The result is

$$a'=V(r)[F(r,k)G(a,k)-F(a,k)G(r,k)]^2\ ,$$
$$a=a(r,k)\ .\qquad(18)$$

Both Eqs. (16) and (18) make clear that $a(r,k)$, if real, increases (decreases) in radial regions where V is positive (negative). This is also clear intuitively. Equation (18) will be our most important starting point for the considerations of Sec. III.

By differentiating Eqs. (8) and (9) it is found that $a(r)$ satisfies a differential equation. For $n>2$ $(m>0)$ the result is

$$a'=V(r)ar\left[\frac{1}{2m}\left[\left[\frac{r}{a}\right]^m-\left[\frac{a}{r}\right]^m\right]\right]^2\ ,\quad a=a(r,0)$$
$$(19)$$

and for $n=2$ we get the equation

$$a'=V(r)ar\left[\ln\frac{r}{a}\right]^2\ ,\qquad(20)$$

of which the right-hand side may also be considered as the limit obtained for $m\to0$ from Eq. (19). For $n=3$ we have

$$a'=V(r)(r-a)^2\ .\qquad(21)$$

These equations show how the local scattering length $a(r)$ builds up starting from $r=0$. In addition they show again that the concept of scattering length that was proposed in Ref. 1 for two-dimensional scattering fits naturally in the general definition of an equivalent hard-sphere radius. For the following considerations it is of importance to point out that the right-hand sides of Eqs. (19)–(21) are the limit for $k\to0$ of the right-hand side of Eq. (18). Note that our $a(r)$, although being very similar to the quantity $a(r)$ introduced in Ref. 3, coincides with it only for $n=3$. The reason for introducing it in a different way for other n values is to avoid difficulties for $n=2$.

III. DERIVATION OF EFFECTIVE-RANGE EXPANSION FOR $r=\infty$

In this section we want to derive the low-energy behavior of the phase shift $\delta(k,r=\infty)$. As a first step we prove that $a(r,k)$ is an analytic function of k^2 in a vicinity of $k=0$ for any finite radius r for which $a(r,0)$ is not singular, i.e., finite and nonvanishing.

We equate the right-hand sides of Eqs. (3) and (14) mul-

125

tiplied by k^{2m}. The result is the equation

$$T(a,r,k^2)$$

$$\equiv k^{2m}\left[\frac{G(a,k)}{F(a,k)} - \frac{G'(r,k)u(r,k)-G(r,k)u'(r,k)}{F'(r,k)u(r,k)-F(r,k)u'(r,k)}\right]$$

$$=0 . \qquad (22)$$

If we introduce low-k expansions[5] for F, G, u, and their first derivatives, the logarithmic k dependence for even dimensions is found to cancel. The function T is extended by means of its $k=0$ limit

$$\ln\frac{a}{r}-\frac{2u_0}{U_0} \quad (m=0) , \qquad (23)$$

$$\frac{[\Gamma(m+1)]^2 2^{2m}}{2m}\left[\frac{1}{r^{2m}}\left(1-\frac{4mu_0}{U_0}\right)-\frac{1}{a^{2m}}\right] \quad (m>0) . \qquad (24)$$

For $k=0$ the solution of Eq. (22) is then given by the quantity $a(r)$ given in Eqs. (8) or (9). For fixed r, T is analytic in a in any bounded region in the complex a plane not containing the origin, and analytic in k^2 in a corresponding environment of $k=0$. Furthermore, for $k\to 0$ the derivative

$$T_a \equiv k^{2m}\frac{d}{da}\frac{G(a,k)}{F(a,k)} = \frac{k^{2m}}{F^2(a,k)} \qquad (25)$$

goes to nonvanishing value for nonsingular $a(r)$. According to the implicit-function theorem of complex-function theory,[6] this implies that in a vicinity of $k=0$ a solution $a(r,k)$, analytic in k^2, exists with $a(r,0)=a(r)$. We stress that this result has been shown to be valid for any finite r in which $a(r)$ is not singular.

We subsequently make the step to $r=\infty$, starting from a radius r_0 beyond which $a(r)$ is not singular and excluding the exceptional case that $a(r)$ tends to a singular value. We transform the infinite interval $[r_0,\infty)$ into a finite one by the transformation $s=1/r$. The differential equations (18)—(21) then take the form

$$\frac{da}{ds}=f(s,a,k^2) \qquad (26)$$

with

$$f=-\frac{1}{s^2}V\left(\frac{1}{s}\right)\left[F\left(\frac{1}{s},k\right)G(a,k)-F(a,k)G\left(\frac{1}{s},k\right)\right]^2 \qquad (27)$$

for $0<s\leq s_0=1/r_0$. We now want f to be continuous at $s=0$. For $k\neq 0$ this implies that $f(0,a,k^2)=0$, taking into account the rapid oscillations of f near $s=0$. Requiring in addition that $f(0,a,k^2)$ is continuous at $k=0$, $f(s,a,0)$ has also to go to zero for $s\to 0$. In view of Eqs. (19)—(21) we therefore conclude that V should go to zero faster than $1/r^{n+1}$. It is then possible to extend the function f by defining it to be zero in an arbitrary closed interval $[s_1,0]$, $s_1<0$. We assume $V(r)$ to be continuous or to have a finite number of discontinuities. We stress that it is not our purpose to find the weakest possible mathematical condition for V.

With respect to $a(r,k)$ for $k=0$ the possibility mentioned in the previous paragraph to choose r_0 and the existence of a finite limit $a(\infty)=a$ now follow from a theorem in the theory of ordinary differential equations.[7] Furthermore, we may conclude[8] the following. (i) $a(\infty,k)$ is continuous as a function of k^2 in a vicinity of $k=0$. For $a(\infty,k)$ to have a continuous derivative of order i, the requirement on V should be correspondingly strengthened: V should go to zero faster than $1/r^{n+2i+1}$. A stronger result follows[9] from a stronger condition for V: (ii) $a(\infty,k)$ is analytic in a vicinity of $k=0$, if V decreases faster than $\exp(-\lambda r)$ $(\lambda>0)$.

The third step in our derivation concerns the low-energy behavior of $\cot\delta(k,\infty)$. From Eq. (14) we have

$$\cot\delta(k)\equiv\cot\delta(k,\infty)=\frac{N_m(ka(\infty,k))}{J_m(ka(\infty,k))} , \qquad (28)$$

which equals

$$\frac{2}{\pi}[\ln\tfrac{1}{2}ka(\infty,k)+\gamma]+\frac{2}{\pi}[\tfrac{1}{2}ka(\infty,k)]^2+\cdots \qquad (29)$$

for $n=2$ and

$$\frac{1}{\pi}[2\ln\tfrac{1}{2}ka(\infty,k)+\gamma-\psi(m+1)]\delta_{n,\text{even}}$$

$$-\frac{2^{2m}[\Gamma(m+1)]^2}{\pi m[ka(\infty,k)]^{2m}}+\cdots \qquad (30)$$

for $n>2$. We now use the analyticity or C^i property of $a(\infty,k)$ to expand $a(\infty,k)$ in powers of k^2 in this expression. This leads us to

$$\cot\delta(k)=\frac{2}{\pi}(\ln\tfrac{1}{2}ka+\gamma)+\frac{1}{2\pi}r_e^2 k^2+\cdots \quad (n=2) \qquad (31)$$

$$\cot\delta(k)=-\frac{4}{\pi a^2}\frac{1}{k^2}+\frac{2}{\pi}(\ln\tfrac{1}{2}kr_e+\gamma-\tfrac{3}{4})+\cdots$$

$$(n=4) \qquad (32)$$

$$\cot\delta(k)=-\frac{2^{2m}[\Gamma(m+1)]^2}{\pi ma^{2m}}\frac{1}{k^{2m}}$$

$$-\frac{2^{2m-1}[\Gamma(m+1)]^2}{\pi(m^2-1)r_e^{2m-2}}\frac{1}{k^{2m-2}}+\cdots , \qquad (33)$$

the last expression being valid for $n>2$, $n\neq 4$. Here the effective range r_e is given by

$$r_e=\begin{cases} a\exp\dfrac{4\dot{a}}{a^3} & (n=4) \qquad (34) \\[2ex] a/[1-4(m^2-1)(\dot{a}/a^3)]^{1/(2m-2)} & (n\neq 4) \qquad (35) \end{cases}$$

with $\dot{a}=\partial a(\infty,k)/\partial k^2$ for $k=0$. The effective range r_e is normalized for all dimensions in such a way that its value equals d for hard-sphere scattering [see $O(k^2)$ term in Eq. (13)]. This corresponds to the convention chosen for $n=2$ in Ref. 1. For $n=3$ our convention differs from the usual one by a factor of $\tfrac{3}{2}$.

For even dimensions the $(m+1)$th term in Eq. (33) has a logarithmic k dependence, as in Eqs. (31) and (32). Apart from this logarithmic term the expansion of $k^{2m}\cot\delta(k)$ in the three equations is to be interpreted as a convergent Taylor series of a function analytic in k^2, or, in the more general situation, (i) as an asymptotic expansion.

Note that analogous to the case of Eqs. (8) and (9) the present equation (34) can be considered as the limit for dimension approaching 4 of Eq. (35). Apart from the usefulness of the $n \geq 2$ formulas in providing a generalized framework for the special $n=2$ and $n=3$ cases, the equations for $n \geq 4$ may also have applications in studies of the energy dependence for higher partial waves in two and three dimensions which are also described by Eq. (1).

Note that the k dependence in Eqs. (31)—(33) is identical to that found by Bollé and Gesztesy[4] (neutral case). A difference is that we introduce both the scattering length a and the effective range r_e, each of which has the physical significance of a radius of an equivalent hard sphere giving rise to the same energy dependence of the scattering phase shift in a specific order of the effective-range expansion. In addition, we believe our method of derivation to be more transparent, due to the use of the (adapted) variable-phase approach.[3]

Looking especially at our $n=2$ formula (31) [see also Eq. (13) of Ref. 1] and comparing with the corresponding equation

$$\cot\delta(k) = \frac{2}{\pi}\left[\ln\tfrac{1}{2}k - \frac{1}{a_B} + \gamma\right] + O(k^2) , \tag{36}$$

obtained by Bollé and Gesztesy,[4] we indeed observe the same k dependence. Equation (36), in which for distinction we indicate the scattering length as a_B, has been derived in dimensionless quantities. Inserting dimensions one would either have to insert a length scale r_0 to the logarithmic argument, changing it into $\ln\tfrac{1}{2}kr_0$, which would keep a_B dimensionless but dependent on r_0, or one would replace $\ln\tfrac{1}{2}k - 1/a_B$ by $\ln\tfrac{1}{2}ka$ which is our choice. By our approach, in which dimensions are taken along in the derivation, a (and r_e) has the dimension of length from the beginning for all n. It is of importance to point out that the problem does not provide a natural length scale r_0.

In this paper we met some examples in which an equation for a specific dimension could be seen as a limit of an equation for general dimension. Equations (31)—(33) seem to be exceptions in this respect. We note, however, that an analogous derivation for any real dimension $n \geq 2$ gives rise to an additional term $\cos(\mu\pi)/\sin(\mu\pi)$ in the $\cot\delta(k)$ expression $(\mu = \tfrac{1}{2}n - 1)$. Adding this to Eq. (33) with m replaced by μ, one does obtain Eq. (31) in the limit $\mu \to 0$, Eq. (32) in the limit $\mu \to 1$, and similarly the equations for all other dimensions ≥ 2.

IV. EXAMPLES AND APPLICATIONS

We start by considering the scattering length for scattering from an (attractive) square well with radius r. For $k=0$, Eqs. (8) and (9) lead to

$$a(r) = \begin{cases} r\exp\left[\dfrac{J_0(Kr)}{KrJ_1(Kr)}\right] & (n=2) \tag{37} \\[4mm] r\Big/\left[1 - 2m\dfrac{J_m(Kr)}{KrJ_{m+1}(Kr)}\right]^{1/2m} & (n>2) . \tag{38} \end{cases}$$

The $k=0$ wave number within the well is denoted by K. The strength of the potential enters the formulas for $a(r)$ only through K. For other potential strengths $a(r)$ can be obtained by simple scaling. In Figs. 1—3 these quantities are given for $K=1$ as a function of r for $n=2$, 3, and 4, respectively. The $\cot(Kr)$-like behavior due to the ratio of the oscillating Bessel functions is clearly visible. We repeat that for $n=2$, $a(r)$ varies between the equivalent values 0 and ∞. For $n=3$, the variation is between ∞ and $-\infty$. For $n=4$, the solid parts are those with $a(r)$ real. The dashed parts have complex phase $\tfrac{1}{2}\pi$. Note that due to the factor Kr in the denominator of Eq. (38) the intervals in which $a(r)$ varies along a complex axis, become gradually narrower. In Fig. 1 the dashed curves represent $a(r,k)$ for $k=0.5$. As mentioned in Sec. III, we select from the infinity of possible values at each r that $a(r,k)$ value which goes continuously to $a(r)$ for $k \to 0$. The magnitude of the jumps increases for decreasing k. The value 4.82... of $a(0,k)$ corresponds with the first zero of $J_0(ka)$. Turning the attractive well into a repulsive barrier leads to similar equations with K imaginary. The corresponding curves show less structure.

For the scattering of adsorbed H atoms we show in Fig. 4 how $a(r)$ and $r_e(r)$ build up as a function of r starting from 0 at the origin. We describe the scattering as a two-dimensional phenomenon, accounting[10] for the spatial extent of the bound states $\phi_0(z_1)$ and $\phi_0(z_2)$ of the H atoms by averaging the H-H interaction potential. For the weight function
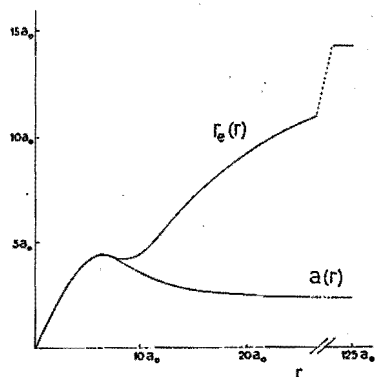

FIG. 4. Local scattering length $a(r)$ and effective range $r_e(r)$ for triplet scattering of H atoms adsorbed at a superfluid helium film. The horizontal scale has been interrupted to indicate the asymptotic values at $125a_0$.

$$\int d(\tfrac{1}{2}(z_1+z_2))\phi_0^2(z_1)\phi_0^2(z_2) \qquad (39)$$

we choose a Gaussian function of z_1-z_2 with maximum value $0.05026a_0^{-1}$, taken from Mantz and Edwards.[11] For small r, $a(r)$ and $r_e(r)$ are both seen to be almost equal to r. This is due to the extreme hardness of the inner repulsive part of the potential. At about $7a_0$ the curves start to diverge; $a(r)$ continues to decrease due to the attractive part of the potential. Note that apparently $r_e(r)$ converges more slowly than does $a(r)$. The asymptotic values are found to be $a=2.3a_0$ and $r_e=14.3a_0$. These parameter values can be used for the analysis of low-energy H-H scattering at a helium surface. To give some feeling for the influence of the width of the z_1-z_2 probability distribution we here present the corresponding values for a truly two-dimensional gas (i.e., no averaging): $a=2.0a_0$ and $r_e=17.4a_0$.

V. CONCLUSIONS

We have shown that for low-energy scattering, the introduction of a scattering length a and an effective range r_e for $n=2$ in Ref. 1 fits naturally in the definition of a and r_e for general dimensions. A very useful tool for generalizing the discussion to long-range potentials has been the introduction of the function $a(r,k)$. We showed that $a(\infty,k)$ is an analytic function of k^2 under the condition that $V(r)$ goes to zero faster than $\exp(-\lambda r)$ $(\lambda>0)$, and that $a(\infty,k)$ is i times continuously differentiable in k^2, if $V(r)$ goes to zero faster than $1/r^{n+2i+1}$,

As as a result the effective-range expansions are convergent and asymptotic series in k^2, respectively (apart from a logarithmic term for even dimensions). The expansions presented contain earlier expansions for $n=2$ and $n=3$ as special cases.

[1]B. J. Verhaar, J. P. H. W. van den Eijnde, M. A. J. Voermans, and M. M. J. Schaffrath, J. Phys. A **17**, 595 (1984).

[2]L. P. H. de Goey, J. P. J. Driessen, B. J. Verhaar, and J. T. M. Walraven, Phys. Rev. Lett. **53**, 1919 (1984).

[3]F. Calogero, *Variable Phase Approch to Potential Scattering* (Academic, New York, 1967).

[4]D. Bollé and F. Gesztesy, Phys. Rev. Lett. **52**, 1469 (1984); Phys. Rev. A **30**, 1279 (1984).

[5]P. M. Morse and H. Feshbach, *Methods of Theoretical Physics* (McGraw-Hill, New York, 1953), pp. 1322 and 1573.

[6]L. Bieberbach, *Lehrbuch der Funktionentheorie* (Chelsea, New York, 1945), p. 190.

[7]E. A. Coddington and N. Levinson, *Theory of Ordinary Differential Equations* (McGraw-Hill, New York, 1955), p. 10.

[8]E. A. Coddington and N. Levinson, Ref. 7, p. 30.

[9]E. A. Coddington and N. Levinson, Ref. 7, p. 36.

[10]J. P. H. W. van den Eijnde, C. J. Reuver, and B. J. Verhaar, Phys. Rev. B **28**, 6309 (1983).

[11]D. O. Edwards and I. B. Mantz, J. Phys. (Paris) Colloq. C7, 257 (1980).

Scattering length and effective range for charged-particle scattering in a plane and in higher dimensions

B. J. Verhaar, L. P. H. de Goey, and E. J. D. Vredenbregt

Department of Physics, Eindhoven University of Technology, Postbus 513, 5600 MB, Eindhoven, The Netherlands

(Received 24 January 1985)

The concepts of scattering length a and effective range r_e previously introduced for low-energy scattering from a potential $V(r)$ in a plane and in higher dimensions are extended to include a $1/r$ potential (strength parameter γ). Both a and r_e have the physical significance of being equal to the radius of an equivalent hard sphere giving rise to the same $O(k^0)$ and $O(k^2)$ terms in the expression for the phase shift. The method used is based on the properties of the "local scattering length" $a(r,\gamma)$ for the potential $V(r)$ cut off at radius r and an "equivalent hard-sphere radius" $a(r,k,\gamma)$ for wave number $k\neq0$. It is shown that these quantities have a smooth behavior for $\gamma\to0$ and for dimension $n\to2$.

I. INTRODUCTION

In view of applications to scattering phenomena in two-dimensional spin-polarized atomic hydrogen gas we introduced[1] a year ago the concepts of scattering length and effective range for scattering in a plane. In the same paper we showed that the H + H scattering phase shift could be described by a simple effective-range formula, even at the highest collision energies occurring significantly in the relevant experimental temperature range. In a subsequent paper[2] we applied this effective-range theory in a calculation of the two-dimensional H + H recombination rate on the basis of the Kagan dipole mechanism.

In the preceding paper[3] we showed that a consistent effective-range theory could be derived, making use of the concepts of "local scattering length" and "equivalent hard-sphere radius." This enabled us to dispense with our previous restriction to a finite-range potential and to dimension $n=2$. Furthermore, we related the formalism to that proposed by Bollé and Gesztesy.[4] The purpose of the present paper is to remove the single remaining restriction of our work[3] compared to that of Ref. 4: the absence of a $1/r$ potential. The main result of this paper is the derivation of the elegant analyticity (or continuity) properties of the equivalent hard-sphere radius $a(r,k,\gamma)$ as a function of k^2 and of γ, the strength parameter of the $1/r$ potential. The smoothness of $a(r,k,\gamma)$ contrasts strongly with the singular behavior of the phase shift near $k=0$ and $\gamma=0$ which we shall also derive.

In Sec. II an effective-range theory is presented in general dimension $n\geq2$ for $\gamma\neq0$, starting from the properties of $a(r,k,\gamma)$. Section III deals with the behavior of that quantity and the phase shift as a function of γ and briefly also as a function of dimension n. Some conclusions are presented in Sec. IV.

II. LOW-ENERGY SCATTERING FOR $\gamma\neq0$

The radial Schrödinger equation for scattering of the lowest partial wave in n dimensions from a potential $V(r)+\gamma/r$ is given by

$$\left[-\frac{d^2}{dr^2}+V(r)+\frac{\gamma}{r}+\frac{l(l+1)}{r^2}-k^2\right]u(r,k,\gamma)=0 , \quad (1)$$

in which $l=\frac{1}{2}(n-3)$ and a factor of $2\mu/\hbar^2$ is absorbed in V (μ is the mass or reduced mass). For $V\equiv0$ we have the basis solutions

$$F(r,k,\gamma)=k^{-1/2}F_l(\rho,\eta) , \quad (2)$$

$$G(r,k,\gamma)=-k^{-1/2}G_l(\rho,\eta) , \quad (3)$$

normalized in order to make the Wronskian equal to unity. We use conventional notation[5,6] for the regular and irregular Coulomb functions F_l and G_l for integer and half-integer l values $l\geq-\frac{1}{2}$.

The regular solution $u(r,k,\gamma)$ of Eq. (1) is chosen with normalization such that it satisfies the energy-independent boundary condition

$$\lim_{r\to0} r^{-l-1}u=1 . \quad (4)$$

Then by Poincaré's theorem[7] both u and its radial derivative $u'\equiv\partial u/\partial r$ are known to be entire functions of k^2 for any fixed value of r. This is true under rather general conditions for the behavior of V. If a factor $c_l(\eta)k^{l+1/2}$, in conventional notation, is split off from F, the remaining function also satisfies Eq. (4) and therefore has the same analyticity properties as u.

As in Ref. 3 we consider the phase shift $\delta(k,\gamma,r)$ for the potential V cut off at r. Again it satisfies the equation

$$\cot\delta(k,\gamma,r)=\frac{G'u-Gu'}{F'u-Fu'} . \quad (5)$$

Inserting the low-energy behavior[6] of G and that of u and F, as well as their derivatives, we find

$$\cot\delta = -\frac{2}{\pi}[e^{2\pi\eta}-(-1)^{2l}]$$

$$\times \left[\frac{K_{2l+1}(2\sqrt{\gamma a})}{I_{2l+1}(2\sqrt{\gamma a})} \right.$$

$$+\tfrac{1}{4}(-1)^{2l}\mathrm{Re}[\,\psi(l+1-i\eta)+\psi(-l-i\eta)$$

$$\left. -2\ln\eta]+O(k^2) \right] \qquad (6)$$

for both $n=2$ and $n>2$. The order symbol represents a convergent expansion in k^2. For practical purposes an asymptotic expansion is equally useful. Its zero-order term is obtained by leaving out the Re term between the large parentheses which is $O(k^2)$. The local scattering length $a(r,\gamma)$ in Eq. (6) is defined by the implicit equation

$$\frac{K_{2l+1}(2\sqrt{\gamma a})}{I_{2l+1}(2\sqrt{\gamma a})}$$

$$=\frac{K_{2l+1}(2\sqrt{\gamma r})U_0-2\sqrt{\gamma r}K_{2l+2}(2\sqrt{\gamma r})u_0}{I_{2l+1}(2\sqrt{\gamma r})U_0+2\sqrt{\gamma r}I_{2l+2}(2\sqrt{\gamma r})u_0}\,, \qquad (7)$$

where K and I represent modified Bessel functions[5] and

$$u_0=u(r,0,\gamma)\,, \qquad (8)$$

$$U_0=(2l+2)u_0-2ru_0'\,, \qquad (9)$$

analogous to neutral-particle scattering.[3]

Note that for three dimensions and $\gamma\neq0$ this definition of the scattering length differs from the usual one. As we shall see in Sec. III, our scattering length has the advantage that it behaves smoothly as $\gamma\to0$ also for $n=2$. In addition it has the physical significance of an equivalent hard-sphere radius. As in the neutral case this can be seen by extrapolating the local solution of the wave equation including V, characterized by u_0 and u_0', by means of the wave equation for $k=0$ without V. The extrapolated wave function cuts the axis at $a(r,\gamma)$. Again, a can be negative or even complex if this point of intersection is not on the positive r axis. For positive right-hand side of Eq. (7), γa can be chosen to be positive and is then uniquely defined. This follows from the fact that on the real x axis $K_{2l+1}(2\sqrt{x})/I_{2l+1}(2\sqrt{x})$ varies monotonically from 0 to ∞ for x approaching the origin from $+\infty$. If the right-hand side of Eq. (7) is negative, we take another path in the complex x plane where the K/I ratio is monotonic but now negative: the path which starts at $2\sqrt{x}=+\infty+i\tfrac{1}{2}\pi$. Along this path, which is shown in Fig. 1 for $n=2$, 3, and 4, the K/I ratio varies from 0 to $-\infty$. For all dimensions $n>2$ the path ends at $x=0$, for $n=2$ at $x_0=-1.445\ldots$, corresponding to the first zero of the Bessel function $J_0(2\sqrt{x})=J_0(2\sqrt{-x})$. This defines a uniquely. The above-mentioned monotonicity of K/I follows from the fact that its derivative with respect to $2\sqrt{x}$ equals $(IK'-I'K)/I^2=-1/(2l^2\sqrt{x}I)$, which does not vanish anywhere in the x plane and can only be infinite on the negative real axis. Along the $n\geq3$ paths the derivative is infinite only at the origin and along the $n=2$ path only at x_0. This is consistent with the above-mentioned infinite value of K/I at these points.
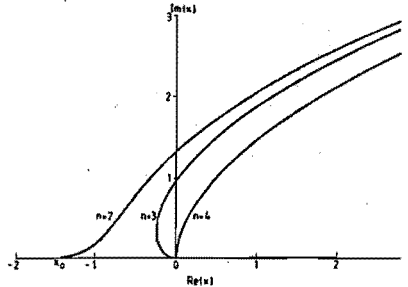

FIG. 1. Definition of scattering length by means of complex $x=\gamma a(\gamma)$ plane. For positive right-hand side of Eq. (7), γa is taken to be positive real; for negative values, γa is chosen along a complex path, shown for $n=2$, 3, and 4. Function K/I varies from 0 at $2\sqrt{x}=+\infty+\tfrac{1}{2}\pi i$ to $-\infty$ at the origin ($n\geq3$) or at $x_0=-1.445\ldots$ ($n=2$; $2\sqrt{-x_0}=$ first zero of J_0). For $\gamma\to0$ γa tends to the origin with slope $\pi/(n-2)$ or 0 corresponding to the neutral case.

Anticipating the discussion of the analyticity property of a as a function of γ to be derived in Sec. III, we note that a, thus defined for $\gamma\neq0$, approaches continuously the value[3] for $\gamma=0$. Replacing the K and I functions in both members of Eq. (7) by their asymptotic expressions for small arguments, we recover the equations

$$a(r)=\begin{cases} r\exp(2u_0/U_0) & (n=2) \qquad (10) \\[2mm] r\Big/\left[1-(2l+1)\dfrac{2u_0}{U_0}\right]^{1/(2l+1)} & \\[2mm] & (n=3,4,\ldots) \quad (11) \end{cases}$$

for the local scattering length in the neutral case. In the limit $\gamma\to0$ the slopes near the origin of the paths in Fig. 1, i.e., $\pi/(n-2)$ or 0, correspond to the phases of the neutral-particle $a(r)$, chosen in Ref. 3.

The aim of the following derivation is to obtain equations such as (6) for $r\to\infty$. To that end we generalize $a(r,\gamma)$ to an equivalent hard-sphere radius $a(r,k,\gamma)$ for $k\neq0$:

$$\cot\delta(k,r,\gamma)=\frac{G(a(r,k,\gamma),k,\gamma)}{F(a(r,k,\gamma),k,\gamma)}\,. \qquad (12)$$

This defines a uniquely, if we require it to go continuously to $a(r,\gamma)$ for $k\to0$.

A number of radial equations for a can be derived as in the neutral case. We mention only one of them, to be used in the following:

$$a'=V(r)[F(a,k,\gamma)G(r,k,\gamma)-F(r,k,\gamma)G(a,k,\gamma)]^2\,. \qquad (13)$$

An analogous equation for $a=a(r,\gamma)$ follows by differentiation of Eq. (7) and some tedious algebra:

$$a'=4arV(r)[\,K_{2l+1}(2\sqrt{\gamma a})I_{2l+1}(2\sqrt{\gamma r})$$
$$-I_{2l+1}(2\sqrt{\gamma a})K_{2l+1}(2\sqrt{\gamma r})]^2\,. \qquad (14)$$

The right-hand side of this equation may be seen to be the limit for $k \rightarrow 0$ of the term on the right-hand side of Eq. (13).

In the remaining part of this section we derive the low-energy behavior of $\delta(k,\gamma,r=\infty)$. First of all we show that $a(r,k,\gamma)$ is analytic in k^2 near $k=0$ for fixed r and γ, if $a(r,0,\gamma)$ is not singular, i.e., finite and nonvanishing. We equate the right-hand sides of Eqs. (5) and (12), multiplied by $c_l^2 k^{2l+1}$:

$$T(a,r,k^2,\gamma) \equiv \frac{u(r)u_{HS}'(r) - u'(r)u_{HS}(r)}{F(a)[F(r)u'(r) - F'(r)u(r)]/[c_l^2 k^{2l+1}]} \quad (15)$$

$$= 0 .$$

In the second member of this equation we left out the arguments k and γ, while $u_{HS}(r)$ represents a (extrapolated) wave function for scattering from a hard sphere with radius a:

$$u_{HS}(r) = F(a)G(r) - G(a)F(r) . \quad (16)$$

Since for sufficiently small $|k|$ the function $G(a,k,\gamma)/F(a,k,\gamma)$ is an analytic function[5,6] of a in any bounded region of the complex a plane not containing the origin, T is analytic in a in the same region. From the radial wave equation for the function $u_{HS}(r)$ and the boundary conditions $u_{HS}(a)=0$, $u_{HS}'(a)=1$ we derive by applying Poincaré's theorem[7] (if a is complex, along a straight line in the complex plane through a and r) that $u_{HS}(r)$ and $u_{HS}'(r)$ are entire functions of k^2. A similar statement was already made with respect to the other functions occurring in Eq. (15). We conclude that T is analytic in k^2 in a neighborhood of $k=0$ where the denominator is nonvanishing. Furthermore, for $k \rightarrow 0$ the derivative of T with respect to a,

$$T_a \equiv c_l^2 k^{2l+1} \frac{d}{da} \frac{G(a,k,\gamma)}{F(a,k,\gamma)} = \frac{c_l^2 k^{2l+1}}{F^2(a,k,\gamma)} \quad (17)$$

goes to a nonvanishing value. From the implicit-function theorem of complex-function theory[8] we may then conclude that in a vicinity of $k=0$ a local scattering length $a(r,k,\gamma)$ exists, analytic in k^2 and with $a(r,0,\gamma) = a(r,\gamma)$.

As a second step we derive the low-k behavior of $a(\infty,k,\gamma)$. To that end we start from a finite radius r_0 beyond which $a(r,\gamma)$ is not singular, excluding the exceptional case that $a(r,\gamma)$ tends to a singular value. We follow the method of derivation of the neutral case.[3] We merely repeat the essential points. (a) The infinite r interval $r_0 \leq r < \infty$ is transformed into a finite one by introducing the variable $s=1/r$. (b) For $s>0$ the function f in the transformed equation (13) $da/ds = f(a,s,k^2,\gamma)$ is analytic in k^2 and in a for $a \neq 0$. In addition it is required to be continuous and therefore, taking into account its rapid oscillations, to go to 0 as $s \rightarrow 0$ for fixed $k \neq 0$. (c) For reasons of continuity in k^2, f is also required to go to 0 as $s \rightarrow 0$ for $k=0$. From Eq. (14) we then find (i) $a(\infty,k,\gamma)$ is continuous as a function of k^2 in a vicinity of $k=0$, if

$$V(r) = \begin{cases} o\left[\dfrac{\exp(-4\sqrt{\gamma r})}{r^{5/2}}\right] & (\gamma > 0) \quad (18) \\[3ex] o\left[\dfrac{1}{r^{5/2}}\right] & (\gamma < 0). \quad (19) \end{cases}$$

Here we used the asymptotic expression for the modified Bessel functions in Eq. (14) for $r \rightarrow \infty$. For $a(\infty,k,\gamma)$ to be continuously differentiable in k^2 up to a certain order these conditions have to be correspondingly strengthened. This is necessary if in the asymptotic k^2 expansion of $\cot\delta$ further terms are desired in addition to the k^0 term [see Eq. (21) below]. If V satisfies the stronger condition

$$V(r) = o(\exp(-\lambda r)) \quad (\lambda > 0) \quad (20)$$

we have the stronger result (ii) $a(\infty,k,\gamma)$ is analytic in k^2 in a vicinity of $k=0$. Note that the conditions on V for continuity do not depend on the dimension, contrary to the neutral case.

The third and final step is to take the limit $r \rightarrow \infty$ in Eq. (12) and thus to derive effective-range expansions for the phase shift at infinity. The result to lowest order in k^2 is again given by Eq. (6), but with a replaced by $a(\gamma) \equiv a(r=\infty,\gamma)$. For completeness we also give an expression which includes the terms of order k^2:

$$\cot\delta(k,\gamma) = -\frac{2}{\pi}[e^{2\pi\eta} - (-1)^{2l}]\left[\frac{K_{2l+1}(2\sqrt{\gamma a})}{I_{2l+1}(2\sqrt{\gamma a})} - \frac{k^2}{\gamma^2}\frac{\gamma r_e}{6 I_{2l+1}^2}[2l(K_{2l+3}I_{2l+1} - K_{2l+1}I_{2l+3}) - 1] + O(k^4)\right], \quad (21)$$

where the arguments of a and r_e are γ, and those of the K and I functions in the second term in large parentheses are $2\sqrt{\gamma r_e}$. The scattering length $a(\gamma)$ and the effective range $r_e(\gamma)$ have been defined such that the k^0 and k^2 terms in large parentheses are the same as for scattering from a hard sphere with radius a and r_e, respectively. The effective range may be expressed in terms of a and $\dot{a} = \partial a(\infty,k,\gamma)/\partial k^2|_{k=0}$.

For $n=3$, Eq. (21) is more complicated than the usual effective-range expansion, in which the expression in large parentheses reads simply

$$-\frac{1}{2\gamma}\left[-\frac{1}{a} + \frac{1}{2}r_e k^2\right] + O(k^4) . \quad (22)$$

For any $n \geq 2$, Bollé and Gesztesy[4] generalized the first term in expression (22). Upon comparing their $\cot\delta$ formulas for even and odd dimensions with Eq. (21) we have

$$\frac{K_{2l+1}(2\sqrt{\gamma a})}{I_{2l+1}(2\sqrt{\gamma a})} = \frac{[(2l+1)!]^2}{2\gamma^{2l+1}a_B}, \tag{23}$$

denoting the scattering length introduced by Bollé and Gesztesy by a_B. It is interesting to compare a and a_B for small γ. To that end we approximate the K/I ratio for small arguments and find

$$a_B = \begin{cases} (n-2)a^{n-2} & (n \ge 3) \tag{24} \\[2mm] \dfrac{-1}{2C + \ln(\gamma a)} & (n=2,\ \gamma \ne 0) \tag{25} \end{cases}$$

denoting Euler's constant 0.577215... by C instead of γ as in Refs. 1 and 3, to avoid confusion with the strength parameter of the $1/r$ potential. Anticipating the results of Sec. III, we already note here that Eq. (24) implies a_B to be continuous for $\gamma \to 0$, although not differentiably, while for $n=2$, Eq. (25) shows a_B to have a discontinuity. This contrasts with the smooth charge dependence of our scattering length for all $n \ge 2$ under rather general conditions on V. We confirmed the above-mentioned behavior of a and a_B with γ by means of numerical calculations.

III. COULOMB-CORRECTED SCATTERING LENGTHS AND PHASE SHIFTS

In this section we pay attention to a problem often studied in the literature: the problem of how to take into account the effect of charges on the value of the neutral scattering length and phase shift.[9-12]

We extend the derivation of the preceding section following Eq. (14) by including the dependence on γ. The first step concerns the analytic dependence of $a(r,\gamma)$ on γ for finite r, taking into account that $T(a,r,k^2,\gamma)$ is also analytic in γ by Poincaré's theorem, the boundary conditions for u, u_{HS}, and $F/(c_l k^{l+1/2})$ being independent of γ. The second step concerns the dependence of $a(r=\infty,k,\gamma)$ on γ. We again start from a finite radius r_0 beyond which $a(r,\gamma=0)$ is not singular, excluding the exceptional case that it tends to a singular limit. Essentially, the derivation of the preceding section then applies, since in the first place the function $f(a,s,k^2,\gamma)$ is entire in k^2 and γ for $s > 0$. This follows from Eq. (13), the function $u_{HS}(r)$ between square brackets satisfying k^2- and γ-independent boundary conditions. Turning to the point $s=0$, again for reasons of continuity f also has to go to 0 as $s \to 0$ at $k^2 = \gamma = 0$. This implies the condition

$$V(r) = o\left[\frac{1}{r^{n+1}}\right] \tag{26}$$

of Ref. 3, together with conditions (18) and (19) for $\gamma > 0$ and $\gamma < 0$, respectively (the preceding conditions automatically imply continuity of f as $s \to 0$ for real $k \ne 0$). Thus a is continuous in γ for $|\gamma|^{1/2} < \lambda$, if the strongest of these is satisfied, i.e., if $V(r)$ goes to zero faster than $\exp(-4\lambda/\sqrt{r})$. The same condition is needed, if we want a to be analytic in γ for real k. For complex k we again have to impose the stronger condition (20). A survey of

conditions on V is given in Table I.

We conclude that $a(\gamma)$ goes smoothly to $a(\gamma=0)$ for any dimension $n \ge 2$. As a consequence $a_B(\gamma)$ for $n \ge 3$ also behaves continuously, Eq. (24) also being valid[3,4] for $\gamma = 0$. Note, however, that it is certainly not analytic in γ, since the left-hand side of Eq. (23) contains a $\ln(\gamma a)$ term. This has also been pointed out in Ref. 4. A Taylor series expansion of a_B is thus impossible: Eq. (24) is an asymptotic expression. Furthermore, for $n=2$, $a(\gamma)$ goes to a real positive value $a(\gamma=0)$. Therefore, according to Eq. (25), $a_B(\gamma)$ tends to 0 both for $\gamma \to +0$ and $\gamma \to -0$. Its value for $\gamma=0$, however, is, in general, different from 0.

The continuity of our scattering length for $\gamma \to 0$ makes it possible to derive for any $n \ge 2$ an explicit expression for the Coulomb correction to our scattering length in terms of the $\gamma=0$ scattering length. The right-hand side of Eq. (14) being an entire function of γ, we consider its first derivative relative to γ. As mentioned before, its zero-order form corresponds to the radial equation[3] for the neutral scattering length. Taking first-order terms and integrating over r from 0 to ∞ we are able to express $a(\gamma)$ in the $\gamma=0$ quantities

$$a(\gamma) = a(0) + \gamma \int_0^\infty f(r)g(r)dr + O(\gamma^2). \tag{27}$$

In this equation f and g are given by

$$f(r) = \exp - \int_r^\infty \frac{2tV(t)}{(2l+1)^2} \\ \times \left\{ l\left[\frac{t}{a}\right]^{2l+1} - (l+1)\left[\frac{a}{t}\right]^{2l+1} \\ + 1 \right\}dt \quad (n \ge 3), \tag{28}$$

$$f(r) = \exp \int_r^\infty tV(t)\ln\frac{a}{t}\left[\ln\frac{a}{t} + 2\right]dt \quad (n=2), \tag{29}$$

$$g(r) = \frac{2arV(r)}{(2l+1)^2(2l+2)} \\ \times \left\{ \left[\left[\frac{r}{a}\right]^{2l+1} - \left[\frac{a}{r}\right]^{2l+1}\right](r-a) \\ + \frac{r}{l}\left[1 - \left[\frac{a}{r}\right]^{2l+1}\right] \\ + \frac{a}{l}\left[1 - \left[\frac{r}{a}\right]^{2l+1}\right] \right\} \quad (n > 3), \tag{30}$$

$$g(r) = arV(r)\left[\frac{r^2}{a} + \frac{a^2}{r} - a - r + 2(r-a)\ln\frac{a}{r}\right] \quad (n=3), \tag{31}$$

$$g(r) = 2arV(r)\ln\frac{a}{r}\left[(a+r)\ln\frac{a}{r} - 2(a-r)\right] \quad (n=2). \tag{32}$$

In Eqs. (28)–(32) a stands for the $\gamma=0$ local scattering length $a(r)$. We stress that no approximations have been

TABLE I. Conditions on V at infinity for continuity and analyticity properties of $a(\infty,k,\gamma)$ in k^2 and γ.

Property of $a(\infty,k,\gamma)$	Condition on V
Continuous in k^2 for $\gamma < 0$	$o\left[\dfrac{1}{r^{5/2}}\right]$
Continuous in k^2 and γ at $\gamma = 0$	$o(1/r^{n+1})$
Continuous in k^2 for $\gamma > 0$	$o\left[\dfrac{\exp(-4\sqrt{\gamma r})}{r^{5/2}}\right]$
Analytic in γ for real k	$o(\exp(-4\lambda\sqrt{r}))$, $\lambda > 0$
Analytic in k^2 and γ	$o(\exp(-\lambda r))$, $\lambda > 0$

made in deriving these lowest-order terms in γ. We note furthermore that again expression (29) is the limit for $n \to 2$ of Eq. (28). Similarly, Eqs. (31) and (32) are limits of Eq. (30).

It does not make much sense to turn to an expansion of the phase shift δ or $\cot\delta$ itself in γ: the availability of an explicit expression via Eq. (21) makes it possible to substitute directly an order-γ approximated scattering length in the K/I ratio.

In the present paper and in Ref. 3 we have pointed several times to the fact that our equations show a natural behavior for varying dimension n. In particular the equations for two dimensions fitted naturally in those for general $n \geq 2$. To show this was in fact one of the main objectives of Ref. 3 and this paper. It is appropriate to point out that this formal behavior as a function of dimension can be put on a more rigorous basis by treating n (i.e., l) as a third parameter besides k^2 and γ. Poincaré's theorem can also be applied to prove the smooth behavior of the equivalent hard-sphere radius and the scattering length as a function of n near $n = 2$.

IV. CONCLUSIONS

We have thus extended the concepts of scattering length and effective range introduced in Refs. 1 and 3, so as to include a $1/r$ potential. Both of them have the physical significance of the radius of an equivalent hard sphere giving rise to the same $O(k^0)$ and $O(k^2)$ terms in the expression for $\cot\delta$. The derivation was based on the introduction of an equivalent hard-sphere radius $a(r,k,\gamma)$ for general k and γ, cutting off the potential V at r. The smooth energy dependence of this quantity made it possible to derive the effective-range expansion for fixed γ, both for finite r and for r going to infinity.

Making extensive use of Poincaré's theorem it was subsequently possible to derive a similar smoothness property for $a(r,k,\gamma)$ and $a(\infty,k,\gamma)$ as they depend on γ and on the dimension.

[1]B. J. Verhaar, J. P. H. W. van den Eijnde, M. A. J. Voermans, and M. M. J. Schaffrath, J. Phys. A **17**, 595 (1984).

[2]L. P. H. de Goey, J. P. J. Driessen, B. J. Verhaar, and J. T. M. Walraven, Phys. Rev. Lett. **53**, 1919 (1984).

[3]B. J. Verhaar, L. P. H. de Goey, J. P. H. W. van den Eijnde, and E. J. D. Vredenbregt, preceding paper, Phys. Rev. A **32**, 1424 (1985).

[4]D. Bollé and F. Gesztesy, Phys. Rev. Lett. **52**, 1469 (1984); Phys. Rev. A **30**, 1279 (1984).

[5]*Handbook of Mathematical Functions*, edited by M. Abramowitz and I. A. Stegun (Dover, New York, 1968).

[6]F. S. Ham, Q. Appl. Math. **15**, 31 (1957): Eqs. (9), (23), (A14), (A16), and (A17). Using the Watson definition of the K func-

tion, we omit the $\cos(\pi m)$ factor in Eq. (A17).

[7]H. Poincaré, Acta Math. **4**, 201 (1884); R. G. Newton, *Scattering Theory of Waves and Particles*, 2nd ed. (McGraw-Hill, New York, 1982), p. 334.

[8]L. Bieberbach, *Lehrbuch der Funktionentheorie* (Chelsea, New York, 1945), p. 190.

[9]G. F. Chew and M. L. Goldberger, Phys. Rev. **75**, 1637 (1949).

[10]H. A. Bethe, Phys. Rev. **76**, 38 (1949).

[11]A. M. Badalyan, L. P. Kok, M. I. Polikarpov, and Yu. A. Simonov, Phys. Rep. **82**, 32 (1982).

[12]J. Fröhlich, L. Streit, H. Zankel, and H. Zingl, J. Phys. G **6**, 841 (1980).

SUMMARY

The study of atomic hydrogen gas, stabilized against the formation of H_2 molecules by the parallel direction of the electron- and proton-spins (H↓↕ or H↑↕), has attracted much attention in recent years. This thesis deals with the theoretical aspects of some interesting quantummechanical collision phenomena appearing in such a spin-polarized gas at densities and temperatures for which degeneracy effects do not play a role.

The thesis is divided in eight chapters. Chapter 1 serves as an introduction and gives the motivation for the research. We start with a brief summary of the progress during the last years, in which we come to the conclusion that óne of the possibilities to obtain Bose-Einstein condensation in H↓↕ gas is under present experimental circumstances blocked by a rapid decay of the gas via the exothermal recombination reaction $H+H+H \rightarrow H_2+H$. This process can take place when one or two electron spins are flipped by the magnetic-dipole interaction during a collision of three polarized hydrogen atoms. A study of this collision process, taking place in the volume and in the H↓↕ gas adsorbed to the helium surface, is óne of the main topics of this thesis. As a preparation for this study, we give in Chapter 1 also an overview of the interactions in the atomic gas and a summary of some aspects of (non-relativistic) quantummechanical scattering theory of two and three particles.

A calculation of the decay constant of the three-body dipolar recombination process at the surface is presented in Chapter 2. This calculation is based on a mechanism, first described by Kagan for the volume. The results display important differences with experiment: the magnetic-field dependence is wrong as in the case of the volume, while also the order of magnitude is roughly a factor of 10 too small. In Chapter 3 the theory of this surface reaction is more extensively studied and the effect of some approximations further investigated. Apart from this, Chapter 3 contains also the more general theory of exchange and dipolar recombination in atomic hydrogen gas: on the basis of scattering theory and via the quantum Boltzmann equation expressions are deduced for the decay constants in terms of transition matrix elements.

In view of the discrepancies between the experimental and theoretical behavior of the surface and volume recombination constants for fields B≲10 T, we introduce in Chapter 4 the dipole-exchange mechanism as an alternative to the Kagan process. Two ways to estimate its contribution turn out to be promising, but too uncertain to come to definite conclusions.

Therefore a start is made in the same Chapter 4 with a more exact determination of the decay constant for the volume. This calculation is continued in Chapter 5. An almost rigorous starting point here is the first-order matrix element of the extremely weak magnetic-dipole interaction between the H+H+H initial state and the H_2+H final state, in which the central (singlet/triplet) interactions are included to all orders. A major part of such a project has already been realized: the H+H+H initial state is determined exactly by means of the Faddeev formalism, while in the H_2+H final state all three-body correlations are included, except for the correlations giving rise to the dipole-exchange mechanism. The results of this calculation are still not in agreement with the experiment, so that we may conclude that the latter mechanism must be responsible for the discrepancies for fields B≲10 T.

A parametrizetion of the low-energy behavior of two- and three-particle collision phenomena is of special importance to describe the low-temperature phenomena in a gas of H↓↑. In Chapters 6-8 attention is given to formulate such a theory for scattering in arbitrary dimension n≳2, so that it can be used in particular for H+H and H+H+H collisions in the bulk and in the two-dimensional gas of atoms adsorbed to the helium surface. Chapter 6 contains a summary of this effective-range theory in general, while Chapters 7 and 8 are especially devoted to scattering of neutral and charged particles, respectively.

SAMENVATTING

De studie van atomair waterstof gas, gestabiliseerd tegen de vorming van H_2 moleculen door het gelijk richten van de electron- en proton-spins $(H\downarrow\uparrow$ of $H\uparrow\uparrow)$, heeft de laatste jaren veel aandacht getrokken. Dit proefschrift behandelt de theoretische aspecten van enkele interessante quantummechanische botsingsverschijnselen die in zo'n spin-gepolariseerd gas optreden, bij dichtheden en temperaturen waarvoor degeneratie effecten nog geen rol spelen.

Het proefschrift is verdeeld in acht hoofdstukken. Hoofdstuk 1 is een inleiding en geeft de motivatie voor het onderzoek. We starten met een korte samenvatting van de ontwikkeling gedurende de laatste jaren, waarin we tot de conclusie komen dat één van de mogelijkheden om Bose-Einstein condensatie in $H\downarrow\uparrow$ gas te verkrijgen onder de huidige experimentele omstandigheden wordt geblokkeerd door een snel verval van het gas via de exotherme recombinatie reactie $H+H+H \rightarrow H_2+H$. Dit proces kan optreden als een of twee electron spins worden geflipt door de magnetische dipool interactie tijdens een botsing van drie gepolariseerde waterstof atomen. Een studie van dit botsingsproces, dat plaats vindt in het volume en in het aan de heliumwand geadsorbeerde $H\downarrow\uparrow$ gas, is één van de hoofdpunten van dit proefschift. Als voorbereiding op die studie geven we in Hoofdstuk 1 tevens een overzicht van de interacties in het atomaire gas en een samenvatting van enkel aspecten van de (niet-relativistische) quantummechanische verstrooiings-theorie van twee en drie deeltjes.

Een berekening van de vervalsconstante van het drie-deeltjes dipolaire recombinatie proces aan het oppervlak wordt in Hoofdstuk 2 weergegeven. Deze berekening is gebaseerd op een mechanisme, dat voor het eerst beschreven is door Kagan voor het volume. De resultaten vertonen belangrijke verschillen met het experiment: net als in het volume is de magneetveld afhankelijkheid fout, terwijl ook de orde van grootte ruwweg een factor 10 te klein is. In hoofdstuk 3 wordt de theorie van deze oppervlakte reactie meer uitgebreid bestudeerd en het effect van enkele benaderingen verder onderzocht. Daarnaast bevat Hoofdstuk 3 nog de meer algemene theorie van exchange en dipolaire recombinatie in atomair waterstofgas: via de verstrooiingstheorie en via de quantum Boltzmann vergelijking worden uitdrukkingen afgeleid voor vervalsconstanten in termen van overgangs matrix elementen.

Met het oog op de discrepanties tussen het experimentele en theoretische gedrag van de oppervlakte en volume recombinatie constanten voor velden B≲10 T, introduceren we in Hoofdstuk 4 het dipool-exchange mechanism als een alternatief voor het Kagan proces. Twee manieren om de bijdrage hiervan af te schatten blijken hoopgevend te zijn, maar toch te onzeker om er definitieve conclusies aan te verbinden.

Derhalve wordt nog in hetzelfde Hoofdstuk 4 een aanzet gedaan tot een meer exacte berekening van de vervalsconstante voor het volume. Deze berekening wordt voortgezet in Hoofdstuk 5. Een bijna-rigoreus uitgangspunt hierbij is het eerste-orde matrix element van de extreem zwakke magnetische-dipool interactie tussen de H+H+H begintoestand en de H_2+H eindtoestand, waarin de centrale (singlet/triplet) interacties zijn verdisconteerd tot alle orden. Een groot deel van een dergelijk project is reeds gerealiseerd: de H+H+H begintoestand is exact berekend met behulp van het Faddeev formalisme, terwijl in de H_2+H eindtoestand alle drie-deeltjes correlaties zijn verdisconteerd, behalve de correlaties die tot het dipool-exchange mechanisme leiden. De resultaten van de berekeningen zijn nog altijd niet in overeenstemming met het experiment, zodat we kunnen concluderen dat dit laatstgenoemde mechanisme verantwoordelijk moet zijn voor de discrepanties voor velden B≲10 T.

Een parametrisatie van het lage-energie gedrag van twee- en drie-deeltjes botsingsverschijnselen is van speciaal belang voor het beschrijven van lage-temperatuur verschijnselen in H↓↑ gas. In Hoofdstukken 6-8 wordt aandacht geschonken aan een formulering van zo'n theorie voor verstrooiing in algemene dimensie n≥2, zodat deze in het bijzonder gebruikt kan worden voor H+H en H+H+H botsingen in het volume en in het twee-dimensionale gas van atomen geadsorbeerd aan het helium oppervlak. Hoofdstuk 6 bevat een samenvatting van deze effectieve dracht theorie in het algemeen, terwijl Hoofdstukken 7 en 8 speciaal gericht zijn op respectievelijk verstrooiing van neutrale en geladen deeltjes.

LEVENSLOOP

4 Nov. 1958:   Geboren te Budel.

Aug. 1971 - Juni 1977:   Gymnasium B aan het Bisschoppelijk College te
                               Weert

Aug. 1977 - Dec. 1982:   Studie Natuurkunde aan de Katholieke
                               Universiteit Nijmegen.
                               Afstudeerrichting: Theoretische elementaire
                               deeltjes fysica bij Prof. dr. R.P. van Royen.

Dec. 1982 - Juni 1983:   Eerste graads lesbevoegdheid natuurkunde aan de
                               Katholieke Universiteit Nijmegen.
                               Hospitium: Vincent van Gogh Havo te Oss.

Aug. 1983 - Jan. 1984:   Eerste graads leraar natuurkunde aan de
                               R.K. Havo de Naulande te Drunen.

Jan. 1984 - Jan. 1988:   Promotieonderzoek in de vakgroep Theoretische
                               Natuurkunde aan de Technische Universiteit
                               Eindhoven onder leiding van
                               Prof. dr. B.J. Verhaar.

STELLINGEN

behorende bij het proefschrift van

L.P.H. de Goey

1. Uit het τ-matrix formalisme, geïntroduceerd door H.T.C. Stoof et
    al., volgt dat het anti-hermitische deel van de T(ransition)
    operator die de verstrooiing beschrijft aan een
    rotatie-symmetrische potentiaal exact separeert.

    H.T.C. Stoof, L.P.H. de Goey, W.M.H.M. Rovers, P.S.M. Kop Jansen
    en B.J. Verhaar, ingezonden ter publicatie.

2. De recente ontwikkeling m.b.t. hoge-T_c supergeleiding opent
    perspectieven voor de (verdere) stabilisatie van atomair
    waterstof.

    T.K. Worthington, W.J. Gallagher en T.R. Dinger, Phys. Rev. Lett.
    59, 1160 (1987).

3. De generalisatie van de effectieve-dracht theorie van 3 dimensies
    tot algemene dimensie n$\geq$2 zoals gepresenteerd in dit proefschrift
    is superieur t.o.v. formuleringen van andere auteurs.

    D. Bolle'en F. Gesztesy, Phys. Rev. Lett. 52, 1469 (1984).
    S.K. Adhikari, W.G. Gibson en T.K. Lim, J. Chem. Phys. 85, 5580
    (1986).

4. De beschrijving van de relatieve beweging van twee aan de helium
    wand geadsorbeerde H atomen wisselwerkend via de triplet
    interactie, zoals toegepast door Kagan, is een slechte benadering
    voor subkelvin temperaturen.

    Yu. Kagan, G.V. Shlyapnikov, I.A. Vartan'yants en N.A. Glukhov,
    Zh. Eksp. Teor. Fiz. 81, 1131 (1981).

5. Het is mogelijk om een experimentele benedengrens te bepalen voor
    de bulk recombinatie-constante van dubbel-gepolariseerd atomair
    waterstof gas voor magneetvelden tot 40 Tesla via metingen bij
    velden variërend tussen 0 en 20 Tesla.

6. De uitdrukking die Bogoliubov, op basis van een suggestie van
    Landau, gebruikt voor het T-matrix element van een binaire botsing
    om zijn microscopische theorie van verdunde gedegenereerde Bose
    systemen te generaliseren tot willekeurig sterke paar-interacties,
    is onjuist.

    N.N. Bogoliubov, J. Phys. (USSR) <u>11</u>, 23 (1947).

7. Het gedrag van een groot deel van de Budelse bevolking ten aanzien
    van de cadmiumvervuiling kan verklaard worden met behulp van de
    cognitieve dissonantie-theorie van Festinger.

    C. Keers en H. Wilke, Oriëntatie in de sociale psychologie.

8. Met name vanuit het oogpunt van het Japanse onderwijs zou het
    grote voordelen bieden als de Kanji tekens in het Japanse
    letterschrift vervangen zouden worden door Kana tekens.

9. Het dient aanbeveling strips als "Kuifje", "Asterix" en
    "Lucky Luke" te verwerken in het lesmateriaal van het
    basisonderwijs.

10. De toekenning van Nobel prijzen in de Natuurkunde doet te weinig
    recht aan belangrijke bijdragen met een minder spectaculair
    karakter.